J. Gianelos and E. A. Grulke, Some studies of chlorinated PVC using XPS, *Adv. X-ray Anal.*, **22**, 473 (1979).

J. Knecht and H. Baessler, An ESCA study of solid 2,4-hexadiyne-1,6-diol bis (toluene sulphonate) and its constituents before and after polymerisation, *Chem. Phys.*, **33**, 179 (1978).

K. Knutson and D. J. Lyman, Morphology of block copolyurethanes (II). FTIR and ESCA techniques for studying surface morpholy, *Org. Coat Plast.* Chem., **42**, 621 (1981).

P. C. Lacaze and G. Tourillon, Spectroscopic study (XPS-SIMS) of the aging of polyacetonitrile thin films electrochemically deposited on a platinum electrode, *J. Chim. Phys., Phys. Chim. Biol.*, **76**, 371 (1979).

H. J. Leary and D. S. Campbell, Surface analysis of aromatic polymide films using ESCA, *Surf. Interface Anal.*, **1**, 75 (1979).

S. Nagarajan, Z. H. Stachurshi, M. E. Hughes and F. P. Larkins, A study of the PE-PTFE system (II). ESCA measurements, *J. Polym. Sci. Phys. Ed.*, **20**, 1001 (1982).

J. J. O'Malley and H. R. Thomas, Surface studies of multicomponent polymer solids, *Contemp. Top Poly. Sci.*, **3**, 215 (1979).

D. Shuttleworth *et al.*, XPS study of low molecular weight polystyrene-polydimethylsiloxane black copolymers, *Polym. Prepr., Am. Chem. Soc., Div. Polym. Chem.*, **20**, 499 (1979).

J. H. Stone-Masui and W. E. E. Stone, Characterisation of polystyrene latexes by photo-electron and infrared spectroscopy, *Polym. Colloids*, **2**, 331 (1980).

C. Sung, S. Paik and C. B. Hu, ESCA studies on surface chemical composition of segmented polyrethanes, *J. Biomed. Mater. Res.*, **13**, 161 (1979).

Y. Takai *et al.*, Photoelectron spectroscopy of poly-*p*-xylyene polymerised from the vapour phase, *Polym. Photochem.*, **2**, 33 (1982).

R. H. Thomas and J. J. O'Malley, Surface studies on multicomponent polymer studies by XPS : polystyrene/poly(ethyleneoxide) homopolymer blends, *Macromolecules*, **14**, 1316 (1981).

Practical Surface Analysis
by Auger and X-ray Photoelectron Spectroscopy
Edited by D. Briggs and M. P. Seah
© 1983, John Wiley & Sons, Ltd

Chapter 10

Uses of Auger Electron and Photoelectron Spectroscopies in Corrosion Science

N. S. McIntyre
Surface Science Western, University of Western Ontario
London, Ontario, Canada N6A 5B7

10.1 Introduction

The processes of corrosion begin and terminate at very thin surface layers. Corrosive attack of a metal is initiated when a protective or 'passivating' oxide surface film is ruptured, allowing contact between the active metal and an invading atomic or molecular species. Re-passivation can result from coverage of the surface by as little as a few atomic layers of a chemically inert substance. Corrosion science involves understanding both aspects—the causes as well as the prevention of the chemical degradation of a metal. The analysis of such thin surface films using the many techniques available should therefore have been an early topic for exploitation by surface scientists.

The fact that this was not the case has had as much to do with the concern of most corrosion scientists with a vast array of practical materials problems as with the desire of many surface physicists or chemists to study less complex surface interactions. Contacts between the two disparate groups generally occurred when an actively corroding specimen was analysed for surface composition. The results of such investigations often told the corrosion scientists much about the surface in question, but less about the true origin of the corrosion. Thus, only in the past two or three years have there been concerted joint attempts to address the question of corrosion initiation and passivation using surface analysis techniques.

The scope of surface chemistry and physics related to corrosion processes is indeed broad. If the topic is defined as the understanding of the initiation or prevention of metal deterioration in the environment, the scope extends well beyond the traditional testing of metal durability in aqueous media. Electrochemistry has become one of the most important tools in controlling the number and rate of processes occurring at a metal interface. The combined

use of electrochemistry and surface analysis is particularly promising and a number of examples are discussed in this chapter. Many corrosion-related problems involve as much metallurgy as chemistry. Corrosive attack of metals frequently occurs preferentially along boundaries between the metallic grains; heating and mechanical treatments of the metal have strong effects on such intergranular corrosion. Metallurgists, themselves, have made ample use of surface techniques, particularly Auger electron spectroscopy, to understand processes such as grain boundary segregation and alloy sensitization (see Chapter 7). However, few studies have yet used surface techniques to study corrosive invasion within metallic microstructure and fewer still have related surface effects to corrosive cracking under mechanical stress. The related microstructural phenomenon of surface pitting also has just begun to receive attention from surface scientists. The potential importance of such work will also be discussed in this chapter. The development of new methods and materials to provide surface protection is an area where analytical techniques are being more rapidly adopted. Some studies of organic and inorganic corrosion inhibitors are thus described in this chapter.

The earliest tool of the corrosion specialist used in surface studies was the optical microscope. This, coupled with a number of preferential chemical etchants, has allowed analysis of cross-sections cut through a corrosion film on a metal substrate. The surface distribution and homogeneity of corrosion films as thin as 5–10 μm can be determined in this way. Crystallographic structure of such a film (if any) has sometimes been determinable by X-ray diffraction techniques. A major improvement to film analysis came in the 1960s with the general availability of electron probe microanalysis. With the electron microprobe an X-ray fluorescence elemental analysis could be made of a spacial region as small as 2 μm, thus allowing films to be analysed chemically in cross-section.

These techniques were, of course, only applicable to cases where corrosion was rather extensive and uniform and certainly could not provide information on the initial surface attack, on surface microstructure or on the detailed chemistry of any thin film playing a passivating role. The arrival of the electron spectroscopies in the early 1970s thus marks a watershed, beyond which a number of new approaches to corrosion science were possible.

Discussion of surface techniques in this chapter is limited to X-ray photoelectron spectroscopy (XPS or ESCA) and Auger electron spectroscopy (AES), in accord with the topics covered in this volume. Indeed, most of corrosion-related surface studies have used those techniques exclusively. Where limitations to these techniques exist, alternative approaches using other well-known surface techniques will be described.

In an attempt to provide information useful to specialists in either corrosion science or surface analysis, the first section discusses aspects of the electron spectroscopies which are particularly important for corrosion studies. The

second section reviews past analytical use of AES and XPS in corrosion-related experiments. Supplemental information in both areas will be found in earlier reviews by Joshi[1] and Castle.[2, 3]

10.2 Special Aspects of XPS and AES for Corrosion Studies

10.2.1 Surface sensitivity

The 100–1000 eV electrons analysed in typical XPS and AES experiments have mean free paths ranging from 1 to 3 nm.[4] Thus, given the sensitivity of either technique, it is normally easy to detect a single monolayer of a passivating film on a substrate of different elemental composition. In certain cases, where chemical shifts are appreciable, XPS has been able to detect a top monolayer which differed only in *chemical* structure from the substrate.

Where lamellar layers of corrosion products are expected, the thickness of the uppermost layer on an infinitely thick substrate can be determined from the exponential relationship given by equation (5.27) in Chapter 5. It is possible to determine whether distribution of the top layer is lamellar or island-like by measuring the angular[5] or the kinetic energy dependence of the Auger electron or photo-electron intensities from the overlayer and the substrate. Castle[3] was able to use switch between two X-ray sources of different energy and compare the XPS intensity ratios obtained with results calculated for a lamellar model. If lamellar behaviour is confirmed, the uptake of as many as 10–20 monolayers should be measureable. In the future, changes in more complex surface distributions may be able to be followed quantitatively using scanning Auger microscopy (SAM).

Initial oxidation films fequently consist of several very thin layers of different composition; in such cases even very careful angle energy dependence studies may still yield an ambiguous model of the layers. An XPS study of an oxidized Alloy 600 surface showed nickel and iron oxides near the surface and chromium oxides nearer the metal interface. An even more surface-sensitive technique, low energy ion scattering (LEIS), was required to show that the top monolayer consisted uniquely of iron oxide.[6]

10.2.2 Elemental sensitivities

Both XPS and AES are sensitive to all elements of importance to corrosion scientists, excepting hydrogen. Access to the low atomic number elements (below $Z = 11$) has been particularly important for oxygen analysis of corrosion films; knowledge of the O 1*s* intensity and the binding energy have both been extremely valuable in passive film characterization.

The detection sensitivity in XPS is limited by the high background caused by the predominance of energy-degraded electrons in the spectrum. With

most commercial X-ray sources and counting times of practical duration (approximately 1 h), elemental detection limits (signal/noise = 3/1) range between 1.0 and 0.1 per cent of the total composition. This means that many corrosion precursors such as chloride or phosphate are barely or not at all detected by XPS under many circumstances. Unless the count rate can be improved substantially (approximately an order of magnitude) from its present status, XPS will effectively remain a tool for studying only the major phases in a corrosion system.

With a few exceptions, equivalent AES detection limits tend to be somewhat poorer than XPS. There are several reasons for this (see Chapter 3), but for many corrosion specimens, electrical charging of insulating oxides and hydroxides is probably the most significant cause. Such charging is mainly controlled by using very low primary electron beam currents, but this, in turn, greatly increases counting times. The potential of AES for detecting some minor and trace constituents, such as chloride, is greater than for XPS since distribution of these is often quite localized.

The inability of XPS and AES to detect hydrogen is a definite limitation for corrosion research. Hydrogen is an important film constituent in the form of hydrates and hydroxides. In addition, metal hydrides which are formed in some systems are precursors to brittle fracture. Alternative methods for study of hydrogen are secondary ion mass spectrometry (SIMS) or nuclear microanalysis.

10.2.3 Quantitative analysis

A number of quantitative models for XPS and AES, with and without the use of standards, are discussed in Chapter 5. Several adaptations of these, particularly suited to corrosion film analysis have been developed. For XPS studies, probably the most complete 'first-principles' model was developed by Asami, Hashimoto and Shimodaira,[7,8] and is particularly suited to the analysis of thin passive oxides on alloy substrates. Equation (5.27) in Chapter 5 was modified to account for the attenuation effect of a carbon contamination overlayer and the differing densities of the oxide film and the metal substrate. The atomic fractions of chemically differentiated species were obtained in this way, even allowing for hydrogen content, estimated from the —OH and bound water detected (see below). This model has been successful in dealing with a surface oxide composition on a metal alloy substrate of quite a different composition.[9] In Figure 10.1, a comparison is made of the surface oxide compositions on a chromium–molybdenum steel as a function of anodic polarization potential in hydrochloric acid. The Fe $2p_{3/2}$, Cr $2p_{3/2}$ and Mo $3d$ XPS spectra were integrated, and were also curve resolved (see Appendix 3) to separate the lower binding energy metallic component from the oxide component of the

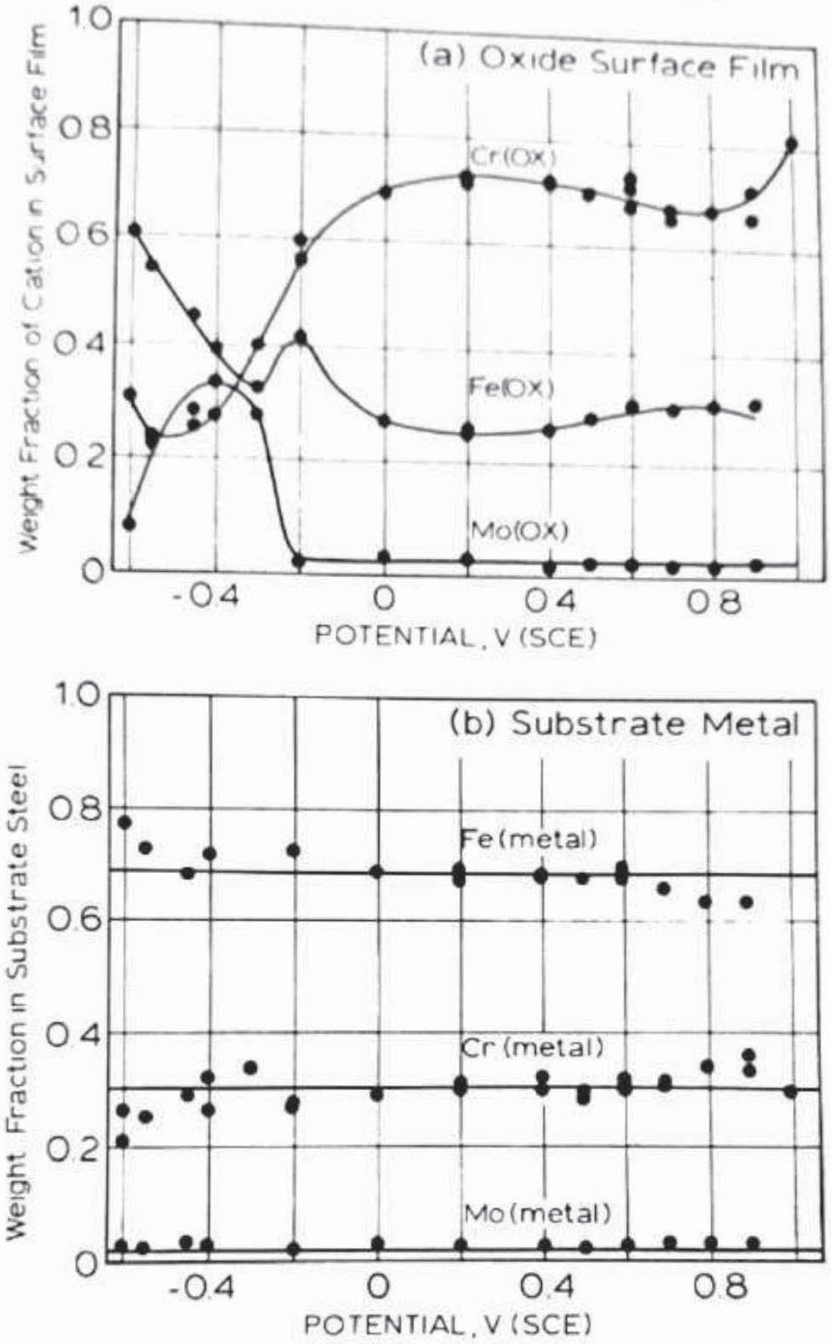

Figure 10.1 Quantitative measurement of compositions of oxide surface films and substrate alloys. Analysis of a chromium–molybdenum steel electrode polarized in 1*M* HCl for 3600 s. (a) Weight fractions of cations in the oxide film are plotted as a function of applied potential. (b) Weight fractions of metal constituents in the stainless steel are plotted as a function of applied potential. The solid lines give the composition of the bulk steel. (Reproduced by permission of K. Hashimoto, K. Asami and K. Teramoto[9])

spectrum. The sums of these separated metal and oxide intensities were used to calculate the thickness of the oxide film, and this, in turn, was used in the calculation of the oxide and metal alloy compositions. The validity of the quantitative model is supported by the agreement between the known bulk

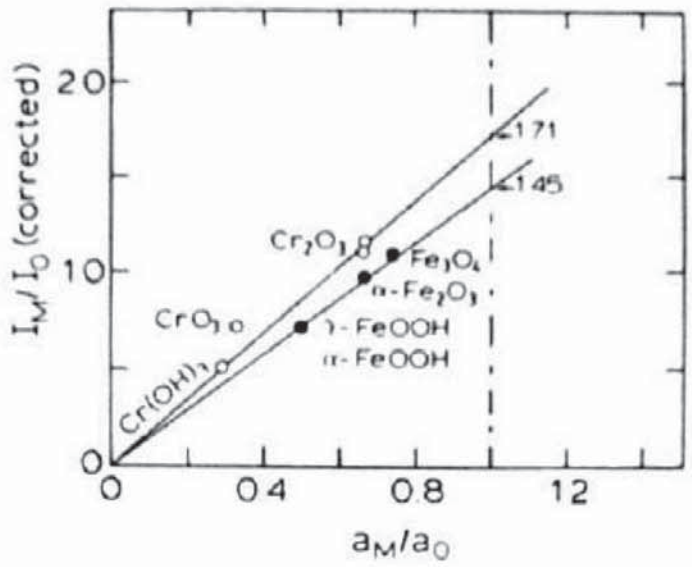

Figure 10.2 Quantitative XPS analysis of well-characterized metal oxides. Bulk oxygen/metal ratios are plotted against corrected O 1*s*/M 2*p* ratios for a number of chromium and iron oxides. (Reproduced by permission of K. Asami and K. Hashimoto[10])

alloy composition and the values consistently obtained for the metal substrate XPS analysis (see Figure 10.1b), despite major changes in the composition of the overlying oxide during the experiments.

Asami and Hashimoto have also calculated the compositions obtained from known oxide structures using this same XPS model.[10] Only one electron mean free path value was used for each photo-electron line, regardless of the chemical structure of the element. Figure 10.2 compares the known oxide/cation ratio for a given oxide with the O 1*s*/M 2*p* intensity ratio, corrected by the model for mean free path and contamination layer. The very good agreement for most oxides shows that it is valid to use a single mean free path value in such studies. Moreover, average O/M photo-electron cross-section ratios for chromium and iron oxides can be derived from the slopes in Figure 10.2.

The determination of the quantity of different types of oxygen present in the corrosion film is important, particularly where hydration and hydroxylation of the surface may affect its passivity. Asami *et al.*[11] have been able to account quantitatively for three different types of oxygen–metal oxide, metal hydroxide and bound water. Metal oxide and metal hydroxide bonding is detected on the basis of chemical shift; the bound water is determined as the difference between the total integrated O 1*s* intensity and the intensity accountable as bonded to cationic species detected over the entire XPS spectrum.

Other quantitative XPS studies of corrosion films have made use of standards to differentiate oxide and metal constituents.[6] Although this approach is less flexible than that described above, it also appears to achieve reasonable

quantitative separation of major oxide and metal phases using a spectrum analysis method that can be automated.

Quantitative analysis by AES appears to have been carried out largely with standards, although a general 'first principles' approach is well documented (see Chapter 5). The problem of the quantitative contribution of underlying atomic layers to the Auger electron spectrum has been treated by Pons, Le Héricy and Longeron[12] using the multiple surface layer model. Quantitative AES depth-profile analysis of a concentration gradient through a 5–6 monolayer corrosion film is made more difficult by contributions from the underlying layers, themselves of somewhat different composition. The differential method uses composition information obtained further into the film during a depth profile to back-correct the preceding compositions. To be most effective, this method requires that new compositions be obtained every monolayer (~0.3 nm) in the depth profile. This method has been used to improve the depth resolution of AES composition profiles through passive films on Alloys 600 and 800.[13] Figure 10.3(a) shows the original depth profile made with AES line intensities, while Figure 10.3(b) shows the profiles of atomic fractions obtained after differential treatment of the data, as discussed above. Distinct maxima in chromium and iron concentrations within the surface oxide become evident in Figure 10.3(b) as a result of the removal of intensity contributions from underlying layers. The model of Pons, Le Héricy and Longeron has been extended by Mitchell[14] to include a simplified expression for the Auger electron absorption of each successive overlayer. In addition, the statistical nature of the sputtering process was taken into account using a modified Poisson distribution.

10.2.4 Spacial resolution

In XPS, the surface area sampled is of the order of several square millimetres, as defined by the solid acceptance angle of the electron optics. The irradiating X-ray flux normally covers a larger area. By contrast, the minimum area analysed by Auger electrons in the most recent scanning Auger microprobes is as small as 0.01 μm^2.

The low spatial resolution of XPS is a serious handicap in studying some corrosion problems. Corrosion processes by their nature are often localized; many reactions are initiated at surface kinks, grain boundaries or crevices. Unless such phenomena can be generated artificially, isolated from generalized surface corrosion, it is difficult to imagine the use of a standard XPS instrument to study localized corrosion chemistry. Recently, a prototype XPS system with a much-reduced X-ray beam diameter has been announced.* This development, as well as the use of powerful synchrotron photon sources with

*Surface Science Laboratories, Inc., Sunnyvale, California.

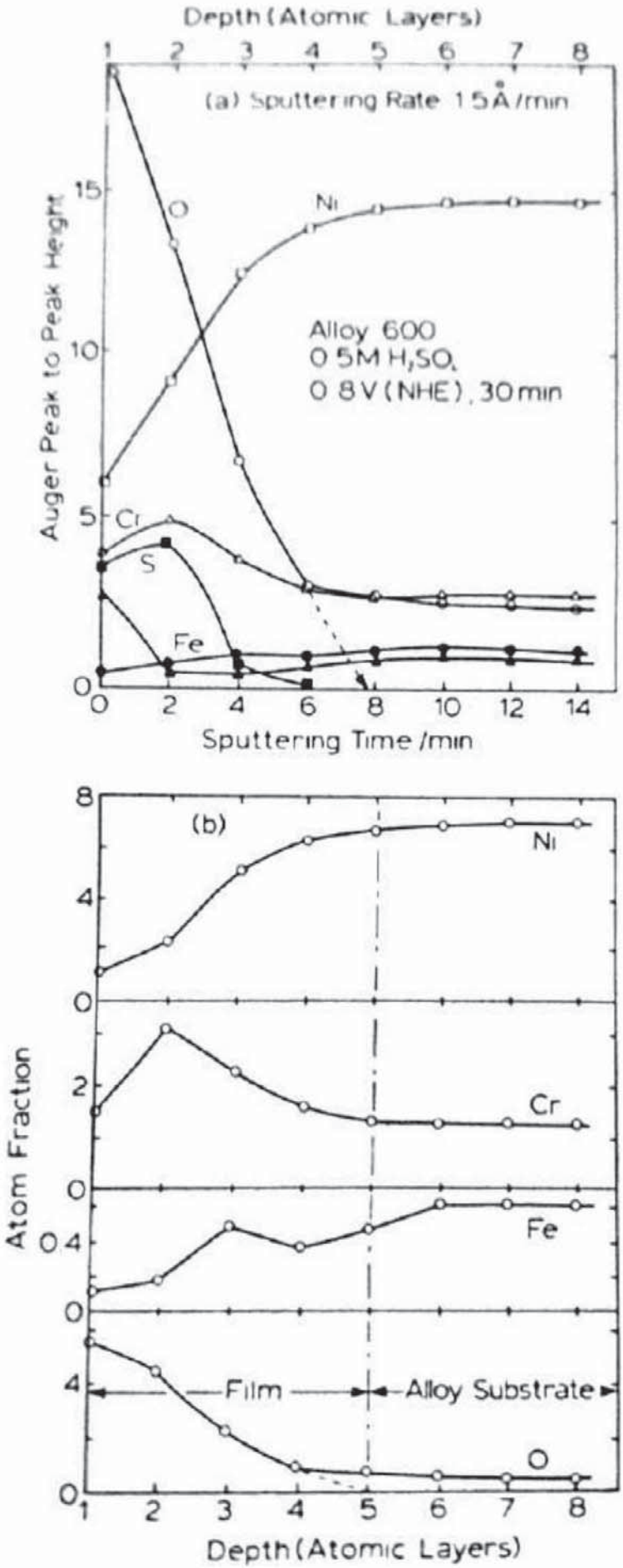
Depth (Atomic Layers)
1 2 3 4 5 6 7 8
(a) Sputtering Rate 1.5Å/min
Auger Peak to Peak Height
15
10
5
0
O
Ni
Alloy 600
0.5M H2SO4
0.8V (NHE), 30min
Cr
S
Fe
0 2 4 6 8 10 12 14
Sputtering Time /min
(b)
Ni
Cr
Fe
O
Atom Fraction
8
4
0
2
0.4
Film
Alloy Substrate
1 2 3 4 5 6 7 8
Depth (Atomic Layers)

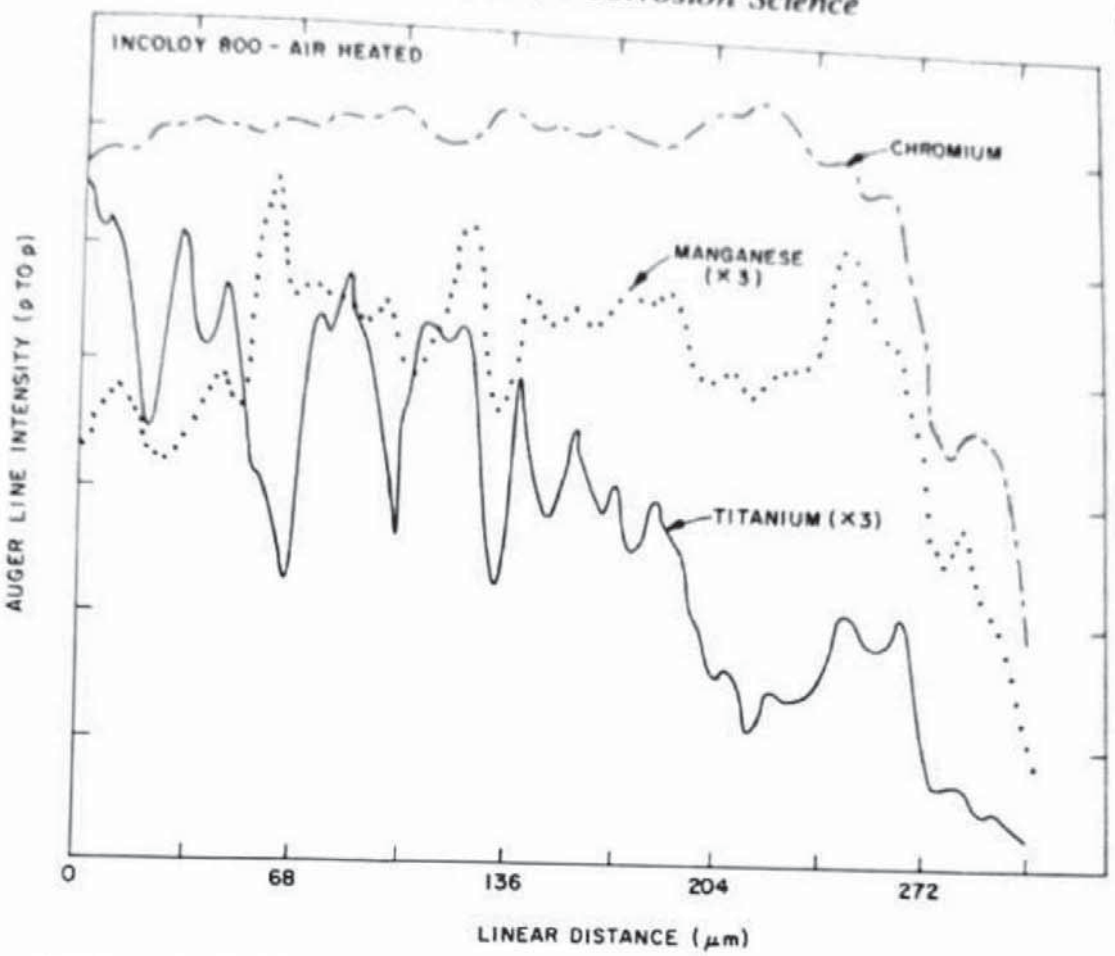

Figure 10.4 AES line scan of chromium, manganese and titanium distributions on an Alloy 800 surface oxidized at 600 °C for 1 min

reduced beam diameters, could lead to exciting new areas of research in corrosion chemistry.

The analysis of localized corrosion products by AES is well known to be a major advantage of the technique. Spot analyses of regions (e.g. pits and crevices) 1 μm apart are routinely made in studies of corrosion films. Line scans across a region changing in composition are particularly valuable, since a number of elements can be monitored simultaneously, and intensity references can be established. Figure 10.4 shows line scans of chromium, manganese and titanium made across an Alloy 800 surface oxidized at 600 °C in a flowing oxygen atmosphere.[15] Manganese and titanium distributions are highly localized and probably affected by the grain boundary intersections

Figure 10.3 Differential treatment of AES depth profile data for improved depth resolution. (a) AES intensity depth profile of an Alloy 600 surface passivated potentiostatically at 0.8 V(NHE) for 30 min in 0.5*N* H_2SO_4. (b) Differential composition profiles of data from (a) expressed in terms of atomic fractions for Ni, Cr, Fe and O. (Reproduced by permission of M. Seo and N. Sato[13])

with the surface. The distribution of titanium is, moreover, a strong function of the temperature which is altered with distance along the surface because of the flow of gas in that direction. The reconstruction of spacial distributions in the form of Auger images is qualitatively useful for corrosion studies. Auger maps showing chromium enrichment along grain boundaries has been obtained for 304 stainless steel heated to 1000 °C.[16] Many other examples of scanning Auger imaging may be found in the literature.

10.2.5 Depth profiling

Analysis of a corrosion film to a depth greater than 2nm usually involves ion bombardment coupled with simultaneous analysis by AES or sequential analysis by XPS. Much has been written of the structural damage imparted by ion beams to oxide surfaces (see Chapter 4). Knowledge of this is important if oxide layers are to be chemically or quantitatively characterized during profiling. Some beam damage has been found to result in chemical alteration of metal oxides—severe in some cases and tolerable in others. Reports of the extent of chemical alterations on the same oxide system vary, suggesting that system geometry is important. For example, numerous workers have reported the decomposition of iron oxides to FeO under low-energy argon ion bombardment. Some[17, 18] find that FeO is reduced further to the metal, while others[19, 20] find that FeO is a stable product. If preservation of steady-state sputtering of an oxide structure does not result in its reduction to a metal, oxide and metallic phases can be distinguished quantitatively during a depth profile. Of the typical first-row 'corrosion' elements, McIntyre and others[6, 21] have found that chromium, cobalt, nickel and iron are not reduced to the metal by ion bombardment, under their experimental conditions.

Such a detailed analysis of the relationship between oxide and metal phases is only possible in XPS, where oxide metal contributions to the spectrum are well separated. Figure 10.5 shows cumulative presentations of oxide and metal phases on Alloy 600 surfaces, oxidized at 300 °C in 5 and 0.01 per cent oxygen gas mixtures. The major difference is the continuation of a nickel oxide phase deep into the substrate for the sample oxidized at higher oxygen partial pressure. Such effects would be unlikely to be detected using AES.

It goes without saying that differentiation of oxide chemical structures after ion bombardment is usually impossible. Higher oxidation states are reduced and dehydration has occurred. Other non-destructive methods for depth profiling may, at times, prove useful, if a bit tedious. Mechanical milling of corrosion surfaces using an *in situ* ball mill may be useful for determination of chemistry changes in oxide surfaces. The technique is now used with AES to profile rapidly through very thick films.[22] Chemical milling, which has been used for chemical depth profiles of semi-conductor surfaces,[23] may also be useful for analysis of some oxide films.

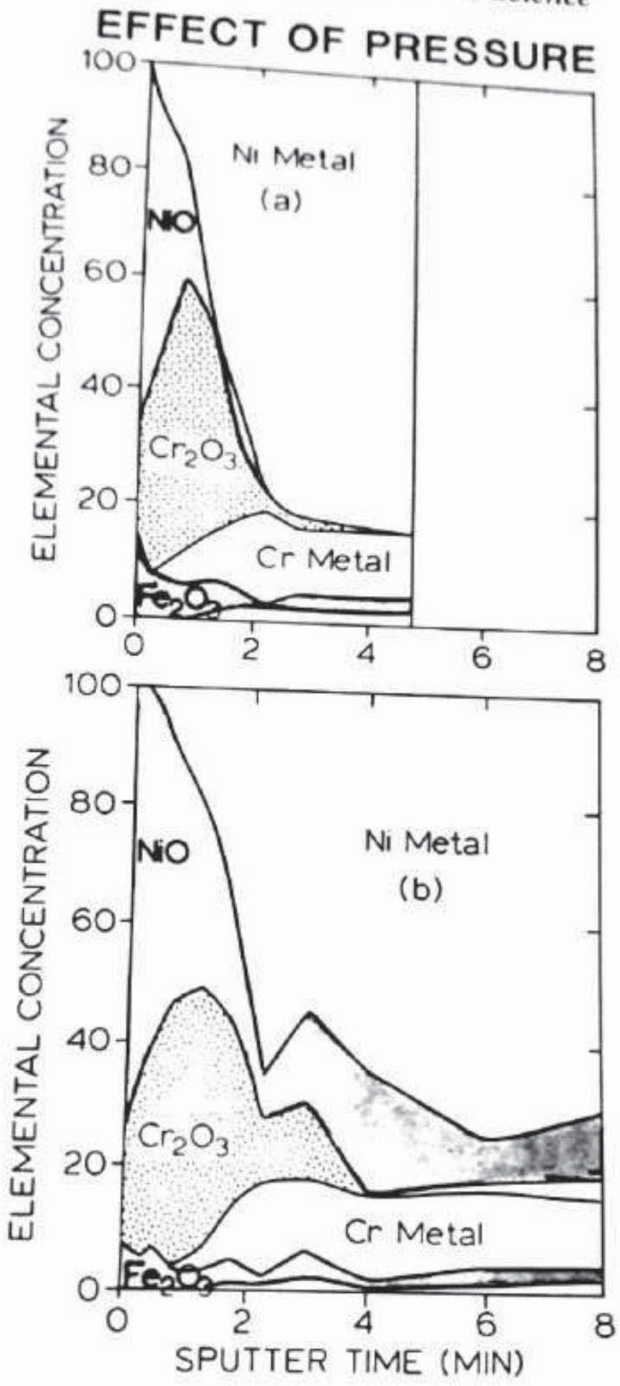

Figure 10.5 XPS depth profiles of surface films on Alloy 600 grown at 300 °C under two different oxygen pressures: (a) 0.01% O_2, 5 min; (b) 5% O_2, 5 min

10.2.6 Experimental techniques

10.2.6.1 The corrosion experiment

Over half of the surface analytical literature on corrosion describes analyses of specimens from contrived corrosion experiments, rather than the study of

material from an actual corrosion problem. A wide range of tests have been documented in the corrosion literature to simulate conditions of pitting, crevice corrosion, stress corrosion or general surface attack. These tests are done in environments resembling 'working' conditions for the material (e.g. high-pressure steam autoclave, replenished aqueous autoclave, *in situ* applied tensile stress, etc.). The balance of studies involving corrosion, generally the more fundamental, are carried out under electrochemical control in a cell. In either situation, the question of specimen surface preparation is important, unless very thick film thicknesses are expected. Surfaces prepared by mechanical polishing (cold-working) exhibit different oxidation behaviour, depending on the degree of roughness of the surface,[6] while those polished electrochemically may lose or gain surface components.[3] Vacuum-annealed specimens are probably best for more basic studies of alloy oxidation; since, however, cold work is inevitably part of 'real-world' specimens, it is frequently desirable to study the effect itself.

10.2.6.2 Specimen transfer

Under many experimental conditions, and particularly for electrochemical studies, it is necessary to protect the specimen from further chemical alteration during transfer to the analytical chamber. The effect of atmospheric exposure will, of course, be greatest when an active metal or alloy is removed from the cell with a non-passive film on the surface. For certain relatively non-reactive films, the specimen can be stored in liquid nitrogen during a transfer.[13] A more elaborate method of transfer is to use an inert atmosphere glove box for the experimental cell and to transfer from this directly into the spectrometer via an air lock. This has proven to be satisfactory for the maintenance of $UO_{2.0}$ surfaces in a reduced state.[24] The most rigorous transfer systems, however, allow no contact with any atmosphere. Such a system for use with AES has been described,[25] and recently vacuum transfer chambers for use with combined electrochemical-XPS studies has been reported.[26, 27]

10.2.6.3 Vacuum effects

It is clear that the vacuum spectrometer results in the desorption of some hydrates and the decomposition of some hydroxides. Asami and Hashimoto[10] found that α-FeOOH decomposed slowly in vacuum at 50 °C, losing 3 per cent of its hydroxide every 100 minutes. Still, there is growing evidence that even water bound within the oxide lattice is being reproducibly detected in XPS O 1*s* spectra.[28,29] Water physically or chemically adsorbed on the surface is, of course, more readily desorbed and creates some scatter in the analytical measurements of XPS O 1*s* 'bound water' intensity.[9] The detection of bound water is an encouraging development for corrosion film characterization,

since its presence has been linked to a degradation of the passive layer.[30] Further correlations of water content could be made using nuclear microprobe measurements before and after XPS analysis.

10.2.6.4 Beam effects

The X-ray source in XPS causes much less surface damage than an equivalent flux of electrons. However, X-ray-induced partial reductions of some metal oxide systems have been reported (e.g. $CuO \rightarrow Cu_2O$, $CoOOH \rightarrow CoO$), and evidence for these is likely to increase with the introduction of more powerful X-ray sources. Electron beams have been found to cause chemical decomposition,[31] desorption of water and adsorbed ions such as chloride[32] and reduction of oxides[33] under intense beam fluxes.

10.2.7 Chemical effects

In XPS the basis of the chemical shift of a core photo-electron peak is the change in electrostatic potential on the core electron when valence electron charge density is accepted or withdrawn from the atom (see Chapter 3). Thus, a relationship exists between the binding energy and the chemical state of the element. The presence of oxidized corrosion product elements can usually be clearly distinguished from the same elements as reduced metals, on the basis of their chemical shifts. Often, it is also possible to differentiate oxides of differing valence (e.g. CrO_4^{2-} and Cr_2O_3) or oxide from hydroxide (e.g. NiO from $Ni(OH)_2$. The chemical structure also influences other photo-electron peak structures and many additional changes in oxidation states. Much of the detail of the spectroscopic lineshapes and chemical shifts, which are characteristic of different corrosion species, has not yet been tabulated in a form that is readily interpretable by corrosion researchers. The characteristic spectroscopic changes are generally not large, and the reported data in the literature often are in conflict or have error limits that are too large to be useful. This situation will improve as energy calibration procedures (Appendix 1) become more standardized and methods for a more accurate definition of peak shape and position are developed. Appendix 4 contains the most complete compilation of chemical shift data on compounds of interest to corrosion scientists (i.e. oxides of the structural elements, iron, nickel, chromium, cobalt, copper and manganese), and greatly extends earlier compilations in Ref. 34.

Well-characterized chemical shifts in AES are, in general, restricted to those between a metal and its oxide. It is quite likely that this situation will change in the future with the growing number of higher resolution energy analysers in AES systems.

A general review of XPS and AES chemical shifts is given elsewhere in this book. There are, however, a number of elements of particular interest to the

corrosion specialist, where a detailed account of available oxide chemical shift data is useful. These are discussed below.

10.2.7.1 Oxygen

The O 1*s* line (approx. 530 eV) has been used extensively in the analysis of oxide surface species. The line has a relatively narrow width and a symmetric shape; this allows more accurate fitting of complex band combinations. An extensive review of O 1*s* binding energies of metal oxides has been reported by Johnson.[35] Although it appears that no simple correlation can be drawn between metal oxide bond character and O 1*s* binding energy, differences between experimental values for some oxides are sufficiently large to allow differentiation. One example of this is the shift between CuO and Cu_2O.[36,37]

Differences between hydroxyl oxygen (OH^-) and oxide oxygen (O^{2-}) are usually recognized by an O 1*s* shift of 1 to 1.5 eV. For example, the oxygen line associated with NiO is located at 529.6 ± 0.2 eV, while that for $Ni(OH)_2$ is located at a distinctly higher binding energy of 531.2 ± 0.2 eV.[37] Further, in the mixed oxide–hydroxide compound FeO(OH), contributions from each oxygen can be clearly distinguished in the O 1*s* spectrum.[19] The identification of water on surfaces from the O 1*s* spectrum is more difficult. Bonding of water molecules in different surface configurations apparently causes binding energy shifts over more than a 3 eV range. Norton[38] found that solid frozen water has a binding energy of ~533 eV, while Asami and coworkers find little difference between a hydroxide O 1*s* binding energy and that for water bound in the lattice (531 eV).[7,8] The broad envelope of O 1*s* intensity frequently detected in the range 531–534 eV suggests a multiplicity of forms of chemically and physically bound water on and within the surface. Unfortunately chemisorbed and physisorbed oxygen and hydroxyl are also found in this energy range.

Experimental Auger electron oxygen linewidths have been too broad for much use in chemical identification. Lattice oxide and chemisorbed oxygen have been identified in one structure.[39]

10.2.7.2 Titanium

XPS studies have shown that TiO_2 can be clearly distinguished from TiO in the Ti $2p_{3/2}$ spectrum.[34,40,41] TiN, a compound potentially formed within some high durability surfaces, can also be distinguished from TiO and TiO_2 on the basis of the Ti $2p_{3/2}$ chemical shift.[40]

The Auger $L_3M_{23}V$ spectra of TiO and TiO_2 are shifted by 2 eV, thus allowing their chemical identification by AES.[42] Lineshape changes in this transition have been used to differentiate metallic titanium and TiH_2.[43]

10.2.7.3 Vanadium

A chemical shift of about 1 eV has been detected between the oxides V_2O_3 and VO_2 using XPS. AES studies in this case have provided more information than those from XPS. A series of oxides of different vanadium–oxygen stoichiometries have been characterized using the $VL_2M_{2,3}V$ and $L_2M_{2,3}M_{2,3}$ Auger transitions.[44–46]

10.2.7.4 Chromium

Chromium oxide species are usually determined in XPS studies with the Cr $2p_{3/2}$ line. Chromium (III) and chromium (VI) oxides are fairly readily separated on the basis of the large (~2 eV) chemical shifts.[47,48] Chromium (III) oxide (Cr_2O_3) and the hydroxides ($Cr(OH)_3$ and CrOOH) can also be distinguished by a smaller shift (~0.5 eV) in binding energy.[10,49] Multiplet splitting of the Cr $2p_{3/2}$ line[10] may be useful in characterization of chromite structures.

10.2.7.5 Manganese

Several manganese oxides of different stoichiometries have been measured by XPS.[50] MnO and MnO_2 appear to be particularly distinguishable on the basis of their Mn $2p_{3/2}$ binding energies and peak shapes.[51]

10.2.7.6 Iron

Several XPS studies of iron oxides have been made.[19,52,53] Fe $2p$ photoelectron spectra of ferric and ferrous oxides are particularly complex, because of the large amount of coupling between the core hole created by photoemission and the high spin states of iron. Some of this complexity can be exploited for analytical purposes, since the spectral line shape is quite sensitive to chemical changes. This can be seen in Figure 10.6 where the Fe $2p_{3/2}$ spectra of α-FeOOH, α-Fe_2O_3, Fe_3O_4 and $Fe(COOH)_2$ are compared. The iron (III) hydroxide peak centre (Figure 10.2a) is shifted about 1 eV to higher binding energy than that for α-Fe_2O_3, α-Fe_2O_3 and γ-Fe_2O_3 (not shown) can be distinguished on the basis of the splitting in the main peak. Magnetite (Fe_3O_4) contains both Fe^{II} and Fe^{III}, both of which contribute to the Fe $2p_{3/2}$ spectrum with the two overlapping components in Figure 10.2(c). In real-life specimens, unfortunately, Fe_3O_4 surfaces are not usually as clearly identifiable since exposure to air causes partial oxidation of Fe_3O_4 to Fe_2O_3. Finally, some organo–iron compounds which are of interest to corrosion studies can be characterized separately from the oxides. In Figure 10.2(d), ferrous oxalate can be characterized on the bases of its prominent shake-up satellite (see arrow.

Several iron (II) oxides are also of interest to corrosion scientists. The Fe

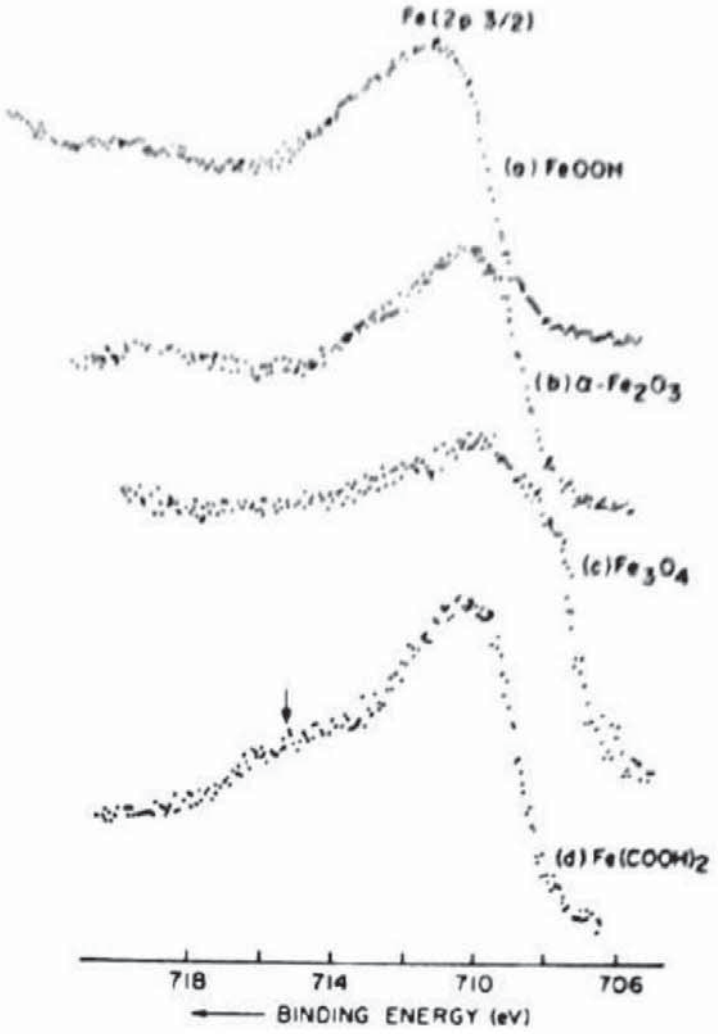

Figure 10.6 X-ray photo-electron spectra for some typical iron corrosion compounds. Fe $2p_{2/3}$ spectra are shown for (a) α-FeOOH; (b) α-Fe_2O_3; (c) Fe_3O_4; (d) Fe $(COOH)_2$

$2p_{3/2}$ spectrum of FeO has a prominent shake-up satellite,[18] as has the mixed oxide $FeMoO_4$.[54]

Sulphides of iron figure prominently in many corrosion studies. Surface iron sulphides frequently undergo hydrolysis to oxides in air, greatly complicating the spectra. However, FeS and FeS_2 are found to have quite different Fe $2p_{3/2}$ spectra, again resulting from differences in multiplet interaction. FeS_2 has a peak shape and position closely resembling that of metallic iron,[55] while FeS has a very broad peak centred nearly 2 eV higher in binding energy than the FeS_2 position.

Several iron oxides have also been characterized by low kinetic energy peaks in the AES spectrum. Ekelund and Leygraf[56] have noted two independent Fe *LVV* peaks at ~43 eV and 51 eV, respectively, and suggest that these are related to Fe^{2+} and Fe^{3+}, respectively. Seo *et al.*[57] also note a third peak at 46 eV and suggest that divalent iron is denoted by peaks at 46 and 51 eV, while trivalent iron is denoted by peaks at 43 and 51 eV.

10.2.7.7 Cobalt

Oxides of cobalt(II) and cobalt(III) are differentiated in XPS using their different magnetic properties. Paramagnetic cobalt(II) oxides have a strong shake-up satellite 6 eV above the Co $2p_{3/2}$ line, while the diamagnetic cobalt(III) oxides do not. Cobalt(II) hydroxide and cobalt(II) oxide are separated by a chemical shift of $\sim 1.0 \pm 0.2$ eV.[18,37] The cobalt mixed oxides, $CoMoO_4$ and $CoAl_2O_4$, are shifted ~ 0.5 eV to a higher binding energy.[38]

10.2.7.8 Nickel

Unlike cobalt, only one oxidation state of nickel is believed to be present, for all practical purposes, on oxidized nickel surfaces. A chemical shift of approximately 2 eV is found between the Ni $2p_{3/2}$ line positions for NiO and $Ni(OH)_2$, thus facilitating identification of surface $Ni(OH)_2$.[37]

The Ni $2p_{3/2}$ spectrum of Ni^{2+} in different oxide lattices also changes significantly with the chemical structure, probably due to multiplet interaction.[6] In

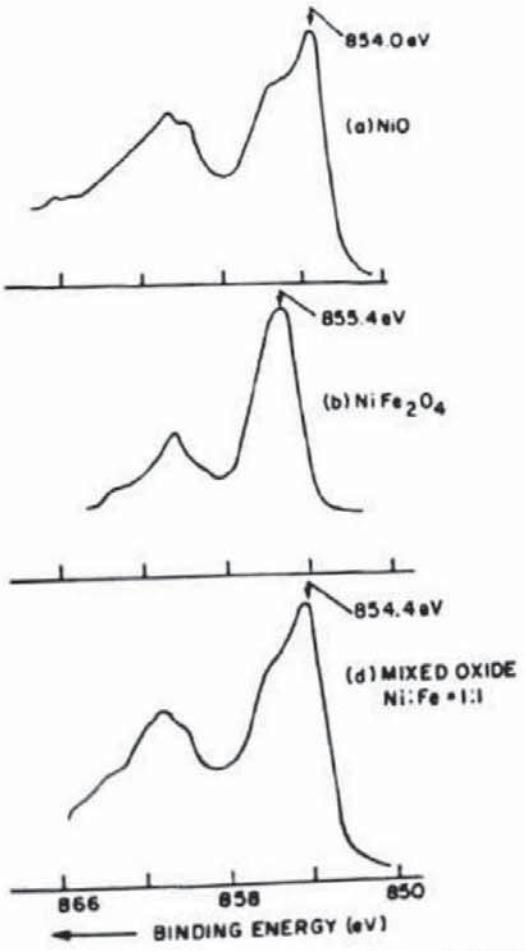

Figure 10.7 Photo-electron spectra of some simple and mixed nickel oxides. Ni $2p_{3/2}$ spectra are shown for (a) NiO; (b) $NiFe_2O_4$; (c) mixed iron–nickel oxide (Ni/Fe ratio = 1)

Figures 10.7(a) and (b) the Ni $2p_{3/2}$ peak maxima for NiO and the spinel $NiFe_2O_4$ are separated by 1.5 eV. In addition the NiO main peak is clearly split, while the peak for $NiFe_2O_4$ is not.

10.2.7.9 Copper

Copper has been one of the elements most extensively studied by XPS. Interpretation of oxide spectral structure is probably more straightforward for copper than for other transition metals. However, the oxides appear to transform more readily on heating or irradiation.

Two stable oxides of copper, Cu_2O and CuO, are found in solid-state films using XPS.[59] In addition, a cupric hydroxide has been characterized by XPS.[37]

All three compounds are likely surface products of the corrosion of copper metal, and their chemical differentiation from the metallic substrate is thus important. In the case of cuprous oxide, photo-electron spectra are identical to those for copper metal, within ± 0.1 eV. However, as initially described by Schoen,[60] the X-ray induced Auger spectra of copper metal and cuprous oxide (Cu $L_3M_{4,5}M_{4,5}$) are significantly different and allow a quantitative characterization[24] of oxide or metal. If contributions from the higher valence oxides are absent, the relative contributions of Cu_2O and metallic copper to the spectrum can be determined by ratioing peak intensities at two different energies. Copper $L_3M_{4,5}M_{4,5}$ Auger spectra of CuO and $Cu(OH)_2$ are both shifted to different kinetic energies, compared to Cu_2O. However, these peaks are broad and are somewhat more difficult to characterize because of the large number of discrete Auger lines under the envelope.

Characterization of CuO and $Cu(OH)_2$ is normally accomplished using the Cu $2p_{3/3}$ line. The principal Cu $2p_{3/2}$ peak maximum for CuO is shifted 1.3 ± 0.2 eV above that for Cu_2O, but this maximum is rather poorly defined with respect to the Cu_2O peak, because of significant broadening, probably associated with multiplet splitting. The Cu $2p_{3/2}$ peak for $Cu(OH)_2$ is shifted 2.5 ± 0.15 eV above that for Cu_2O. Cupric compounds are also characterized, in general, by the two strong shake-up peaks located 6 and 8 eV above the principal Cu $2p_{3/2}$ line.[37] The only difference noted between the shake-up spectra of CuO and $Cu(OH)_2$ is a change in the relative intensities of the two peaks under the shake-up envelope.

10.2.7.10 Molybdenum

The corrosion behaviour of molybdenum, as a component in many stainless steels, has been studied using XPS. Unlike the first-row transition elements, the spectral changes with oxidation state of second-row elements like molybdenum are more predictable and are not accompanied by satellite structure. Thus Mo^{IV} and Mo^{VI} oxides have been clearly characterized by chemical shifts

of the Mo 3*d* line.[58] A chemical shift of ~0.8 eV is also noted between the Mo 3*d* line position for MoO_3 and $CoMoO_4$.

10.3 Review of XPS and AES Applications in Corrosion Science

The following section reviews the contributions XPS and AES to corrosion problems on a material-by-material basis. Studies not covered are those involving surface reactions of semi-conductor materials and reactions felt to be more related to metallurgy than corrosion. Surface reactions involving oxygen, water or other elements are considered, although many of the fundamental studies of surface reactions on metals are not considered if they do not appear to have a direct bearing on corrosion processes.

10.3.1 Light metals

Beryllium oxidation has been studied using AES by Zehner, Barbulesco and Jenkins[61] and the surface segregation of trace silicon has been detected using the energy loss peak below the Be *KLL* line. Anodic oxidation of single-crystal aluminium, studied using AES, has been found to result in stoichiometric Al_2O_3 layers.[62]

By contrast, XPS studies of naturally passivated aluminium foils have identified a number of hydroxides, as well as Al_2O_3.[63] Aluminium films formed on anodization in sulphuric acid have been shown by XPS to contain sulphate and sulphide ion,[64] as well as Al_2O_3. Scanning Auger microprobe studies combined with tensile stress tests on aluminium–zinc–magnesium alloys showed that the average grain boundary concentration of zinc, copper and magnesium could be indirectly correlated with the stress corrosion plateau crack velocity.[65]

10.3.2 First-row metals and their alloys

Almost all of the present surface literature is devoted to the study of alloys involving chromium, iron, cobalt, nickel and copper. These are described in the following sections.

10.3.2.1 Chromium

XPS and AES studies of the solid-state oxidation of chromium metal have been described by Conner.[66] The stability of chromate protective coatings on other metals has been the subject of several XPS investigations[67,68] which monitored, in particular, the oxidation state of chromium. The nature of passivation films on chromium surfaces in neutral and acidic solutions has been studied by AES[69]

10.3.2.2 *Iron and low alloy steels*

The air oxidation of pure iron has been studied by several authors using XPS and AES.[70,71] Several electrochemical surface investigations have been made of the aqueous corrosion of pure iron in a borate buffer.[57,72,73] The consistent presence of boron in the outer portion of the passive film suggests that the inner portion of the oxide results from metal oxidation, while the outer portion results from precipitation of ferrous iron.[57] Depth profile evidence for two different oxide structures based on O/M ratios still requires confirmation that iron oxides are not being reduced by the ion beam. Other solution inhibitors such as CrO_4^{2-}, MoO_4^{2-} and $As_2O_3^{2-}$ were found to be incorporated into passive films to a greater extent than was boron.[74] The effect of chloride ion in penetrating iron oxide passive films is well known. To date, however, no chloride incorporation into the film can be detected by AES[75] or XPS.[76] Recent work[76] has suggested that hydrocarbon content of the iron oxide surface increases with increased chloride exposure; this is attributed to the loss of hydroxyl and bound water groups from the surface during depassivation. In addition, chloride attack was believed to result in an increased surface area of the oxide, as evidenced by the high O 1*s* binding energy (increased physisorbed gas).

The incorporation of iodide into a strained mild steel film has been followed as a function of polarization potential.[77] The measurement of iodine content of the film changes with potential (see Figure 10.8). The film is no longer stable to stress corrosion when iodine is not present.

An AES study of iron corrosion in nitrate solutions shows that the observed intergranular corrosion may be the result of non-passivation of the carbide phase in this solution.[78]

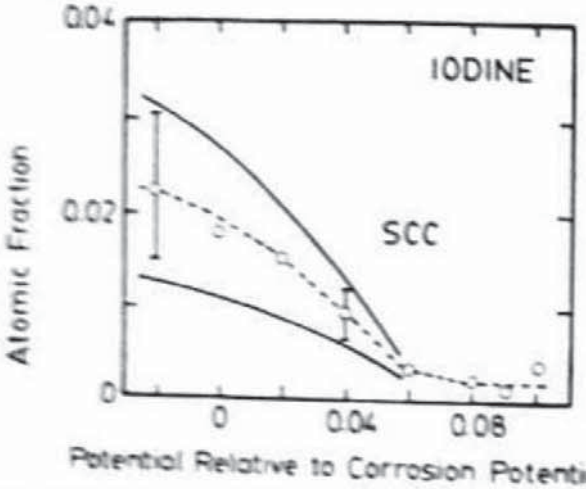

Figure 10.8 Relationship between iodine surface concentration and onset of passivity on an iron surface. (Reproduced by permission of K. Asami, N. Totsuka and M. Takano[77])

10.3.2.3 Binary iron alloys and stainless steels

Gas phase oxidation of iron–chromium alloys and stainless steels has been extensively investigated by AES and XPS.[79,88] For most temperatures studied, a thin chromium oxide layer is observed to form initially, followed by an overlying iron oxide layer. Baer[87] has carried out oxidations of 304 stainless steel at 800 °C using a range of oxygen partial pressures. With the use of scanning Auger microscopy, he showed that lower partial pressures favoured the initial growth of a pure chromium oxide, evenly distributed over the alloy grain surface. At high pressures the chromium oxide was concentrated near boundaries and a mixed oxide was found over the grain itself. In another study[88] the composition of the film formed on the grain surface of an Fe–26Cr alloy was analysed by AES and other methods following oxidation at 10^{-3} torr O_2 and 600 °C. After a few seconds of oxidation time, a duplex film was formed, the outer layer being identified as α–Fe_2O_3 on the basis of the O/Fe AES intensity ratio.[88] An underlying layer of α–Cr_2O_3 was identified, partly with the aid of AES, and the metal alloy substrate adjacent to this layer was shown to be depleted in chromium. Such information will assist efforts to grow protective films on alloys as part of their pre-treatment before service.[89]

The passivation of stainless steels during aqueous corrosion and the composition of its passive films have been one of the most studied subjects in corrosion science. Both AES and XPS studies have shown that the chromium concentration of the surface layer on Fe–Cr steels rises as the passivating potential is approached.[5, 8, 30, 89–93] The chromium enrichment is believed to result from a selective dissolution of iron from the oxide; in some cases, iron is also found to be depleted in the metal as well.[91] Castle and Clayton[5] and Asami, Hashimoto and Shimodaira[91] have examined the nature of the passive film in great detail. Castle and Clayton determined a duplex layer: the inner layer rich in chromium, the outer layer containing much hydroxide or bound water, held together with organic molecules. Asami, Hashimoto and Shimodaira found that both hydroxide and bound water reach a maximum in the film at the passivation potential, forming a hydrated chromium oxyhydroxide (see Figure 10.9).

The addition of molybdenum to stainless steels improves corrosion resistance, particularly from pitting attack. XPS studies[9, 94, 95] have helped to identify the role of molybdenum. It is proposed that hexavalent molybdenum reacts with active sites on a dissolving surface, where the oxyhydroxide cannot form. This leads to a decrease in activity at these sites and formation of a more uniform passive layer[9] (see Figure 10.9). A similar mechanism is proposed for the passivation of iron–molybdenum alloys. Two XPS studies[54,96] have shown that the major portion of passive oxide is an iron oxyhydroxide; only the active regions (i.e. pits) were found to contain molybdenum. In one

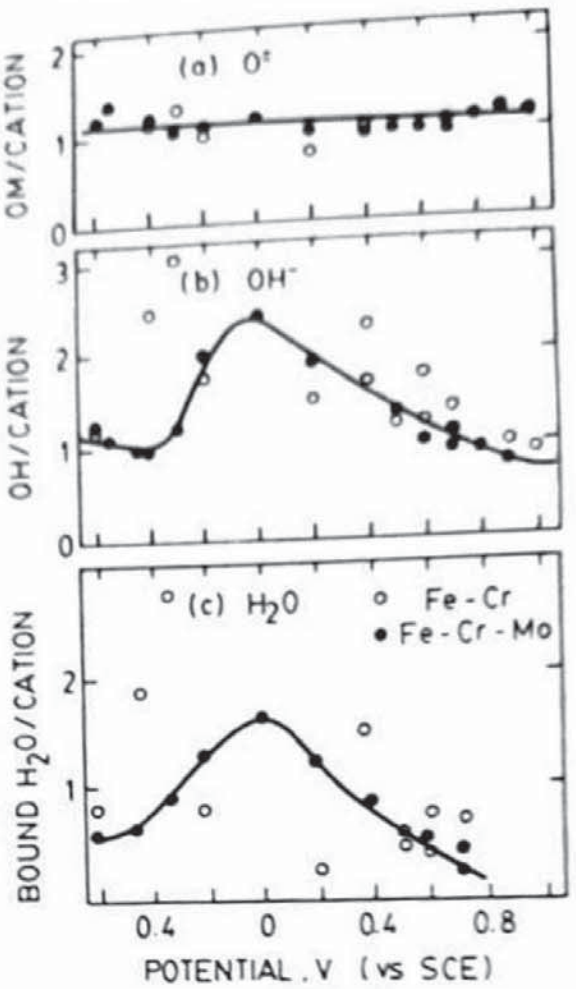

Figure 10.9 Surface concentrations of O^{2-}, OH^- and bound H_2O on steel surfaces measured as a function of polarization potential in 1 *M* HCl. For both Fe–30%Cr and Fe–30%Cr–2%Mo alloys the onset of passivation begins about −0.2 eV(VS SCE). The results here for Fe–30%Cr can be compared with the cation concentrations for the same alloy shown in Figure 10.1(a). Note that the better reproducibility of the analytical data for the iron–chromium–molybdenum alloy may be related to a more uniform passive layer. (After Asami, Hashimoto and Shimodaira[94])

of these studies[94] the molybdenum was identified as $FeMoO_4$. Another study of a molybdenum stainless steel, corroded in Ringers' solution, did not detect any significant molybdenum in the passive film.[97]

Reactions of Fe–Cr alloys with chloride solution have been studied and identification of surface chloride has been easier than for iron. Saniman[98] used XPS to measure the effect of solution chloride concentration on the surface uptake. Analysis of the film concentration and thickness showed that chloride intake resulted from exchange, not incorporation. Oxide film resistance to stainless steel crevice corrosion in chloride solution has also been studied.[99]

Anodic films formed on iron–nickel binary alloys have been compared with films on iron–nickel alloys also containing molybdenum and boron or phosphorus and boron.[100] This latter alloy had oxidized boron and phosphorus in the passive film. Using AES peak shapes, the phosphorus was identified

tentatively as a phosphite; this form was believed responsible for reducing the nickel potential and hence its lower dissolution rate. Another AES–XPS study of the native oxide films on Fe–Ni–Cr–P–B alloys showed that boron and phosphorus are, in fact, enriched within the passive film, with most phosphorus distributed in a layer behind a chromium oxide enriched layer.[101]

AES studies of intergranular corrosion in 304 stainless steel[102] have revealed that many grain boundary inpurities play a role in increasing its susceptibility to attack. For example, sulphur in non-sensitized steels promotes intergranular corrosion in nitrate–dichromate solutions. However, chromium depletion at the grain boundary has been demonstrated by AES for specimens corroded in H_2SO_4–$CuSO_4$ solutions.

10.3.2.4 Cobalt and its alloys

An XPS study of the oxidation of cobalt in moist air[18] showed that $Co(OH)_2$ is an initial reaction product on the metal surface. The anodic oxidation of pure cobalt has been studied by AES and the passive film has been characterized.[103]

The corrosion of cobalt–chromium alloys in neutral or acidic solutions was found to proceed by selective dissolution of the cobalt.[67] McIntyre, Murphy and Zetaruk, using XPS, also showed that cobalt dissolves preferentially from a cobalt–chromium–tungsten alloy in alkaline solution at 300 °C. Gas phase oxidations done concurrently show that a cobalt-rich layer (Co_3O_4) forms in air; such outward migration of cobalt will enhance the preferential dissolution in the aqueous phase.

10.3.2.5 Nickel and its alloys

The oxidation of polycrystalline nickel has been followed by AES.[104–106] Müller *et al.*[106] have been able to identify the formation of NiO 'islands' early in the oxidation process.

Several investigations of Ni–Fe alloys have been reported, including AES analysis of oxidized permalloy surfaces (80%Ni–20%Fe)[107] and XPS analysis of Ni–20% Fe alloy oxidized at 500 °C.[108] An iron-rich oxide formed early on an annealed surface eventually gives way to a $NiFe_2O_4$ spinel.

Smith and Schmidt[109] have studied the oxidation of Ni–20%Cr alloy at 800 °C. A duplex Cr_2O_3–NiO was formed, except near grain boundary intersections. Similar XPS results were found for the short-term gas phase oxidation of Alloy 600 at 500 °C,[6] except that iron, a minor constituent in the bulk alloy, was found concentrated in the outermost layers of the oxide film. Oxygen partial pressure was shown to affect the nickel oxide content of the film.

A number of nickel-rich superalloy surfaces, oxidized near 1000 °C, have

been analysed by XPS.[110] The surfaces were enriched in TiO_2, a minor constituent of all the alloys tested. High temperature reaction with Na_2SO_4 results in oxidation of most of the surface chromium to Cr^{VI}, apparently leading to accelerated corrosion.

XPS has been used to monitor the oxidation of a nickel electrode in contact with a solid electrolyte[27] in acid[111–113] and neutral[113] solutions and in liquid hydrogen fluoride.[114] Two XPS studies of the nickel electrode in acidic solution[111,112] show the passive film to be a NiO underlayer and $Ni(OH)_2$ on the surface. AES was used to measure the thickness of a NiO film during dissolution of nickel under transpassive conditions[115] but no information on film stoichiometry was forthcoming. MacDougall, Mitchell and Graham[113] analysed passive anodic films on polycrystalline nickel. Using AES to image the surface oxygen distribution, they showed that the passive film is one-third thinner on some grains than on others. Depth profiles of the film show a long interface between oxide and metal; the authors interpret this as evidence of a film high in defects which are important to the passivation process.

Anodic oxidation of Ni–25%Fe alloy in acidic solution[116] was shown by XPS to result in a passive film of NiO at the metal interface and nickel and iron hydroxides near the outer surface. By contrast, the duplex passive films found on Ni–Mo[117] and Hastalloy[31] had mixed nickel–molybdenum oxides in the inner film and only nickel oxide or hydroxide on the outer surface.

The surface films formed on Alloy 600 and Alloy 800 in NaOH have been measured by Hashimoto and Asami[118] using XPS. Primary passivation was ascribed to the formula of the chromium oxyhydroxide film and a secondary passive film was $Ni(OH)_2$. McIntyre, Zetaruk and Owen[119] analysed Alloy 600 surfaces following exposure to pressurized water reactor conditions and identified chromium oxyhydroxide under normal reducing conditions. Solution oxidizing conditions were varied to show a thick nickel-rich hydroxide film under highly oxidizing conditions and mixed chromium–nickel hydroxides under intermediate conditions. Passive films on Alloys 600 and 800 were depth-profiled using AES,[13] and the relative thermodynamic surface excess of chromium was found to decrease with increasing pH.

The aqueous corrosion of Ni–Cu alloy (66% Ni) under boiler conditions has been investigated by XPS,[120] and $Ni(OH)_2$ was shown to be the major surface species under active attack near 300 °C. Under reducing conditions, little or no surface oxide is found, in accordance with thermodynamic predictions.

10.3.2.6 Copper and its alloys

Copper and its oxidation have been studied using XPS and AES for almost ten years.[36,121] Oxidation of a 70–30 Cu–Ni alloy results in a NiO-rich surface film, as deduced by XPS[122]

Anodic oxidation of copper metal in weakly alkaline or acidic solution was

found by XPS to result in a duplex film of Cu_2O adjacent to the metal and a surface layer of $Cu(OH)_2$.[123] Recent XPS work of Shoesmith and coworkers has followed the growth of a similar layer in potassium hydroxide during the initial stages of formation.[24] The formation of films on copper–nickel alloys in saline solutions has been followed by XPS[124] and AES.[125] Duplex films were found in the latter work, which consisted of a mixed copper–nickel oxide over a thicker nickel-rich oxide. Oxidation of Cu–2%Be in ammoniacal solution results in a beryllium-rich surface layer.[126]

The chemistry of aluminium–brass condensor tube surfaces (copper 76%, zinc 22%, aluminium 2%) in seawater has been analysed by Castle, Epler and Peplow[127] using XPS. A layer high in magnesium and aluminium concentration is detected on the tubes and it is proposed that the magnesium from the seawater precipitates either by itself or in combination with aluminium from the alloy. In laboratory tests,[128] $Mg(OH)_2$ precipitation on aluminium brass was analysed by XPS as a function of pH. A higher pH at the interface compared with that in the bulk solution is required to rationalize the thickness of $Mg(OH)_2$ measured by XPS.

The surface analysis of organic protective films on copper has been carried out by several groups. The reaction of copper with benzotriazole has been studied by XPS[129,130] and its reaction with a cuprous oxide surface confirmed. The destructive oxidation of the cuprous benzotriazole to the cupric form has been monitored.[131] Mercaptobenzotriazole reactions with copper(I) surfaces to inhibit corrosion have also been investigated by XPS.[132]

10.3.3 Heavy metals

Corrosion-related surface analyses of elements heavier than those in the first row are much less extensive. Indeed, it is difficult to provide a coherent summary of studies of these elements because of the small number of results yet available.

Molybdenum electrochemistry and the oxidation of *molybdenum* have been studied by XPS by Ansell *et al.*[26] using a special inert atmosphere chamber. The cathodic decomposition of *niobium* oxide was shown by XPS to be a hydrated oxide of lower oxidation state.[133] The native oxides on the rare earth-like elements *cerium, ytterium* and *lanthanum* were determined by XPS[134] and *gadolinium* by AES.[135]

A number of studies of *tin* oxidation and corrosion have been reported. Ansell *et al.*[136] studied the electrochemical oxidation of tin in alkaline solution using XPS. In the passive region the surface oxide is determined to be Sn^{IV} rather than Sn^{II}, which grows initially. Investigations of the solid-state oxidation of tin by XPS have also been reported.[137] The passive film on a Sn–Ni alloy surface has been analysed also by XPS.[138] Servais *et al.*[139] examined chromium passivation films (tinplate) on tin surfaces and determined that lack of adhesion of such a film was caused by the growth of tin oxide.

Indium–gold and indium–lead–gold alloys were analysed for surface oxides by XPS.[140] The anodic oxidation of *gold*[141] in sulphuric acid was shown to produce Au_2O_3 as a surface film. *Lead* oxidation has been studied by XPS[142] and the electrochemical oxidation of *uranium oxide* has recently been characterized by Sunder *et al.*,[143] also using XPS.

10.3.4 Organic coatings

Organic protective coatings, applied to metal surfaces, are intended to provide a barrier between any invading species and the metal surface. Moreover, if penetration of the coating does occur, any corrosive attack will be limited to that immediate region and will not spread laterally, as on an uncoated surface. The loss of adhesion of such coatings on iron and steel surfaces has been studied using XPS.

Steel surfaces coated with epoxy-esters,[144] epoxy-urethane and epoxy-amines[145] have been corroded to de-adhesion in saline solutions. Each side of the film rupture was examined by XPS and subsequently the effects of additional chemical tests on the surface were monitored by XPS. Both organic and substrate sides of the rupture showed evidence of having undergone surface saponification to form sodium carboxylate groups. This is believed to result from corrosion-induced hydroxyl groups.

A highly sensitive method of detection of carboxylate groups involved their 'tagging' with silver—an ion with high selectivity for a carboxy group and a high XPS cross-section. Using this method a carboxylate surface concentration of about one per cent. can be detected (see also Chapter 9).

The effect of using a 'conversion' coating between the steel and the organic layer has been examined. The de-adhesion surfaces showed that the conversion coating, a zinc phosphate, remained adhered to the metal substrate, and showed evidence of some residual organics. Thus, de-adhesion takes place near the interface, but in the organic phase.

Hammond *et al.*[146] have analysed C 1*s*, N 1*s* and O 1*s* spectra of interfacial surfaces containing a number of organic coatings. They have detailed binding energy and intensity ratio data for several carboxylic anions and simple polymers.

The effects of mechanical and chemical de-adhesion of polybutadiene films have been compared by XPS.[147] Mechanical de-adhesion was shown to result from cohesive failure. As in earlier studies, chemical de-adhesion appears to result from ester hydrolysis at the metal interface.

10.4 Conclusion

It is clear that XPS and AES are beginning to be extremely effective in assessing the composition and chemistry of corrosion films. Of particular note

is the degree to which both techniques have become truly quantitative over the past few years—not only in terms of elemental composition but also often in terms of the chemical entities present. Also, there is increasing evidence that even fragile structures, e.g. hydrates, can be preserved in the spectrometer vacuum. These two steps have made possible important discoveries about the nature of the passive film.

Significant quantities of data are beginning to accumulate in the subject area of iron–chromium–nickel corrosion. Thus, in some cases, corroborative evidence has been obtained from different types of experiments. This is the mark of a maturing field!

Electrochemical experiments have been particularly important since these allow corrosion conditions to be altered drastically within a convenient time frame. Many situations cannot be simulated in a cell; it is expected that surface analytical data can tie the result obtained in an electrochemical experiment with that obtained during 'open-circuit' corrosion, thus making corrosion in the electrochemical cell more relevant to corrosion in the field.

From this writer's viewpoint, there is a somewhat larger amount of data now coming from XPS than AES. This is related to the more benign excitation conditions and the better present-day knowledge of chemical shifts. Corrosion, however, is very much a microscopic process and the emphasis must again return to a microscopic surface technique such as AES, when XPS studies of a particular system have been exhausted. For this reason, attempts to understand AES electron beam effects are believed to be potentially important, as are Auger chemical shift studies. Microscopic surface studies will be particularly important for understanding the effects of organic and inorganic inhibition layers, as well as crevice and pitting corrosion.

It is hoped that the progress demonstrated by the usage of AES and XPS over the last five years will lead to the deserved inclusion of these techniques in a much larger number of future corrosion experiments.

Acknowledgement

The writer acknowledges the expert assistance of Miss T. Chan in preparing this manuscript.

References

1. A. Joshi, Investigation of passivity, corrosion and stress corrosion cracking phenomena by AES and ESCA, in *Corrosion 77*, Paper 16, National Association of Corrosion Engineers, Houston, Texas (1977).
2. J. E. Castle, *Surf. Sci.*, **68**, 583 (1977).
3. J. E. Castle, Application of XPS analysis to research into the causes of corrosion, in *Applied Surface Analysis*, (Eds T. L. Barr and L. E. Davis), ASTM STP 699, p. 182, American Society for Testing and Materials, Philadelphia, Pennsylvania (1980).

4. M. P. Seah and W. A. Dench, *Surf. Interfacial Anal.*, **1**, 2 (1979).
5. J. E. Castle and C. R. Clayton, *Corrosion Sci.*, **17**, 7 (1977).
6. N. S.McIntyre, D. G. Owen and D. C. Zetaruk, *Appl. Surf. Sci.*, **2**, 55 (1978).
7. K. Asami, K. Hashimoto and S. Shimodaira, *J. Jpn Inst. Metals*, **40**, 438 (1976).
8. K. Asami, K. Hashimoto and S. Shimodaira, *Corrosion Sci.*, **17**, 713 (1977).
9. K. Hashimoto, K. Asami and K. Teramoto, *Corrosion Sci.*, **19**, 3 (1979).
10. K. Asami and K. Hashimoto, *Corrosion Sci.*, **17**, 559 (1977).
11. K. Hashimoto, M. Naka, K. Asami and T. Masamoto, *Corrosion Sci.*, **19**, 165 (1979).
12. F. Pons, J. Le Hérícy and J. P. Longeron, *Surf. Sci.*, **69**, 547 (1977); **69**, 565 (1977).
13. M. Seo and N. Sato, *Corrosion*, **36**, 334 (1980).
14. D. F. Mitchell, *Appl. Surf. Sci.*, **9**, 131 (1981).
15. N. S. McIntyre, Applications of surface analysis in the nuclear industry, in *Industrial Applications of Surface Analysis* (Eds C. J. Powell and L. Casper), ACS Symposium Series No. 99, p. 345, American Chemical Society, Washington, DC (1982).
16. D. R. Baer, *Appl. Surf. Sci.*, **7**, 69 (1981).
17. K. S. Kim, W. E. Baitinger, J. W. Amy and N. Winograd, *J. Elect. Spectrosc.*, **5**, 351 (1975).
18. T. J. Chuang, C. R. Brundle and K. Wandelt, *Thin Solid Films*, **53**, 19 (1978).
19. N. S. McIntyre and D. G. Zetaruk, *Anal. Chem.*, **49**, 1521 (1977).
20. D. F. Mitchell, G. I Sproule and M. J. Graham, *J. Vac. Sci. Technol.*, **18**, 690 (1981).
21. N. S. McIntyre, E. V. Murphy and D. G. Zetaruk, *Surf. Interfacial Anal.*, **2**, 151 (1979).
22. J. M. Walls, D. D. Hall and D. E. Sykes, *Surf. Interfacial Anal.*, **1**, 204 (1979).
23. C. J. Schmidt, P. V. Lenzo and E. G. Spencer, *J. Appl. Phys.*, **46**, 4080 (1975).
24. N. S. McIntyre, S. Sunder, D. W. Shoesmith and F. W. Stanchell, *J. Vac. Sci. Technol.*, **18**, 714 (1981).
25. R. W. Revie, B. G. Baker and J. L'M. Bockris, *Surf. Sci.*, **52**, 664 (1975).
26. R. O. Ansell, T. Dickinson, A. R. Povey and P. M. A. Sherwood, *J. Electroanal. Chem.*, **98**, 69 (1979).
27. C. Y. Yang and W. E. O'Grady, *J. Vac. Sci. Technol.*, **20**, 925 (1982).
28. K. Kudo, F. Shibata, G,. Okamoto and N. Sato, *Corrosion Sci.*, **18**, 809 (1978).
29. J. E. Castle, *Proc. of the Conference on Metal Coatings*, p. 435, Lehigh University (1978).
30. G. Okamoto, *Corrosion Sci.*, **13**, 471 (1973).
31. G. T. Burstein, *Materials Science and Engineering*, **42**, 207 (1980).
32. Z. Szklarska-Smialowska, H. Viefhaus and M. Hanik-Czachor, *Corrosion Sci.*, **16**, 649 (1976).
33. T. Smith, *Surf. Sci.*, **55**, 601 (1976).
34. C. D. Wagner, W. M. Riggs, L. E. Davis, J. F. Moulder and G. E. Muilenberg, *Handbook of X-ray Photoelectron Spectroscopy*, Physical Electronics Division, Perkin-Elmer Corporation, Eden Prairie, Minnesota (1979).
35. O. Johnson, *Chem. Scripta*, **8**, 162 (1975).
36. G. Schoen, *J. Electron. Spectrosc.*, **1**, 377 (1972).
37. N. S. McIntyre and M. G. Cook, *Anal. Chem.*, **47**, 2208 (1975).
38. P. R. Norton, *J. Catalysis*, **36**, 211 (1975).
39. T. Matsushima, D. B. Almy and J. M. White, *Surf. Sci.*, **67**, 89 (1977).
40. L. Ramqvist, K. Hamrin, G. Johansson, A. Fahlmann and C. Nordling, *J. Phys. Chem. Solids*, **30**, 1835 (1969).

J. F. Franzen, M. X. Umana, J. R. McCreary and R. J. Thorn, *J. Solid State Chem.*, **18**, 363 (1976).
J. S. Solomon and W. L. Baun, *Surf. Sci.*, **51**, 228 (1975).
M. L. Knotek and J. Houston, *Phys. Rev.*, **B15**, 4580 (1977).
G. A. Sawatsky and D. Post, *Phys. Rev.*, **B20**, 1546 (1979).
L. Fiermans and J. Vennik, *Surf. Sci.*, **35**, 42 (1973).
F. J. Szalkowski and G. A. Somorjai, *J. Chem. Phys.*, **61**, 2064 (1974).
G. C. Allen, M. T. Curtis, A. J. Hooper and P. M. Tucker, *J. Chem. Soc. Dalton*, **1973**, 1675 (1973).
G. C. Allen and P. M. Tucker, *Inorg. Chim. Acta*, **16**, 41 (1976).
I. Ikemoto, K. Ishii, S. Kinoshita, H. Kuroda, M. A. A. Franco and J. M. Thomas, *J. Solid State Chem.*, **17**, 425 (1976).
M. Oku, K. Hirokawa and S. Ikeda, *J. Electron Spectrosc.*, **7**, 465 (1975).
A. Aoki, *Jpn J. Appl. Phys.*, **15**, 305 (1976).
G. C. Allen, M. T. Curtis, A. J. Hooper and P. M. Tucker, *J. Chem. Soc. Dalton*, **1976**, 1526 (1976).
C. R. Brundle, T. J. Chuang and K. Wandelt, *Surf. Sci.*, **68**, 459 (1977).
D. A. Stout, J. B. Lumsden and R. W. Staehle, *Corrosion*, **35**, 141 (1979).
H. Binder, *Z. fur Naturforsch.*, **B28**, 256 (1973).
S. Ekelund and C. Leygraf, *Surf. Sci.*, **40**, 179 (1973).
M. Seo, M. Sato, J. B. Lumsden and R. W. Staehle, *Corrosion Sci.*, **17**, 209 (1977).
T. A. Patterson, J. C. Carver, D. E. Leyden and D. M. Hercules, *J. Phys. Chem.*, **80**, 1702 (1976).
S. W. Gaarenstroom and N. Winograd, *J. Chem. Phys.*, **67**, 3500 (1977).
G. Schoen, *J. Electron Spectrosc.*, **7**, 377 (1972).
D. M. Zehner, M. Barbulesco and L. H. Jenkins, *Surf. Sci.*, **34**, 385 (1973).
S. Matsuzawa, N. Baba and S. Tajima, *Electrochim, Acta*, **24**, 1199 (1979).
T. L. Barr, *J. Vac. Sci. Technol.*, **14**, 660 (1977).
J. A. Treverton and N. C. Davies, *Electrochim. Acta*, **25**, 1571 (1980).
C. R. Shastry, M. Levy and A. Joshi, *Corrosion Sci.*, **21**, 673 ()1981).
G. R. Conner, *J. Vac. Sci. Technol.*, **15**, 343 (1978).
S. Storp and R. Holm, *Surf. Sci.*, **10**, 68 (1977).
D. R. Baer, Use of surface analytical techniques to examine metal corrosion problems, in *ACS Symposium Series, Industrial Application of Surface Analysis*, American Chemical Society, Washington, DC (1982).
M. Seo, R. Saito and N. Sato, *J. Electrochem. Soc.*, **127**, 1909 (1980).
C. R. Brundle, *Surf. Sci.*, **66**, 581 (1977).
J. K. Gramzewski, B. D. Padalia, S. Affrossman, L. M. Watson and D. J. Fabian, *Surf. Sci.*, **62**, 386 (1977).l
R. W. Revie, B. G. Baker and J. O'M. Bokris, *J. Electrochem. Soc.*, **122**, 1460 (1975).
D. H. Davies and G. T. Burstein, *Corrosion*, **36**, 416 (1980).
J. B. Lumsden, Z. Szklorska-Smialowska and R. W. Staehle, *Corrosion*, **34**, 169 (1977).
M. da Cunha Belo, B. Rondot, F. Pons and J. P. Lanyeron, *J. Electrochem. Soc.*, **124**, 1317 (1977).
D. L. Cocke, P. Nilsson, O. J. Murphy and J. O'M. Bokris, *Surf. Interfacial Anal.*, **4**, 94 (1982).
K. Asami, N. Totsuka and M. Takano, *Corrosion*, **35**, 208 (1979).
G. Tauber and H. J. Grabke, *Corrosion Sci.*, **19**, 793 (1979).
C. Leygraf, G. Hultqvist and S. Ekelund, *Surf. Sci.*, **51**, 409 (1975).

80. J. P. Coad and J. G. Cunningham, *J. Electron Spectrosc.*, **3,** 435 (1974).
81. G. Betz, G. K. Wehner, I. Toth and A. Joshi, *J. Appl. Phys.*, **45,** 5312 (1974).
82. I. Olefjord, *Corrosion Sci.*, **15,** 687 (1975).
83. C. Leygraf and G. Hultqvist, *Surf. Sci.*, **61,** 69 (1976).
84. R. K. Wild, *Corrosion Sci.*, **17,** 87 (1977).
85. T. Smith and I. W. Crane, *Oxid. Met.*, **10,** 135 (1976).
86. T. J. Driscoll and P. B. Needham, *Oxid. Met.*, **13,** 283 (1979).
87. D. R. Baer, *Appl. Surf. Sci.*, **7,** 69 (1981).
88. C. P. Jensen, D. F. Mitchell and M. J. Graham, *Corrosion Sci.* (in press).
89. B. Chattopodhyay and G. C. Wood, *J. Electrochem. Soc.*, **117,** 1163 (1970).
90. I. Olefjord and H. Fischmeister, *Corrosion Sci.*, **15,** 697 (1975).
91. K. Asami, K. Hashimoto and S. Shimodaira, *Corrosion Sci.*, **16,** 387 (1976).
92. K. Asami, K. Hashimoto and S. Shimodaira, *Corrosion Scie.*, **18,** 125 (1978).
93. C. Leygraf, G. Hultqvist, I. Olefjord, B. O. Elfström, V. M. Knyazheva, A. V. Plaskeyev and Y. M. Kolotyrkin, *Corrosion Sci.*, **19,** 343 (1979).
94. K. Sugimoto and Y. Sawada, *Corrosion*, **32,** 347 (1976).
95. K. Hashimoto and K. Asami, *Corrosion Sci.*, **19,** 251 (1979).
96. K. Hashimoto, M. Naka, K. Asami and T. Masumoto, *Corrosion Sci.*, **19,** 165 (1979).
97. J. R. Cahoon and R. Bandy, *Corrosion*, **38,** 299 (1982).
98. E. Saniman, MSc Thesis, University of Surrey, Guildford, Surrey (1977).
99. G. Hultqvist and C. Leygraf, *J. Vac. Sci. Technol.*, **17,** 85 (1980).
100. G. T. Burstein, *Corrosion*, **37,** 549 (1981).
101. D. R. Baer, D. A. Petersen, L. R. Pederson and M. T. Thomas, *J. Vac. Sci. Technol.*, **20,** 957 (1982).
102. A. Joshi and D. F. Stein, *Corrosion*, **28,** 321 (1972).
103. D. H. Davies and G. T. Burstein, *Corrosion Sci.*, **20,** 989 (1980).
104. S. H. Kulpa and R. P. Frankenthal, *J. Electrochem. Soc.*, **124,** 1588 (1977).
105. S. P. Sharma, *J. Electrochem. Soc.*, **125,** 2005 (1978).
106. K.-H. Müller, P. Beckmann, M. Schemmer and A. Benninghoven, *Surf. Sci.*, **80,** 325 (1979).
107. W. Y. Lee and J. J. Eldridge, *J. Electrochem. Soc.*, **124,** 1747 (1977).
108. I. Olefjord and P. Marcus, *Surf. Interfacial Anal.*, **4,** 23 (1982).
109. K. L. Smith and L. D. Schmidt, *J. Vac. Sci. Technol.*, **20,** 364 (1982).
110. S. R. Smith, W. J. Carter, G. D. Mateescu, F. J. Kohl, G. C. Fryburg and C. A. Stearns, *Oxidation of Metals*, **14,** 415 (1980).
111. T. Dickenson, A. F. Povey and P. M. A. Sherwood, *J. Chem. Soc., Faraday Trans. I*, **73,** 327 (1977).
112. P. Marcus, J. Oudar and I. Olefjord, *J. Microsc. Spectrosc. Electron*, **4,** 63 (1979).
113. B. MacDougall, D. F. Mitchell and M. J. Graham, *Corrosion*, **38,** 85 (1982).
114. N. Watanabe and M. Haruta, *Electrochim. Acta*, **25,** 461 (1980).
115. M. Datta, H. J. Mathieu and D. Landolt, *Electrochim. Acta*, **24,** 843 (1979).
116. I. Olefjord and P. Marcus, *Surf. Interfacial Anal.*, **4,** 29 (1982).
117. G. T. Burstein and T. P. Hoar, *Corrosion Sci.*, **17,** 939 (1977).
118. K. Hashimoto and K. Asami, *Corrosion Sci.*, **19,** 427 (1979).
119. N. S. McIntyre, D. G. Zetaruk and D. Owen, *J. Electrochem. Soc.*, **126,** 750 (1979).
120. N. S. McIntyre, T. E. Rummery, M. G. Cook and D. Owen, *J. Electrochem. Soc.*, **123,** 1164 (1976).
121. T. Robert, M. Bartel and G. Offergeld, *Surf. Sci.*, **33,** 128 (1972).
122. J. E. Castle, *Nature Physical Sciences*, **234,** 93 (1971).

123. H.-H. Strehblow and B. Titze, *Electrochim. Acta*, **25**, 839 (1980).
124. L. D. Hulett, A. L. Bacarella, L. LiDonnici and J. C. Griess, *J. Electron Spectrosc.*, **1**, 169 (1972).
125. G. E. McGuire, A. L. Bacarella, J. C. Griess, R. E. Clausing and L. D. Hulett, *J. Electrochem. Soc.*, **125**, 1801 (1978).
126. R. C. Newman and G. T. Brustein, *Corrosion Sci.*, **20**, 375 (1980).
127. J. E. Castle, D. C. Epler and D. B. Peplow, *Corrosion Sci.*, **19**, 457 (1979).
128. J. E. Castle and R. Tanner-Tremain, *Surf. Interfacial Anal.*, **1**, 49 (1979).
129. R. F. Roberts, *J. Electron Spectrosc.*, **4**, 273 (1974).
130. P. G. Fox, G. Lewis and P. J. Boden, *Corrosion Sci.*, **19**, 457 (1979).
131. D. Chadwick and T. Hashami, *Corrosion Sci.*, **18**, 39 (1978).
132. M. Ohsawa and W. Suetaka, *Corrosion Sci.*, **19**, 709 (1979).
133. K. Sugimoto, G. Belanger and D. L. Piron, *J. Electrochem. Soc.*, **126**, 535 (1979).
134. T. L. Barr, in *Quantitative Surface Analysis of Materials* (Ed. N. S. McIntyre), ASTM STP 643, p. 83, American Society for Testing and Materials, Philadelphia, Pennsylvania (1978).
135. A. J. Bevolo, B. J. Beaudry and K. A. Gschneidner, *J. Electrochem. Soc.*, **127**, 2556 (1980).
136. R. O. Ansell, T. Dickinson, A. F. Povey and P. M. A. Sherwood, *J. Electrochem. Soc.*, **124**, 1360 (1977).
137. C. L. Lau and G. K. Wertheim, *J. Vac. Sci. Technol.*, **15**, 622 (1978).
138. J. H. Thomas and S. P. Sharma, *J. Vac. Sci. Technol.*, **14**, 1168 (1977).
139. J. P. Servais, J. Lempereur, L. Renaud and V. Leroy, *Br. Corros. J.*, **14**, 126 (1979).
140. J. M. Baker, R. W. Johnson and R. A. Pollak, *J. Vac. Sci. Technol.*, **16**, 1534 (1979).
141. T. Dickinson, A. F. Povey and P. M. A. Sherwood, *J. Chem. Soc., Faraday Trans. I*, **71**, 298 (1975).
142. R. W. Hewitt and N. Winograd, *Surf. Sci.*, **78**, 1 (1978).
143. S. Sunder, D. W. Shoesmith, M. G. Bailey, F. W. Stanchell and N. S. McIntyre, *J. Electroanal. Chem.*, **130**, 163 (1981).
144. J. S. Hammond, J. W. Holubka and R. A. Dickie, *J. Coatings Technol.*, **51**, 655 (1979).
145. J. W. Holubka, J. S. Hammond, J. E. DeVries and R. A. Dickie, *J. Coatings Technol.*, **52**, 63 (1980).
146. J. S. Hammond, J. W. Holubka, J. E. DeVries and R. A. Dickie, *Corrosion Sci.*, **21**, 239 (1981).
147. R. A. Dickie, J. S. Hammond and J. W. Holubka, *Ind. Eng. Chem., Prod. Res. and Dev.*, **20**, 339 (1981).

Practical Surface Analysis
by Auger and X-ray Photoelectron Spectroscopy
Edited by D. Briggs and M. P. Seah

Appendix 1

Spectrometer Calibration

M. T. Anthony
Division of Materials Applications,
National Physical Laboratory, Teddington, Middlesex, UK

A1.1 Calibration of XPS Instruments

The accurate calibration of X-ray photo-electron spectrometers has been an important and continuing objective of spectroscopists over the last ten years. Without an accurately defined spectral energy scale a full interpretation of the spectra gathered on different instruments is severely limited. Several workers[1–9] have reported energy calibrations by presenting binding energy tabulations for copper, silver and gold. These elements have the advantages of being easily cleaned and chemically inert as well as being stable conductors. For the purposes of calibration, binding energies are most accurately defined by referencing the zero to the Fermi level of conducting samples since this avoids errors arising from work function differences between spectrometers. The *d*-bands of palladium and nickel provide suitably intense and sharp Fermi edges in order to define this zero. The literature calibration values of binding energies for copper, silver and gold defined in this way are given in Table A1.1. It is evident that the accumulated data in this table shows a variability of about 0.3 eV which, surprisingly, has not reduced through the years.

The ASTM E-42 committee organized a round-robin[10] to report on binding energies obtained on a wide range of spectrometers. This highlighted the magnitude of errors arising in energy calibration. Analysis by means of Youden plots enables the contributions of random errors, zero shift and voltage scaling to be separated. The most significant error of around 0.3 eV is due to positioning of the zero point. The random error of about 0.1 eV shows the measurement repeatability. Finally, the voltage scaling of the spectrometer introduces errors of approximately 500 p.p.m. or 0.5 eV at 1000 eV binding energy.

Having regard to both the previous literature results[1–9] and those of the ASTM survey,[10] it was clear that accurate energy calibration would only be possible if there was full traceability of the calibration measurements. The

Table A1.1 XPS calibration binding energies, eV, from the literature

	Schon, 1972[2]	Johansson *et al.*, 1973[3]	Asami, 1976[4]	Richter and Peplinski, 1978[5]	Wagner, Gale and Raymond, 1979[6]	Powell, Erickson and Madey, 1979[10]	Bird and Swift, 1980[7]	Fuggle and Mortensson, 1980[8]	Lebugle *et al.*, 1981[9]
Cu $3p$	75.2 ± .1					75.1		75.1	75.13
Au $4f_{7/2}$	84.0	83.8 ± .2	84.07	84.0	83.8	84.0	83.98 ± .02	83.7	84.0
Ag $3d_{5/2}$	368.2	368.2 ± .2	368.23		367.9		368.21 ± .03	367.9	368.2
Cu $2p_{3/2}$	932.2 ± .1	932.8 ± .2	932.53	932.7	932.4	932.6	932.66 ± .06	932.5	932.57
Cu *LMM*, KE	919.0 ± .1	918.3 ± .2	918.65	918.35	918.6	918.7	918.64 ± .04		
BE	567.6 ± .1	568.35 ± .2	567.96	568.25	567.9	567.9	567.97 ± .04		
F.E. ref.	Pd	Pd	Pd	Pd	Au $4f_{7/2}$		Pd	—	—
Instrument	AEIES100	magnetic	AEIES200	AEIES200	Varian IEE-15	E-42 Survey	AEIES200B	VG ESCA3 Mk 1	HP 5950A

work undertaken at the NPL,[11] on a VG Scientific ESCA3 Mk II, gave particular attention to (a) the reproducibility of the calibration, (b) the correct establishment of the zero binding energy point and (c) the accurate measurement of the energy scale. The work determined in detail the effect of operating parameters on reproducibility and, in addition, concluded that the zero point was best defined by the nickel Fermi edge using Mg $K\alpha$ as the source radiation. The measurement of the energy scale was achieved by first checking the 1:1 energy-to-scan voltage equivalence and then by measuring the scan voltage as accurately as possible. The measurement chain was calibrated against a standard cell itself calibrated against the standard NPL volt. The NPL spectrometer energy scale therefore possessed full traceability to the primary volt standard. For electrons of energy 0–1550 eV a precision of measurement of 0.005 eV was achieved with an overall accuracy of 11 p.p.m. in the energy scale.

Binding energies of copper, silver and gold referenced to the nickel Fermi edge were determined on the NPL spectrometer and represent the first accurately traceable calibration of binding energies. The binding energies for both Al $K\alpha$ and Mg $K\alpha$ radiations are listed in Table A1.2.[11]

A comparison of previous literature values from Table A1.1 with the NPL tabulation shows that the recent careful work of Bird and Swift,[7] which quotes the smallest errors of the literature values, gives very close agreement. Other interlaboratory comparisons[11] have subsequently confirmed that where the appropriate methodology[12] is carried out, the calibration is repeatable to ± 0.02 eV if some effort is taken and to ± 0.05 eV with fair ease.

A1.2 Calibration of AES Instruments

The majority of electron spectrometers presently employed in Auger electron spectroscopy are cylindrical mirror analysers (CMA), as distinct from the

Table A1.2 XPS calibration binding energies, eV (Ni Fermi edge zero)

	Al $K\alpha$	Mg $K\alpha$
Cu $3p$	75.14 ± 0.02	75.13 ± 0.02
Au $4f_{7/2}$	83.98 ± 0.02	84.00 ± 0.01
Ag $3d_{5/2}$	368.27 ± 0.02	368.29 ± 0.01
Cu L_3MM	567.97 ± 0.02	334.95 ± 0.01
Cu $2p_{3/2}$	932.67 ± 0.02	932.67 ± 0.02
Ag M_4NN	1128.79 ± 0.02	895.76 ± 0.02

Notes
1 Al $K\alpha$–Mg $K\alpha$ = 233.02 eV
2 Au $4f_{7/2}$ Al $K\alpha$ BE lowered by Au $4f_{5/2}$ tail
3 Ag $3d_{5/2}$ Mg $K\alpha$ BE raised by Ag $3d_{3/2}$ X-ray satellite

spherical sector analysers (SSA) more common in the higher resolution instruments for XPS. The poorer resolution attainable using single-pass CMA analysers, together with the difficulties of accurate sample positioning, restrict the accuracy of the energy calibration compared with that for XPS. However, for chemical state information in AES, an accurate energy scale calibration is needed.

In contrast to XPS, where kinetic energies, E_K, are referenced to the Fermi level, in AES peaks are quoted for their kinetic energy, E_K, referenced to the vacuum level. As a result, the absolute energy scale will be sensitive to work function differences between spectrometers, although energy differences are not so dependent. In addition, for CMA instruments the precise positioning of the sample is critical, unlike the case for the SSA encountered in XPS instruments. Tests at the NPL[13] using a Varian CMA analyser showed that the position of a copper sample must be set to 15 μm to gain an experimental repeatability of 0.1 eV for the Cu L_3MM peak. This arises through the focal properties of the CMA where a change, Δl, in the focal length l of the analyser appears as a shift, ΔE, in the energy E. Generally l is of the order of 150 mm so that the above positioning accuracy cannot be avoided.

The recent ASTM E-42 round-robin[14] reports on the Auger peak positions for copper and gold reference metals; these peaks were recorded on a wide range of instruments. Peak energies showed substantial deviations about the median ranging from 1.9 eV for the low-energy peaks up to 7.4 eV for the high-energy gold $M_5N_{6,7}N_{6,7}$ transition. Clearly differences of this magnitude arise from calibration problems and make chemical state information unreliable.

As most Auger electron spectra are recorded in the derivative $(\mathrm{d}\{En(E)\}/\mathrm{d}E)$ mode with a modulation voltage applied to the analyser, peak energies are generally reported as the position of the high-energy negative excursion peak. Unfortunately, peak energies defined in this way are very sensitive to the modulation amplitude, as seen in Figure A1.1 for the 100 eV elastic peak, and also to analyser resolution. Accurate calibrations could be established for the copper, silver and gold peaks at a given modulation for various analyser resolutions; however, for most instruments the real modulation in terms of the contribution to the energy spectrum is not known with sufficient accuracy. For many instruments the modulations are not applied to all electrodes in phase in strict proportionality to the d.c. voltages present. This problem is discussed in detail by Seah,[15] who shows why this then makes it very difficult to calibrate the effective energy modulations of the spectrometer. The problem is most prevalent with XPS analysers used for AES but even the CMAs do not behave simply. Tests on two Varian CMAs show that the effective energy modulation of the spectrometer is 20 ± 1 per cent. lower than that predicted from the product of the measured voltage modulation of the mirror electrode and the spectrometer constant. In addi-

tion to this effect, which arises from the analyser design, will be the normal errors associated with ensuring that the voltage oscillator is kept in calibration. These problems are common to most AES instruments and not to any particular model.

In order to avoid the difficulties associated with the imprecision of the modulation and the need to correct for analyser resolution, each peak position in the differential mode may be replaced by the energy at which swing between the positive and negative excursions crosses the zero signal line. This zero crossing point is insensitive to the applied modulation and analyser resolution and can therefore be most accurately assigned. Figure A1.1 shows a series of different modulations for the 100 eV elastic peak and illustrates how the zero crossing point changes by less than 1 per cent. of the shift seen in the customary negative peaks for modulations up to 2 V. For small modula-

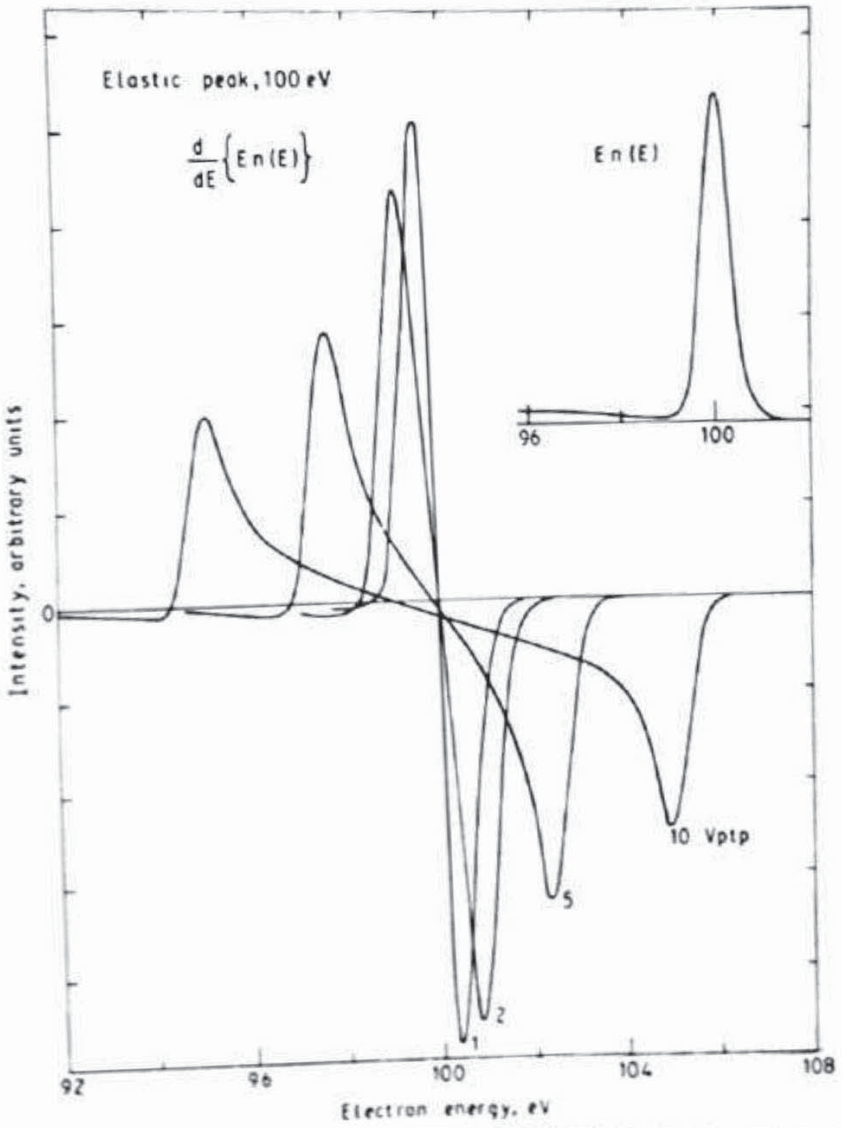

Figure A1.1 100 eV elastic peak in (i) differential (d{$En(E)$}/dE), mode for 1, 2, 5 and 10 volts peak-to-peak modulation and (ii) direct, $En(E)$ mode.

tions the zero crossing point corresponds to the peak positions as recorded in the direct *En(E)* spectrum (shown top right in Figure A1.1). Indeed, for the best possible accuracy of energy calibration, it is strongly advisable to use this *En(E)* mode, since only then is the peak energy entirely independent of the modulation and its associated errors in assessing its magnitude. The *En(E)* peak positions for copper, silver and gold reference metals, using a 5 kV electron beam, are given in Table A1.3.[13] The positions are the same as the zero crossing point in the differential mode for small modulations. The tabulated data were recorded at the NPL on a VG Scientific ESCA3 Mk II spectrometer modified for reference work with its energy scale traceable to the standard volt.[11] The peak positions thus have precise traceability to a primary standard, but, bearing in mind that kinetic energies referenced to the vacuum level (as customarily used) depend on the spectrometer 'work function', a final column in Table A1.3 is added with the kinetic energies referenced to the Fermi level. A further point that should be noted is that, with the varying energy in the deflector field, the effective mass of the electron is involved and not the rest mass, so that a relativistic effect occurs in which the true electron energy E_k is related to that using the low energy approximation for the analyser, E_k^0, by[16,17,18]

$$E_k = E_k^0 + \left(\frac{E_k^0}{1011R}\right)^2 + \cdots \text{SSA}$$

$$E_k = E_k^0 + \left(\frac{E_k^0}{1536}\right)^2 + \cdots \text{CMA}$$

where R is the retard ratio between the kinetic energy of the electron in the SSA deflector field and E_k. Thus, a CMA calibrated to give the correct value for the gold peak at 2020 eV will, if the energy scale is assumed to be linear measure, the copper 914.4 eV peak at 0.43 eV too high an energy, i.e. 914.8 eV.

Table A1.3 Auger electron peak kinetic energies, eV

	E_k	E_K
Cu $M_{2,3}M_{4,5}M_{4,5}$	59.2 ± 0.1	63.5 ± 0.1
Au $N_{6,7}O_{4,5}O_{4,5}$	68.2 ± 0.1	72.5 ± 0.1
Ag $M_4N_{4,5}N_{4,5}$	353.6 ± 0.1	357.9 ± 0.1
Cu $L_3M_{4,5}M_{4,5}$	914.4 ± 0.1	918.7 ± 0.1

Notes
1. Energy of peak recorded in *En(E)* mode, equivalent to the zero crossing point in the differential mode for small modulations.
2. Kinetic energies include the appropriate relativistic correction
   E_k = kinetic energy referenced to vacuum level
   E_K = kinetic energy referenced to Fermi level

Unlike the XPS case the use of Table A1.3 in calibrating AES analysers is not always trivial. For XPS instruments which can also provide AES, the spectrometer will already have been accurately calibrated using XPS. For XPS-style analysers used for AES and with no XPS present, the table can be used directly since the sample position is not critical. However, in CMA-based instruments where the sample will not be repositioned exactly to ± 15 μm an extra procedure must be used. Most CMAs are provided with a stabilized beam energy of 2000 eV so that the sample is positioned until the zero crossing of the elastic peak appears at 2000 eV on the energy scale. In general, the instrument needs to be left on this setting for 10 minutes or so for stability but, even then, the energy will not generally be 2000.0 eV. The spectrometer should be set up on copper or gold and the sample carefully moved until the energy difference of the peaks matches that in Table A1.3, as recorded by the energy DVM. The sample is now in the correct position and the true value of the nominal 2000 eV beam energy may be accurately established. This energy value is then used for all subsequent sample positionings and the instrument is calibrated as given in Table A1.3.

References

1. K. Siegbahn, C. Nordling, A. Fahlman, R. Nordberg, K. Hamrin, J. Hedman, G. Johansson, T. Bergmark, S-E. Karlsson, I. Lindgren and B. Lindberg, *ESCA—Atomic Molecular and Solid State Structure Studied by Means of Electron Spectroscopy*, Almqvist, Uppsala (1967).
2. G. Schon, *J. Electron Spectrosc.*, **1**, 377 (1972).
3. G. Johansson, J. Hedman, A. Berndtsson, M. Klasson and R. Nilsson, *J. Electron Spectrosc.*, **2**, 295 (1973).
4. K. Asami, *J. Electron Spectrosc.*, **9**, 469 (1976).
5. K. Richter and B. Peplinski, *J. Electron Spectrosc.*, **13**, 69 (1978).
6. C. D. Wagner, L. H. Gale and R. H. Raymond, *Anal. Chem.*, **51**, 466 (1979).
7. R. J. Bird and P. Swift, *J. Electron Spectrosc.*, **21**, 277 (1980).
8. J. C. Fuggle and N. Martensson, *J. Electron Spectrosc.*, **21**, 275 (1980).
9. A. Lebugle, U. Axelsson, R. Nyholm and N. Martensson, *Phys. Scrip.*, **23**, 825 (1981).
10. C. J. Powell, N. E. Erickson and T. E. Madey, *J. Electron Spectrosc.*, **17**, 361 (1979).
11. M. T. Anthony and M. P. Seah, *Surf. Interface Anal.*, **6**, 107 (1984).
12. M. T. Anthony and M. P. Seah, *Surf. Interface Anal.*, **6**, 95 (1984).
13. M. P. Seah and M. T. Anthony (to be published).
14. C. J. Powell, N. E. Erickson and T. E. Madey, *J. Electron Spectrosc.*, **25**, 87 (1982).
15. M. P. Seah, *Surf. Interface Anal.*, **1**, 91 (1979).
16. O. Keski-Rahkonen and M. O. Krause, *J. Electron Spectrosc.*, **13**, 107 (1978).
17. O. Keski-Rahkonen, *J. Electron Spectrosc.*, **13**, 113 (1978).
18. M. P. Seah and M. T. Anthony, *J. Electron Spectrosc.* (to be published).

Practical Surface Analysis
by Auger and X-ray Photoelectron Spectroscopy
Edited by D. Briggs and M. P. Seah

Appendix 2

Static Charge Referencing Techniques

P. Swift, D. Shuttleworth
Shell Research Ltd., Thornton Research Centre, PO Box 1, Chester CH1 3SH UK

M. P. Seah
National Physical Laboratory, Teddington, Middlesex, UK

A2.1 Introduction

A problem commonly experienced in the interpretation of an XPS spectrum is that of static charge referencing. Static charging arises as a consequence of the build-up of a positive charge at the surface of non-conducting specimens when the atoms lose electrons in the photo-emission process. This positive charge produces a retarding field in front of the specimen such that the photo-electrons have a kinetic energy, E_K, lower than that predicted by the simple equation:

$$E_K = h\nu - E_B \qquad \text{(A2.1)}$$

where $h\nu$ is the photon energy of the X-ray source, E_B is the binding energy of the appropriate core level and E_K is referenced to the Fermi level of the spectrometer. Conductors in electrical contact with the spectrometer probe do not exhibit such charging effects because the photo-electrons are replaced by electrons flowing through the sample. However, for electrically isolated conductors and insulating materials the rate of photo-electron loss is greater than that of their replacement from within the specimen, and a charged surface ensues.

Generally, in spectrometers using an achromatic X-ray source, this charge is partially neutralized by a background of low-energy electrons (i.e. <5 eV) produced by the bremsstrahlung X-rays striking the X-ray gun window and the internal parts of the apparatus. If the surface charges positively, these low-energy electrons are drawn to the sample so that an equilibrium steady-state static charge results and the photo-electron peaks occur in the spectrum

with an energy now defined by

$$E_K = h\nu - E_B - C \qquad \text{(A2.2)}$$

where C is the steady-state static charge value, usually a positive number.

The steady-state static charge discussed above may be termed an equilibrium static charge, C, and is generally achieved within a few seconds of the irradiation of the specimen by X-rays from an achromatic source, unless the sample is of a changeable conductivity. The latter effect may arise from damage to a specimen by the X-rays, thereby changing its physical nature (e.g. reduction of an insulating compound to contain metallic sites).

The surface charging problem is accentuated if the X-ray source is monochromatized because of the reduced intensity of the photon flux and the loss of the bremsstrahlung X-rays. This leads to a significant decrease in the number of scattered low-energy electrons in the vicinity of the sample and, consequently, a steady-state static charge is seldom attained. If a monochromatized X-ray source is used it is necessary to direct a controlled beam of low-energy electrons from an electron gun at the specimen surface, as discussed in Section A2.6, and this produces a gun-controlled static charge, C_G.

In addition to the change of kinetic energy of the photo-electrons arising from the equilibrium static charge, spectral peak broadening may be observed for insulating materials. This is because, although the surface may attain an overall static charge at equilibrium with the photon flux, not all of the sites have equivalent C values. This effect is particularly noticeable for heterogeneous specimens where components vary in insulating nature (e.g. minerals) and, in extreme cases, spectral peaks arising from photo-electrons emitted from the same atomic level in different regions of the sample may be split by several electronvolts.

Although static charging can significantly shift the kinetic energy of the photo-electron peaks, it does not necessarily preclude the determination of their true binding energy provided the value of C is established. Several methods are discussed below which may be considered as supplementary or alternative to the use of the Auger parameter discussed in Chapter 3.

A2.2 Adventitious Surface Layers

Unless specimens are prepared for analysis under carefully controlled atmospheres, their surfaces generally suffer from adventitious contamination. Once in the spectrometer, further contamination can occur by the adsorption of residual gases, especially in instruments with oil diffusion pumps. These contamination layers can be used for referencing purposes if it is assumed that they truly reflect the steady-state static charge exhibited by the specimen surface and that they contain an element peak of known binding energy. Carbon is the element which is most commonly detected in contamination

layers and the photo-electrons from the C 1*s* atomic energy level are those most generally adopted for referencing purposes. A binding energy of 284.8 eV is often used for the C 1*s* level of this contamination and the difference between its measured position in the energy spectrum and the above value gives the charging value, *C*, of equation (A2.2).

Siegbahn *et al*[1] first reported the presence of a carbon contamination layer and deduced that it originated from pump oil, since the C 1*s* peak increased in intensity with the exposure of the specimen to the spectrometer vacuum. Subsequently, it had generally been assumed that the C 1*s* electrons originate from saturated hydrocarbon components, or from carbon atoms in chemical domains of similar electronegativity to that in a saturated hydrocarbon, in the contamination layer. The experimental considerations and reliability of the use of adventitious carbon for energy referencing have been discussed in a review article by Swift.[2]

The main disadvantage of the technique is the uncertainty caused by the spread of values from 284.6 to 285.2 eV reported in the literature[2] for the C 1*s* electrons. Therefore, it is recommended that if the C 1*s* electrons from a contamination layer are to be used for referencing, their binding energy should be determined by the user on his own spectrometer. Ideally this determination should be carried out on a substrate closely similar in chemical and physical properties to the material to be analysed uniformly covered by only a thin contamination layer (i.e. of the order of a monolayer).

Factors that can affect the measured C 1*s* binding energy from adventitious carbon layers, and its subsequent use for energy referencing, include:

(a) The chemical state of the carbon in the contamination layer.[3]
(b) The thickness of the adventitious layer.[4–6]
(c) The chemical and physical nature of the substrate on which the measurements are made.[2,4]
(d) Specimen preparation and surface treatment effects.[4,7,8]
(e) The accuracy of the energy calibration of the spectrometer on which it is determined.[9]

Despite the apparent limitations and uncertainties associated with the use of adventitious carbon for static-charge referencing, it is the most convenient and commonly applied technique. However, for the reasons listed above and discussed in the review article by Swift,[2] the interpretation of binding energies must be regarded with caution. Furthermore, if results from different laboratories are to be compared, the absolute energy calibration of the spectrometers must be defined and a reliable reference binding energy (e.g. Au $4f_{7/2}$) reported. This information, together with the C 1*s* electron binding energy used and the substrate on which it was measured, should provide a reasonable basis to allow a meaningful comparison of results to be made.

A2.3 Deposited Surface Layers

In cases where a suitable adventitious overlayer is not present it is necessary to introduce a calibrant by deliberate deposition. In general, organic compounds and metals are used for the calibrating species as they can often be reliably condensed onto surfaces under UHV conditions. Unknown calibrants, such as pump oils, can be used if they re-evaporate without decomposition in UHV.

Care should be taken to ensure that the calibrant neither decomposes nor reacts with the substrate upon condensation and that the binding energy observed for the reference material, which may deposit either as a thin overlayer or in islands, is characteristic of the bulk. This can be done by taking spectra as a function of time and amount of calibrant deposited. It may also be advantageous to characterize the form of the deposition (i.e. as uniform overlayer or islands) by carrying out angular studies. This, of course, is not applicable to powder samples.

The deliberate deposition of oil vapour in diffusion pumped systems is frequently used for calibration purposes since it may be accomplished by allowing the liquid nitrogen cold traps to partially warm up. Alternatively,[10] in certain types of spectrometer the cooled X-ray source window may be allowed to warm to release condensed adventitious species directly onto the specimen. In both cases condensation may be accelerated by cooling the sample. When employing this method care should be exercised to avoid the 'memory effect' from previously introduced volatile material, which is not intended to be used as a calibrant, condensing onto the sample and possibly leading to an erroneous reference.

Another method employing organic materials as calibrants involves their introduction from outside the vacuum chamber, as described by Connor.[11] This little-used method allows the organic compound chosen to be compatible with the sample under investigation, for instance in regard to wettability and freedom from spectral overlap of core-level lines.

Metals are also frequently employed as calibrants in XPS and, because of their general inertness and ease of evaporation, the noble metals are most often used. In practice about a monolayer of, for example, gold is deposited, preferably *in situ*. The method is one of the few charge-correction methods to receive detailed study,[12–15] where it has been demonstrated[12,14,15] that the conditions necessary to obtain electrical equilibrium, and therefore accurate charge correction, depend on the surface coverage. An optimum thickness of gold exists for effective charge correction, which for polyethylene and PTFE is approximately 0.6 nm.[15] Such thicknesses should be regarded as equivalent thicknesses since it is known[16] that gold deposits in the form of islands at these low coverages. Care must be exercised here since there are indications that small binding energy shifts ($\leq$0.25 eV) for the Au $4f_{7/2}$ peak occurs at low

A2.3 Deposited Surface Layers

In cases where a suitable adventitious overlayer is not present it is necessary to introduce a calibrant by deliberate deposition. In general, organic compounds and metals are used for the calibrating species as they can often be reliably condensed onto surfaces under UHV conditions. Unknown calibrants, such as pump oils, can be used if they re-evaporate without decomposition in UHV.

Care should be taken to ensure that the calibrant neither decomposes nor reacts with the substrate upon condensation and that the binding energy observed for the reference material, which may deposit either as a thin overlayer or in islands, is characteristic of the bulk. This can be done by taking spectra as a function of time and amount of calibrant deposited. It may also be advantageous to characterize the form of the deposition (i.e. as uniform overlayer or islands) by carrying out angular studies. This, of course, is not applicable to powder samples.

The deliberate deposition of oil vapour in diffusion pumped systems is frequently used for calibration purposes since it may be accomplished by allowing the liquid nitrogen cold traps to partially warm up. Alternatively,[10] in certain types of spectrometer the cooled X-ray source window may be allowed to warm to release condensed adventitious species directly onto the specimen. In both cases condensation may be accelerated by cooling the sample. When employing this method care should be exercised to avoid the 'memory effect' from previously introduced volatile material, which is not intended to be used as a calibrant, condensing onto the sample and possibly leading to an erroneous reference.

Another method employing organic materials as calibrants involves their introduction from outside the vacuum chamber, as described by Connor.[11] This little-used method allows the organic compound chosen to be compatible with the sample under investigation, for instance in regard to wettability and freedom from spectral overlap of core-level lines.

Metals are also frequently employed as calibrants in XPS and, because of their general inertness and ease of evaporation, the noble metals are most often used. In practice about a monolayer of, for example, gold is deposited, preferably *in situ*. The method is one of the few charge-correction methods to receive detailed study,[12-15] where it has been demonstrated[12,14,15] that the conditions necessary to obtain electrical equilibrium, and therefore accurate charge correction, depend on the surface coverage. An optimum thickness of gold exists for effective charge correction, which for polyethylene and PTFE is approximately 0.6 nm.[15] Such thicknesses should be regarded as equivalent thicknesses since it is known[16] that gold deposits in the form of islands at these low coverages. Care must be exercised here since there are indications that small binding energy shifts ($\leq$0.25 eV) for the Au $4f_{7/2}$ peak occurs at low

coverages.[17] Also, with certain types of substrate, notably halides and cyanides, reaction with the gold has been reported.[18-21] However, when the appropriate precautions are taken[13-15] the gold decoration technique may often be used to obtain charge-corrected binding energies using the calibrated binding energy of 84.0 eV for the Au $4f_{7/2}$ line.[9]

Should, of course, one be dealing with a sample that may safely evaporate without decomposition in UHV then referencing becomes relatively straightforward. In this case a suitably thin layer of sample is first characterized by condensation onto a clean metal substrate (e.g. gold) and referenced by using a known core-level binding energy of the substrate. The reliability of the electrical contact should be verified by accumulating spectra at various sample thicknesses and by ensuring that all peaks in the spectrum shift by the same amount when an electrical bias is applied.

A2.4 Mixtures

The possibility of carrying out static charge energy referencing for insulating materials, by preparing finely ground mixtures with powders containing a component of known binding energy, has been investigated. Powdered graphite has been the most commonly used reference material for this technique,[4,22-24] whilst lithium fluoride,[25] potassium salts,[26,27] triplumbic tetroxide,[28] molybdenum trioxide[29,30] and gold[30] have also been considered. Generally, the experimental difficulty of obtaining intimate homogeneous mixtures (i.e. approaching atomic proportions) has been regarded as the main limitation of this technique.

Factors which must be considered when interpreting the data include:

(a) The particle size of the powders, which can affect the intimacy of the mixture.
(b) Particle–interface interaction between different components.
(c) Differential charging of the particles of the different components.

Results for mixed powders are usually very poor and Wagner[31] has recently shown that, for some systems, errors of up to 10 eV can be produced.

It is possible to achieve mixing at a molecular scale for a limited range of materials by fusion of a calibrant with an unknown compound; however, the data will rarely be characteristic of the original compounds. The co-condensation of a volatile calibrant with an unknown compound is also a method of energy referencing that has been extensively used by Connor,[11] who obtained good internal consistency leading to binding energies with a reproducibility of ±0.2 eV. The results were found to be independent of the relative proportions of the calibrant and unknown compound co-condensed and also of the specific calibrant molecule used.

Of the three mixture referencing techniques discussed above, the last has been shown to be the most reliable. However, this method is limited to stable volatile compounds. In general, the use of mixture techniques is not recommended as a means of energy referencing, either with or without static charge correction considerations.

A2.5 Internal Standards

Perhaps the most reliable method of spectral referencing lies in the use of an internal standard[32] which depends upon the invariance of the binding energy of a chosen chemical grouping in different molecules. It is attractive because the referencing specie is now 'locked' into the unknown material and must reflect the static charge of the system if it is uniform over the surface.

The method has found widespread use in the study of carbon-containing material[33] and, in particular, polymer systems, where it has found most reliable application in the study of chemical shift. The use of this method, of course, requires a knowledge of the molecular formula of the material being studied. The binding energy of the chemical grouping employed must be known to be invariant in a range of environments by some independent method (e.g. preparation of thin conducting films).

A novel variation on this method is in the use of bulk solvent as reference in quick-frozen solutions.[34] Although this is of limited application it is nonetheless valuable.

A2.6 Low-energy Electron Flood Gun

Low-energy electron flood guns may be used to stabilize the static charging of insulators examined by XPS[35] and, in particular, when monochromatized X-rays are employed. Recent work [36,37] into the design and operation of flood guns has shown that the best results are achieved with an electron beam of a low energy (< 1 eV), with respect to the vacuum chamber at earth, from a source very close to the specimen. Optimum operating conditions, e.g. sample position, exist for particular configurations and must, in general, be determined by the user. Low electron energies should be used to maximize the neutralization effect and reduce the number of electron bombardment induced reactions.

A low-energy electron flood gun is potentially of use for three types of XPS application; these are:

(a) Studies using monochromatized X-rays where charging shifts for insulators are usually very large and not corrigible by the methods discussed previously. Flood guns compensate for the loss of bremsstrahlung-excited secondary electrons in changing from an achromatic to a mono-

chromatic X-ray source. Operation in this manner normally overcomes the major problem but still leaves a small correction to be made using a method outlined in previous sections.

(b) Absolute calibration of spectra may be achieved by using a flood gun suitably calibrated for a particular instrument configuration.[36] In this way the value of C in equation (A2.2) can be reduced or even made negative. C_G, defined earlier in relation to equation (A2.2), is equal to the cathode voltage minus a gun constant. With a calibrated gun and for smooth samples the surface potential can be set to ± 0.01 eV, allowing a precise definition of binding energies. At the present time the design of flood guns does not enable this accuracy to be achieved with the type of powdered samples often studied with XPS. Here the absolute accuracy is reduced to about ± 0.50 eV.

(c) In situations where static charging is not homogeneous across the sample surface, peak broadening may occur and the electron flood gun can be used to minimize or even eliminate this broadening.[38]

Of the five energy referencing methods discussed in this appendix, the low-energy electron flood gun technique shows the greatest potential because of its applicability to all types of sample encountered in XPS.

References

1. K. Siegbahn, C. Nordling, A. Fahlman, R. Nordberg, K. Hamrin, J. Hedman, G. Johansson, T. Bergmark, S. Karlsson, I. Lindgren and B. Lindberg, *ESCA, Nova Acta Regiae, Soc. Sci. Ups.*, **IV**, 20 (1967).
2. P. Swift, *Surf. Interface Anal.*, **4**, 47 (1982).
3. E. S. Brandt, D. F. Untereker, C. N. Reilley and R. W. Murray, *J. Electron Spectrosc.*, **14**, 113 (1978).
4. G. Johansson, J. Hedman, A. Bendtsson, M. Klasson and R. Nilsson, *J. Electron Spectrosc.*, **2**, 295 (1973).
5. S. Kinoshita, T. Ohta and H. Kuroda, *Bull. Chem. Soc. Jpn*, **49**, 149 (1976).
6. D. T. Clark, A. Dilks and H. R. Thomas, *J. Polym. Sci., Polym Chem. Ed.*, **16**, 1461 (1978).
7. C. D. Wagner, *Applied Surface Analysis*, ASTM STP 699, American Society for Testing and Materials, Philadelphia (1980).
8. A. Jaegle, A. Kait, G. Nanse and J. C. Peruchetti, *Analysis*, **9**, 252 (1981).
9. R. J. Bird and P. Swift, *J. Electron Spectrosc.*, **21**, 227 (1980).
10. D. T. Clark, H. R. Thomas, A. Dilks and D. Shuttleworth, *J. Electron Spectrosc.*, **40**, 455 (1977).
11. J. A. Connor, in *Handbook of X-ray and Ultraviolet Photo-electron Spectroscopy* (Ed. D. Briggs), Chap. 5, p. 183, Heyden, London (1977).
12. D. J. Hnatowich, J. Hudis, M. L. Perlman and R. C. Ragnini, *J. Appl. Phys.*, **42**, 4883 (1971).
13. M. F. Ebel and H. Ebel, *J. Electron Spectrosc.*, **3**, 169 (1974).
14. C. R. Grinnard and H. M. Riggs, *Anal. Chem.*, **46**, 1306 (1974).
15. Y. Uwamine, T. Ishizuka and H. Yamatera, *J. Electron Spectrosc.*, **23**, 55 (1981).

16. D. W. Pashley, *Adv. Phys.*, **14**, 327 (1965).
17. I. Adams, Ph.D. Thesis, p. 137, University College of Wales, Aberystwyth (1972).
18. D. Betteridge, J. C. Connor and D. M. Hercules, *Electron Spectrosc.*, **2**, 327 (1973).
19. D. S. Urch and M. Webber, *J. Electron Spectrosc.*, **5**, 791 (1974).
20. L. I. Matienzo and S. O. Grim, *Anal. Chem.*, **46**, 2052 (1974).
21. V. I. Netedov, Va. V. Salyn, G. Leonhardt and R. Scheibe, *J. Electron Spectrosc.*, **10**, 121 (1977).
22. R. Nordberg, H. Brecht, R. G. Albridge, A. Fahlman and J. R. Van Wazer, *Inorg. Chem.*, **9**, 2469 (1970).
23. V. I. Netedov and M. M. Kakhana, *Zh. Anal. Khim.*, **27**, 2049 (1972).
24. G. Kumar, J. R. Blackburn, R. G. Albridge, W. E. Moddeman and M. M. Jones, *Inorg. Chem.*, **11**, 296 (1972).
25. W. Bremser and F. Linnemann, *Chem.*, **1971**, Fig. 95, 1011 (1971).
26. J. J. Jack and D. M. Hercules, *Anal. Chem.*, **43**, 729 (1971).
27. L. D. Hulett and T. A. Carlson, *Appl. Spectrosc.*, **25**, 33 (1971).
28. W. J. Stec, W. E. Morgan, R. G. Albridge, A. Fahlman and J. R. Van Wazer, *Inorg. Chem.*, **11**, 219 (1972).
29. W. E. Schwartz, P. H. Watts, J. P. Watts, J. W. Brasch and E. R. Lippincott, *Anal. Chem.*, **44**, 2001 (1972).
30. W. P. Dianis and J. E. Lester, *Anal. Chem.*, **45**, 1416 (1973).
31. C. D. Wagner, *J. Electron. Spectrosc.*, **18**, 345 (1980).
32. J. J. Ogilvie and A. Wolburg, *Appl. Spectrosc.*, **26**, 401 (1972).
33. D. T. Clark and H. R. Thomas, *J. Polym. Sci., Polym. Chem. Ed.*, **14**, 1671 (1976).
34. K. Burger, *J. Electron Spectrosc.*, **14**, 405 (1978).
35. D. A. Huchital and R. T. McKeon, *Appl. Phys. Lett.*, **20**, 158 (1972).
36. C. P. Hunt, C. T. H. Stoddart and M. P. Seah, *Surf. Interface Anal.*, **3**, 157 (1981).
37. C. P. Hunt, M. T. Antony, C. T. H. Stoddart and M. P. Seah, NPL Chem. Report 108, March 1980.
38. H. Windawi, *J. Electron Spectrosc.*, **22**, 373 (1981).

Practical Surface Analysis
by Auger and X-ray Photoelectron Spectroscopy
Edited by D. Briggs and M. P. Seah

Appendix 3

Data Analysis in X-ray Photoelectron Spectroscopy

P. M. A. Sherwood
Department of Inorganic Chemistry, The University, Newcastle-upon-Tyne NE1 7RU, UK

A3.1 Introduction

There is an increasing interest in the collection of data of high quality which can then be analysed by accurate data analysis methods. This has arisen because there is a growing awareness of the importance of being able to distinguish small changes in photo-electron spectra, and the availability of cheap microcomputers allows automation of data collection and many digital methods of data analysis to be applied without having to resort to large and expensive mainframe computers. This appendix will attempt to review the range of data-collection and analysis techniques, and provide examples from the work of the author which illustrate the application of the methods described.

A3.2 Data-collection Systems

The majority of X-ray photo-electron spectroscopic (XPS) data is still collected using analogue ratemeters and chart recorders. Analogue data are subject to problems of uncertainty in peak position and peak area due to dependence upon the instrument time constant and scanning speed. Analogue data give almost no idea of data quality due to the effective smoothing due to the choice of a high time constant. If smoothing of data is to be carried out it is much better to smooth digital data in a controlled way (to be discussed below) than to rely upon the correct selection of the time constant and scanning speed by the operator. Once the digital data have been collected it can be treated by various methods, but once analogue data have been collected it cannot be modified since it has already been altered by the analogue collection system. In addition the data analysis is often carried out

using analogue methods such as curve fitting using a Du Pont curve resolver. This approach is highly subjective and, thus, often misleading. One of the most serious limitations of analogue data is that it prevents data accumulation to improve the signal-to-noise (S/N) levels in a spectrum.

Most commercial spectrometers can be purchased with a data system to control the spectrometer and to carry out some data analysis. Such data analysis systems may be fairly expensive, but the availability of cheap microcomputers allows data systems to be provided at a substantially reduced cost. The microcomputers have the advantage that even though they are generally single-task machines their cost allows one to have a number of them performing particular tasks. In addition, the programs can always be adjusted to accommodate the latest developments and improvements in data analysis and collection which would not be possible with dedicated apparatus such as multichannel analysers.

The way in which a microcomputer-based data analysis system might be constructed is illustrated in Figure A3.1, which shows the way in which micro- and mainframe computers are associated with the spectrometer in the author's laboratory. This system uses two microcomputers and five terminals associated with the mainframe computer. Printers and a plotter are all linked together through a local distribution board, which allows devices such as the printers to be shared by the microcomputers and the mainframe computer

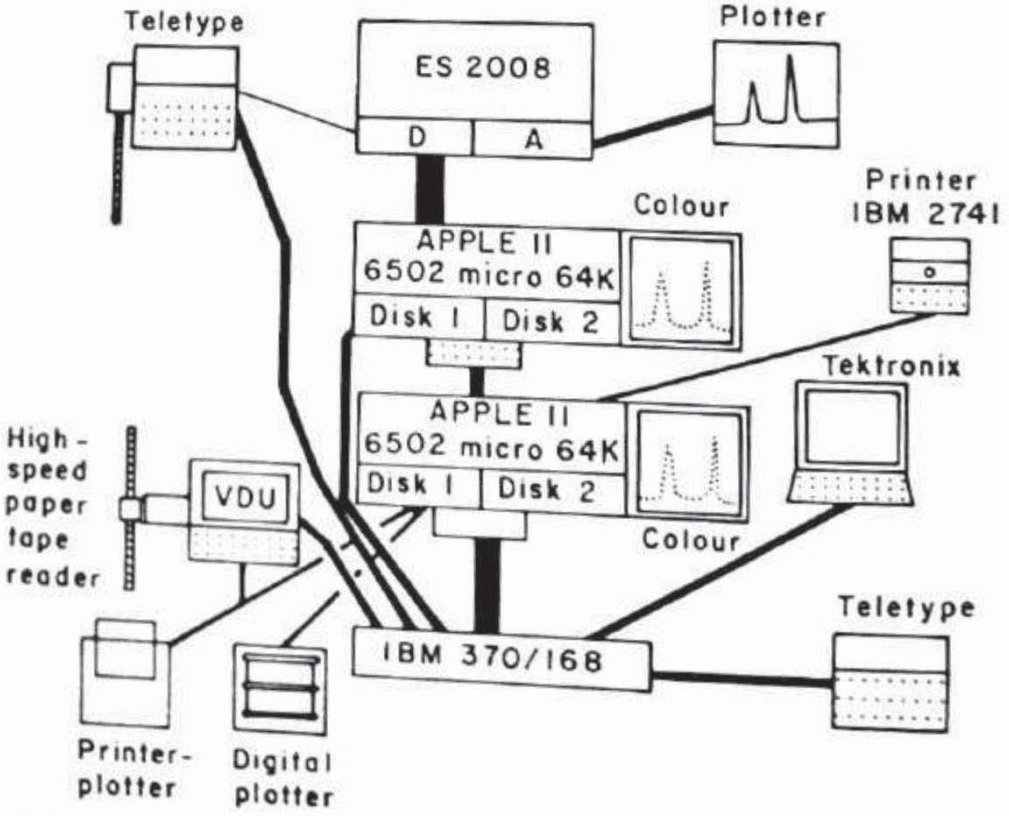

Figure A3.1 Diagram of a microcomputer and mainframe computer data system

terminals, and the microcomputers and the terminals to talk to the mainframe computer through six hard-wired lines.

The data are collected simultaneously by an analogue ratemeter (A) and a digital ratemeter(D). The analogue ratemeter gives an X–Y analogue plot which is useful for collection of an overall spectrum and for monitoring any changes in the spectrum with time (which might be caused by decomposing samples or a drifting sample potential). The digital ratemeter can also be used to monitor any changes in the spectrum with time by an additional output which allows data, when required, to be punched out on paper tape simultaneously with the main output which is transferred to the Apple II microcomputer system.

The Apple II microcomputer system has 64K of random access memory available which gives good space for complex data-collection programs with full graphics facilities. This micro is programmed to communicate with the operator to ensure that the machine is being operated in the correct manner, as well as to collect all the relevant spectral information. The program is so designed that an inexperienced operator is provided with a considerable amount of information on an 80 × 24 upper and lower case screen. The experienced operator can ignore the information since it is printed at a very fast rate. The spectrum is then displayed while it is collected on an additional graphics screen displayed simultaneously with the text screen. This allows simultaneous display of the program instructions with the generation of graphics, allowing instruction manuals to be eliminated and making it possible to easily construct self-teaching programs. This is of particular value when the microcomputer system is being used to analyse the data. The data are stored on floppy disc, which can be transferred to another 64K Apple II system for data analysis, while the first Apple II system is used to collect another spectrum, thus eliminating any dead time.

The spectra are stored permanently on floppy disk (a 5.25 inch floppy disk can store approximately seventy reasonable length spectra), but are also transferred to the mainframe computer where they are stored on magnetic tape. The mainframe computer is used for data analysis and for large calculations (such as molecular orbital calculations) for data interpretation. Mainframe computing power is needed for some data analysis methods, but the microcomputers are being increasingly used for this purpose in the author's laboratory.

A3.3 Simple Data Operations

Many data systems control most of the spectrometer functions, such as starting kinetic energy, range, number of scans, scanning to a predetermined S/N ratio, X-ray gun voltage and current settings, and the operation of an argon ion gun. The data collection may be displayed as it is collected or after the

spectrum is terminated. Some caution has to be exercised in the way in which the data collection is carried out, since some manufacturers pre-treat the data (by smoothing and background subtraction) as an automatic part of their data system. This is a very regrettable practice since it should be clear from this appendix that there is no 'correct' way for carrying out such operations, and thus this practice can lead to misleading results. In general, then, all the data treatment methods must be treated with caution, and the original untreated data should always be retained as a permanent record.

In particular, some very simple operations can be carried out, and these are discussed below. All these operations can easily be carried out on a microcomputer system. Such a system has the value that the altered spectrum can be instantly displayed after the process has been applied.

A3.3.1 Spectral display and expansion

The display is generally made as a series of points representing each digital data point collected for a particular time at a specific kinetic energy, or sometimes at a particular time over a small lineraly varied kinetic energy range. This dot display of points is in the author's view to be preferred over a display which links the points by a line to give a continuous spectrum. The spectrum often has cross wires superimposed upon it so that individual points in the spectrum can be identified in terms of their x (kinetic energy or binding energy) and y (counts) position which is generally printed out at the bottom of the spectrum. Simple x and y expansion of the scale is generally made available. A facility to normalize the spectrum so that the point with maximum counts is at the graphics display maximum is generally useful, especially if there is a facility to remove part of a spectrum in order to concentrate upon particular spectral features.

A3.3.2 Integration and area measurement

Some facility for area measurement is useful, and this generally takes the form of a facility where the area between two points (identified by positioning the cross wires at these points) is calculated as the area between a line joining the points and the spectrum. The whole spectrum is sometimes integrated by adding all the data points together (after the removal of some horizontal background value) and displaying the integrated curve as the total sum at that point counting from left to right.

A3.3.3 Spike removal

Spikes can sometimes be generated in a spectrum as a result of power surges or the switching on of apparatus, and a facility to remove a particular point

and replace it by another point is valuable. Obviously this process should only be applied to a limited number of points!

It is very important to remove spikes before further data analysis is carried out since only one or two such spurious points can very seriously effect data analysis operations such as smoothing and non-linear least squares curve fitting.

A3.3.4 Satellite subtraction

Some commercial data systems provide for the X-ray radiation satellites to be removed, and even claim that such an approach is as good as using an X-ray monochromator, which of course removes such satellites. Satellite subtraction must be carried out with great care. Firstly, the background in the region of interest must be accurately subtracted, and it will be seen below that this is by no means an operation that can be performed with complete accuracy. Secondly, any Auger peaks present in the region of interest must be identified (since these, of course, will have no X-ray satellite contribution) and their spectral contribution accurately calculated, so that this intensity can be removed from the intensity that contributes to the X-ray radiation satellite intensity. Thirdly, any satellites due to other peaks outside the region of interest must be identified, e.g. X-ray satellites, satellites of Al $K\alpha_{12}$ radiation from magnesium anode systems with aluminium X-rays windows and cross-over in two anode systems, and discrete energy loss satellites from photoelectron peaks at a higher binding energy than the region of interest (see Chapter 3).

A3.3.5 Baseline removal

The removal of the background of a spectrum is a non-trivial operation which will be discussed below. The removal of a horrizontal baseline is a trivial operation, however, which is a convenient method for the visual improvement of a spectrum which consists of small spectroscopic changes superimposed over a large background.

A3.3.6 Addition and subtraction of spectra

For comparative purposes two spectra may be added together or substracted one from the other. Many data systems provide such a facility for direct addition and subtraction. If the subtraction technique is to be used in a more thorough manner the subtraction technique must be carried out in a non-trivial manner, such methods being discussed below.

A3.3.7 Peak maximum location

A procedure to locate the maximum count, i.e. peak maximum, in a spectrum is easily done. Such a procedure generally allows a genuine peak to be distinguished from a stray point.

A3.4 Smoothing

Nearly all data systems provide a facility to smooth the data. Such an operation must be carried out with care and this section is concerned with the effect that smoothing has upon data and suggests how smoothing might be carried out in the most effective and least distorting way. In general it is always much better to use unsmoothed data, since any smoothing procedure is bound to introduce some sort of distortion to the spectra. Nevertheless, there are many cases where some smoothing is required, such as when very weak signals are recorded with a prohibitively long time needed to record a spectrum with a good signal-to-noise ratio or when a sample is decomposing and it is necessary to record a spectrum over a very small period of time. In addition it is often necessary to smooth data with a fairly good signal-to-noise ratio as a prerequisite to further analysis involving processes such as difference or derivative spectra.

Smoothing is a process that attempts to increase the correlation between points while suppressing uncorrelated noise. Smoothing is achieved by convolution of the data with a suitable smoothing function in an appropriate way. Two different types of smoothing process can be used, namely the least squares central point smoothing techniques proposed by Savitsky and Golay[1] and related methods, and the Fourier transform approach. The first method is the most common, and in its simplest form is found on most data systems.

A3.4.1 Least squares approach

This method involves convoluting the data with a convoluting function such that

$$y(0) = \sum_{i=-m}^{m} \frac{C_i f(i)}{\mathrm{NORM}} \qquad \text{(A3.1)}$$

where $y(0)$ is the smoothed point, which corresponds to the centre of an odd number interval of points, P ($p = 2m + 1$); $f(i)$ are experimental data points in the given interval, which are convoluted with the appropriate integers, C_i; and NORM is a normalizing factor.

In the simplest case, that of a moving average, $C_i = 1$ for all i and NORM = P. A least squares fit to the data over the interval P using a polynomial of degree n can be achieved exactly by using the above formula

since discrete integers, C_i, exist for distinct values of P and n. Hildebrand[2] and Proctor and Sherwood[1] quote a general formula for the necessary set of polynomials p.

In general a number of points concerning the use of this type of smoothing can be identified:[3]

(a) Smoothing increases with the number of points used in the smoothing interval. The optimum value for the smoothing interval is 0.7 (peak width at half maximum).

(b) Smoothing decreases as the degree of the smoothing polynomial increases. In general, fits to quadratic or cubic polynomials are more effective than those to higher order polynomials.

(c) Normal methods of smoothing cause a loss of points at each end of the spectrum. If the smoothing interval is of N points then the number of points lost from each end of the spectrum is $(N\text{-}1)/2$; thus the effect becomes more serious as the smoothing interval is increased. This effect can be eliminated by estimating the points lost by a suitable equation (equation 8 in Ref. 3). This allows the smoothing operation to be repeated as many times as desired.

(d) Smoothing can be repeated (especially when no points are lost when carried out as described in point c) in order to increase the amount of smoothing, though the largest amount of smoothing occurs during the first passage through the smoothing process. Repeat smoothing has the effect of generating a new smoothing polynomial which gives more emphasis to positive values, is broader than the original, has a height that falls as the function gets broader and causes ripples to occur at the extreme ends of the functions. This wide range of smoothing functions makes repeat smoothing a valuable process.[3] It is found that the smallest interval possible, repeated as many times as possible, is a good way to perform such a repeat smoothing operation, though the choice of smoothing interval and repeat number is not critical provided that the interval chosen is not too large with respect to the peak width.

Figure A3.2 and Table A3.1 show how the methods described above can be successfully applied to a typical core photo-electron spectrum. Thus a noisy O 1s spectrum (which can be fitted to three peaks) can be smoothed by a twenty-one-point interval repeated a hundred times (21 is 0.7 × peak width at half maximum), and the result compared with the same spectrum run for a long period of time. The smoothed spectrum contains no new information, of course, since smoothing is a cosmetic process,but the smoothed spectrum makes some spectral features more evident to the observer and so is more useful than the unsmoothed spectrum. Thus the smallest of the three peaks is more clearly present visually and in terms of the fitted information (Table

(a)

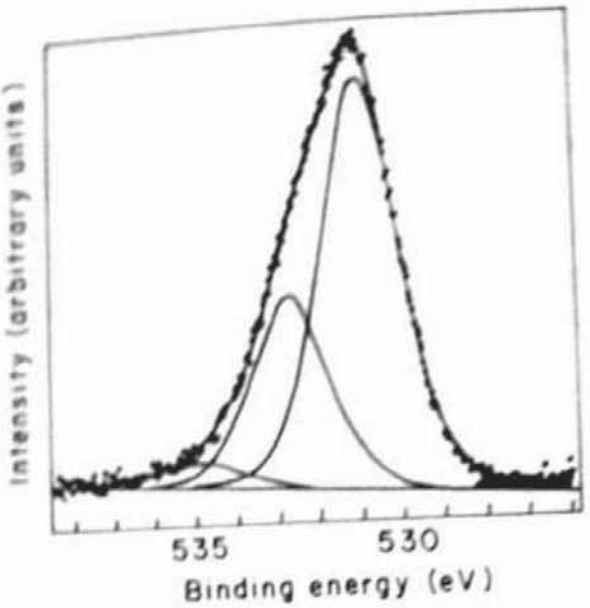
Intensity (arbitrary units)
535
530
Binding energy (eV)

(b)

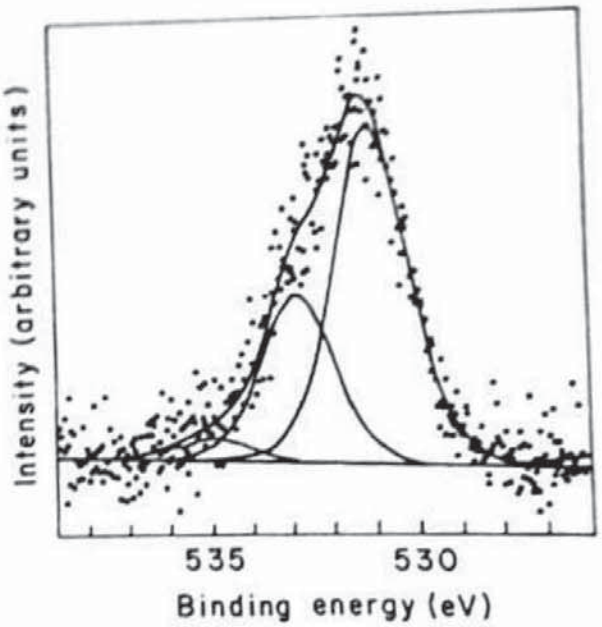
Intensity (arbitrary units)
535
530
Binding energy (eV)

(c)

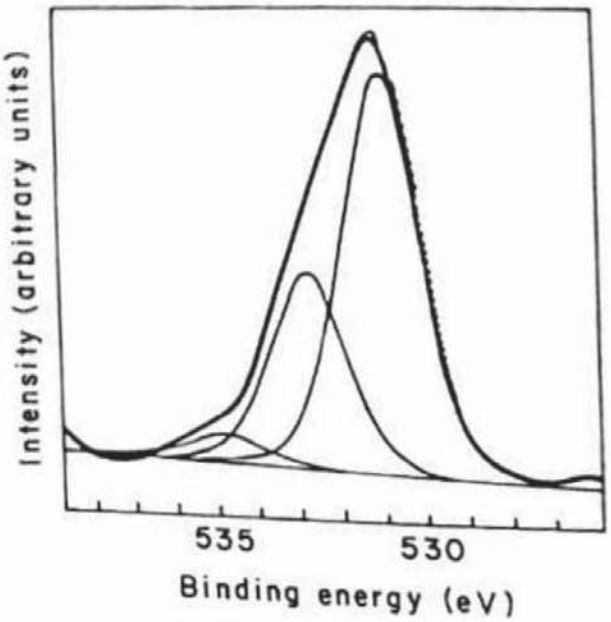
Intensity (arbitrary units)
535
530
Binding energy (eV)

Table A3.1 Non-linear least squares curve fitting results for and O 1s spectrum obtained with good statistics, poor statistics, and poor statistics smoothed

Parameter	Good statistics (Figure A3.2a)	Poor statistics (Figure A3.2b)	Poor statistics smoothed (Figure A3.2c)
Binding Energy, eV	534.81(16) 532.66(04) 530.95(02)	534.79(76) 532.74(18) 530.99(08)	534.73(12) 532.71(03) 530.99(01)
FWHM, eV	2.10(04)	2.04(15)	2.10(03)
Area ratio	1/7.77/16.90	1/7.44/14.94	1/7.08/14.34
Chi-squared	584.4	15636.9	321.97

Note. Figures in brackets refer to 95 per cent confidence limits.

A3.1) in the smoothed spectrum. Thus the chi-squared value (*vide infra*) falls to 42 per cent. of the original value when the third peak is added to the smoothed spectrum, but to only 97 per cent. of the original value in the unsmoothed spectrum.

A3.4.2 Fourier transform approach

Smoothing can be carried out by a very different approach which involves the use of Fourier transform analysis.[4–7] Fourier transformation of a spectral array containing noise results in a spatial frequency distribution for both the signal and the noise. It is possible to truncate the noise contribution in the spatial frequency distribution by multiplication with a suitable weighting function whereupon subsequent transformation back will result in a smoothed spectrum.

The problem with this approach is that a suitable weighting function must be chosen. Various approaches have been used[7–11] but much depends upon the degree of smoothing desired. An optimum S/N filter has been suggested by Turin,[11] but as the S/N ratio is increased so the peak resolution decreases.

Any smoothing methods involves many subjective factors and all methods must be used with great caution.

Figure A3.2 Oxygen 1s spectra illustrating the effect of smoothing. In all cases the spectra are fitted to three peaks, the details being given in Table A3.1. (a) Data for the same material obtained with good statistics by running the spectrum for a long period, (b) data for the same material with bad statistics by running the spectrum for a short period and (c) the result of smoothing the spectrum (b) 100 times with a smoothing interval of 21

A3.5 The Analysis of Overlapping Spectral Features

In many cases the information provided by photo-electron spectroscopy is contained in a spectrum that consists of a number of overlapping peaks, often of different peak shapes and intensities. In the core region the peaks will be a series of chemically shifted peaks, satellites, energy loss features and Auger peaks. In the valence region the spectra will reflect all the complex features of the ground-state valence band, together with complications due to the need to include the excited state (i.e. joint density of states) at low photon energies. In both cases no spectrum can be unambiguously analysed and there is no definite way to proceed with the analysis. Experimentally it is best to employ a monochromatized photon source, especially in the X-ray region, but this is not always available, and in any case the substantial loss of intensity may lead to unacceptable spectral collection times. There are two main ways to try to unscramble this information, namely deconvolution and curve fitting. Neither method can give a unique solution. Most attention has been given to curve fitting, though deconvolution has been applied with success to a number of spectra. Curve fitting is very dependent upon the initial 'guess', i.e. the number of peaks and their peak parameters, and deconvolution can provide valuable assistance in making the most suitable initial guess. Suitable initial guesses can also be assisted by derivative methods and curve synthesis. Certainly the application of as many approaches as possible will provide the best chance of a reasonable spectral interpretation.

A3.5.1 Deconvolution methods

A photo-electron spectrum has an observed spectral width that includes a broadening due to instrumental factors. These factors include the resolving power of the spectrometer and the line width of the photon source used (see Chapter 3). If one knew the exact contribution due to these factors and could construct a function (B) that described them, then it would be known that the observed spectrum was a convolution of the 'true' spectrum (f_t) and this instrumental function. The 'true' spectrum could then be obtained by the deconvolution of the observed spectrun (f_o) that arises from the way in which the experiment is constructed. The observed spectrum is related to the desired 'true' spectrum by a 'convolution' equation:

$$f_o = f_t B \qquad (A3.2)$$

The retrieval of f_t from f_o is referred to as 'deconvolution'. Random high-frequency noise leads to the addition of a noise term to equation (A3.2) which accounts for noise present in all real data to some extent. This noise term means that the deconvolution process is not unique, which has the effect of possibly introducing noise and spurious oscillations into the deconvoluted

spectrum. This serves to highlight the fact that such resolution improvement of enhancement is only achieved at the expense of the signal-to-noise (S/N) ratio in the same way that improvement in S/N ratio by smoothing is generally accompanied by a loss of resolution.[12,13]

Several methods have been used to deconvolute the effects of data distortion. These include differentiation techniques (*vide infra*). However, the three main methods used are:

(a) Direct solution of the convolution equation.
(b) Fourier transform analysis.
(c) Iterative techniques.

It is found that the success of the process depends less upon the method of deconvoltion chosen than upon the quality of the initial data. Data with very good statistics are an important starting point.

The whole subject has been very effectively reviewed by Carley and Joyner[14] and the reader is strongly advised to read this paper for a full discussion of this subject.

A3.5.2 Derivative spectra

Derivative spectra provide a useful method for peak location in appropriate cases. A number of workers[15–21] have pointed out the usefulness of derivative spectra. Automatic peak searching routines, based upon the properties of ideal derivatives, have been suggested, but in XPS these are only of limited use. Second-derivative spectra have been used[15,16] as a quick and easy method for the prediction of peak positions as well as providing useful information in themselves. In second-derivative spectra negative peaks occur corresponding approximately to overlapping peak positions in the original spectrum.

Derivative spectra cannot give accurate peak positions since one is examining the envelope of overlapping peaks so that the observed maximum of each peak is always shifted by the presence of other peaks. Nevertheless derivative spectra provide useful information. In general the most accurate peak position is observed when the differentiating convoluting interval[15] is similar to the FWHM of the component peaks, though there is a need to balance convoluting interval with resolution.

Figure A3.3 illustrates how second-derivative spectra can be used to predict the position and relative intensity in a simple two-component test spectrum based upon two overlapping O 1*s* peaks. The second-derivative spectrum shows two peaks of varying intensity, corresponding well to the amounts of the two overlapping peaks in the original spectrum. In addition to slight errors in peak position due to the factors discussed above the relative intensity of the two peaks is only approximate. This is due to the cancellation

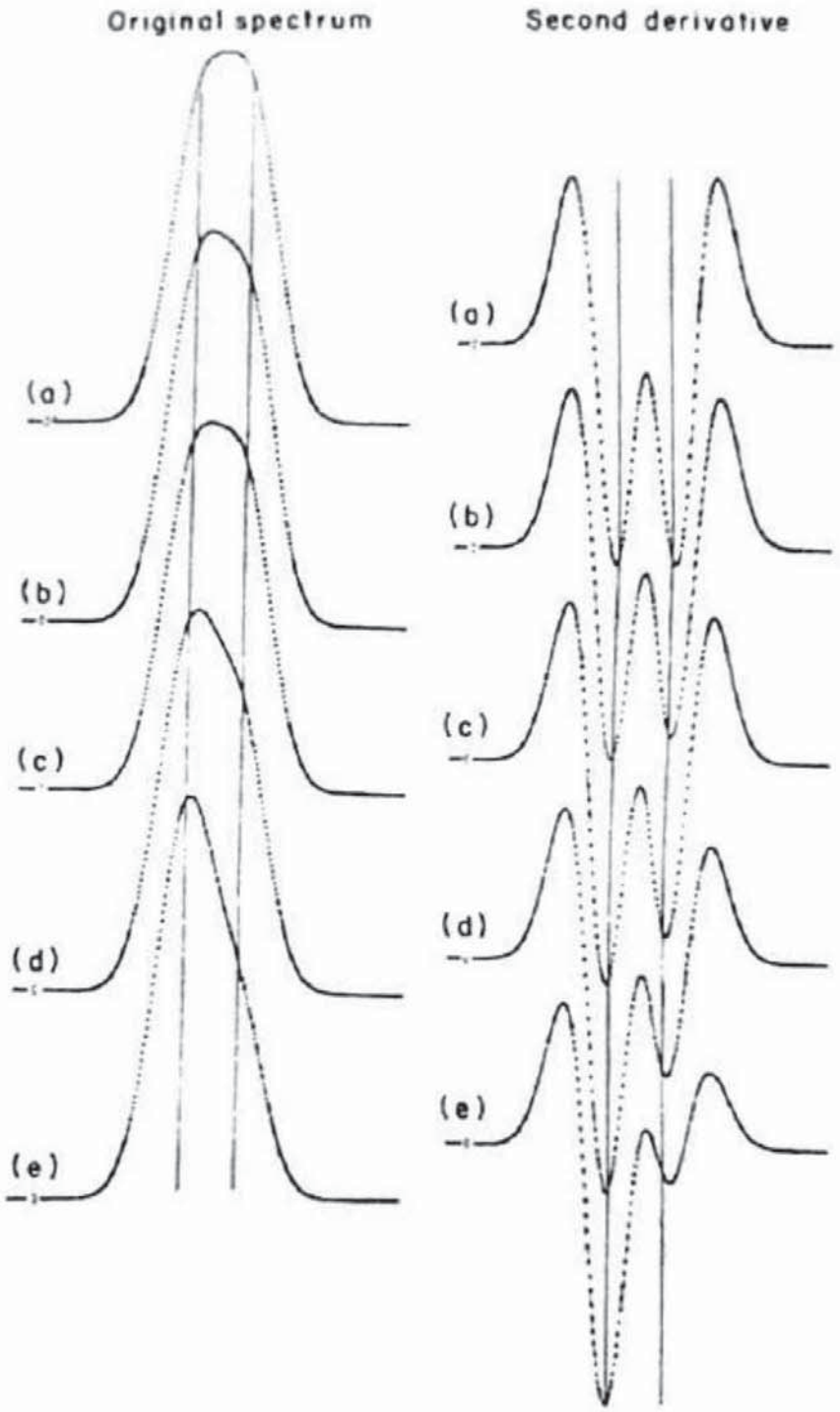

Figure A3.3 Second-derivative spectra of original model spectra consisting of two overlapping peaks of varying intensity: (a) 1 : 1, (b) 1 : 0.95, (c) 1 : 0.90, (d) 1 : 0.75, (e) 1 : 0.5. Convoluting interval = 21, FWHM = 60, separation = 50 channels

effects that occur when the positive lobe of one component peak overlaps with the negative lobe of the other peak. In general this effect will depend upon the number of component peaks, their widths and intensities.

Figure A3.4b shows the second derivative spectrum of a C 1*s* spectrum of a carbon fibre (Figure A3.4a) which consists of overlapping peaks. The ratio $Q = A/B$ gives some indication of the asymmetry of the C 1*s* peak, in the same way that measurement of peak width could indicate peak asymmetry.

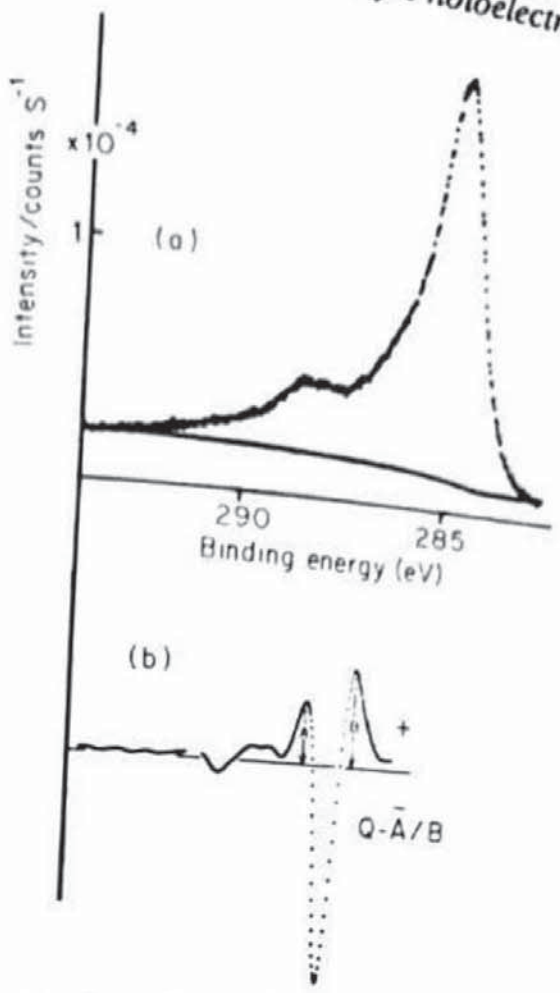

Figure A3.4 Second-derivative of a C 1*s* spectrum of a carbon fibre. (a) original spectrum, (b) second-derivative spectrum showing the way in which the Q factor is evaluated

However, accurate determination of Q is much simpler than any such width measurement, once the second derivative is obtained.

Figure A3.5 compares the smoothed second derivative of an O 1*s* spectrum with the curve fitted spectrum clearly illustrating the value of second-derivative spectra in providing a suitable guess to peak positions that can then be used in curve fitting.

Two relatively simple methods for calculating derivative spectra are available.

A3.5.2.1 Fourier methods

In this approach,[5,22] if $y(x)$ has the Fourier transform $F(s)$, then dy/dx has the Fourier transform $(i2\pi s)F(s)$. Extending this to the general nth derivative:

$$y(x) \rightleftarrows F(s) \quad \frac{d^n y}{dx^n} \rightleftarrows (i2\pi s)^n F(s) \tag{A3.3}$$

Thus, by applying the relevant weighting function in the Fourier domain,

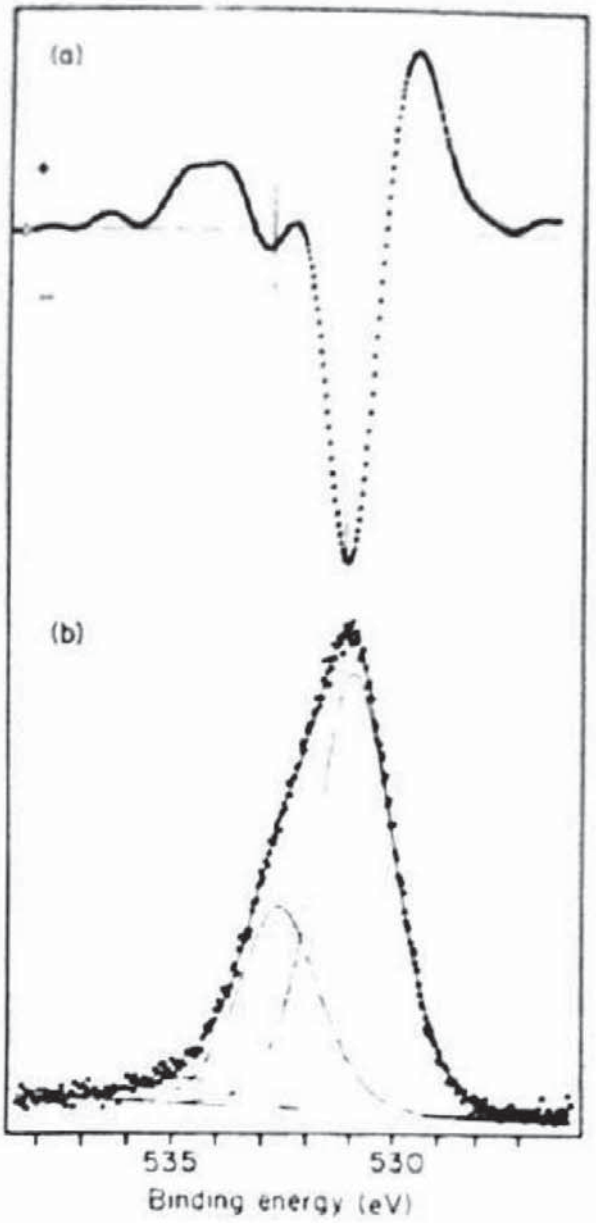

Figure A3.5 Comparison of peak prediction in an O 1*s* spectrum by means of (a) a second-derivative spectrum and (b) a non-linear least squares curve fitting to the original spectrum

the subsequent transformation will result in the generation of the *n*th derivative of the original data. However, because more weight is given to higher spectral frequencies (large *S*) the resultant derivatives will have increased noise associated with them.

A3.5.2.2 Polynomial methods

The derivative of a spectral point is simply the derivative of an initially fitted *n*th-order polynomial at that point. Thus the whole derivative spectrum can be obtained by sliding convolution processes exactly analogous to the

extended least squares smoothing approach.[3] The examples discussed here have all been calculated using this method.

As in the Fourier transform case, differentiation using this method also enhances noise characteristics[15] and so even spectra with high S/N characteristics require some prior smoothing.

Repeating the derivative process does produce a fairly satisfactory higher derivative (i.e. first-derivative procedure repeated n times gives an approximation to the nth derivative) and so initial convoluting functions of greater complexity than first or second need not be known. However, practical use of derivatives greater than $n = 2$ is very limited.

A3.5.3 Curve synthesis

A spectrum can be synthesized by using digital or analogue methods to sum a series of functions representing individual peaks in order to produce a final function that closely represents the experimental spectrum. The peak function is generally designed to be a function of appropriate peak variables such as position, intensity, width, function type and peak tail characteristics. Simple curve synthesis can readily be carried out on a microcomputer system or an analogue curve-fitting device such as a Du Pont curve analyser. The microcomputer system has the advantage that a wider range of functions can be used, and the result of the fit can be rapidly displayed graphically together with the appropriate statistical information to allow the quality of the fit to be evaluated. Such a curve synthesis provides a useful initial guess for the more thorough process of non-linear least squares curve fitting which is described below.

A number of types of function have been used for this purpose, the most common being Gaussian or Lorentzian functions. In a work of the author and others[23] a mixed Gaussian/Lorentzian function is used, the one found to be most effective in practice being a product function:

$$f(x) = \frac{\text{peak height}}{[1 + M(x - x_0)^2/\beta^2]\exp\{(1 - M)[\ln 2(x - x_0)^2]/\beta^2\}} \quad \text{(A3.4)}$$

where x_0 is the peak centre and β is a parameter that is nearly 0.5 (FWHM). The actual FWHM is calculated from β using an iterative method. M is the mixing ratio and takes the value 1 for a pure Lorentzian peak and the value 0 for a pure Gaussian peak.

Curve fitting of this type assumes that a particular peak profile(Gaussian or Lorentzian) is uniquely characterized once its peak width at half maximum (PWHM) has been fixed, and cannot be resolved into subcomponents. In 1968 Perram[24] showed that a single Gaussian profile ($y = \exp(-x^2/2.05)$) could be represented by the sum of two separate Gaussian profiles ($y = \pm 0.515359 \exp[-(x \mp 0.244622)^2/2(0.988937)^2]$), suggesting that the

numerical decomposition of a structureless contour is not unique. However Baruya and Maddams[25] have shown that this result is atypical since it relates to two component peaks of equal intensity and half width, symmetrically separated by −10 per cent of their half widths on either side of the initial Gaussian peak. They conclude that in most practical situations, Gaussian and Lorentzian profiles are unique and curve fitting may be undertaken. The scope and limitations of curve fitting in general have been discussed by Maddams.[13]

A3.5.3.1 Chi-square (X^2)

The quality of the curve fit obtained can usefully be evaluated by evaluation of the weighted χ^2, which is defined as

$$\chi^2 = \sum_{r=1}^{n} w_r[y_r - f(x_r/q)]^2 \qquad \text{(A3.5)}$$

where y_r is the observed count at $x = x_r$, $F(x/q)$ is the fitted peak envelope, k is the total number of points in the spectrum and w_r is a weighting function which in this case is chosen as y_r^{-1}, thus making χ^2 equal to the χ^2 statistic.[26–28]

A3.5.3.2 Goodness of fit

The value of χ^2, or more particularly $\Delta\chi^2$ from one fit to another on the same data, provides the statistical information about the 'goodness of fit'.

Strictly speaking, only χ^2 values with the same number of degrees of freedom f ($f = k$ − number of free parameters) can be directly compared. Athough f may vary slightly from fit to fit this is generally insignificant. Also by the very nature of χ^2, the larger the spectral intensity, the larger the associated χ^2 values for a similar quality fit. Thus, although a change in χ^2 from fit to fit for the same data is meaningful, comparison of χ^2 values for different spectra is meaningless unless the peak intensities are equal.

A3.5.3.3 Tail information

Three tail parameters have been used by the author, namely a constant tail ratio(CT), an exponential tail ratio (ET) and the tail mixing ratio (TM. The tail function (T) used then becomes

$$T = \mathrm{TM} \cdot \mathrm{CT} + (1 - \mathrm{TM})\exp(-D_r \cdot \mathrm{ET}) \qquad \text{(A3.6)}$$

where D_r is the separation from the peak centre in channels. The peak function to the right of the peak centre is chosen to have no tail and can be represented as $\mathrm{H} \cdot GL$, where H is the peak height and GL the peak function.

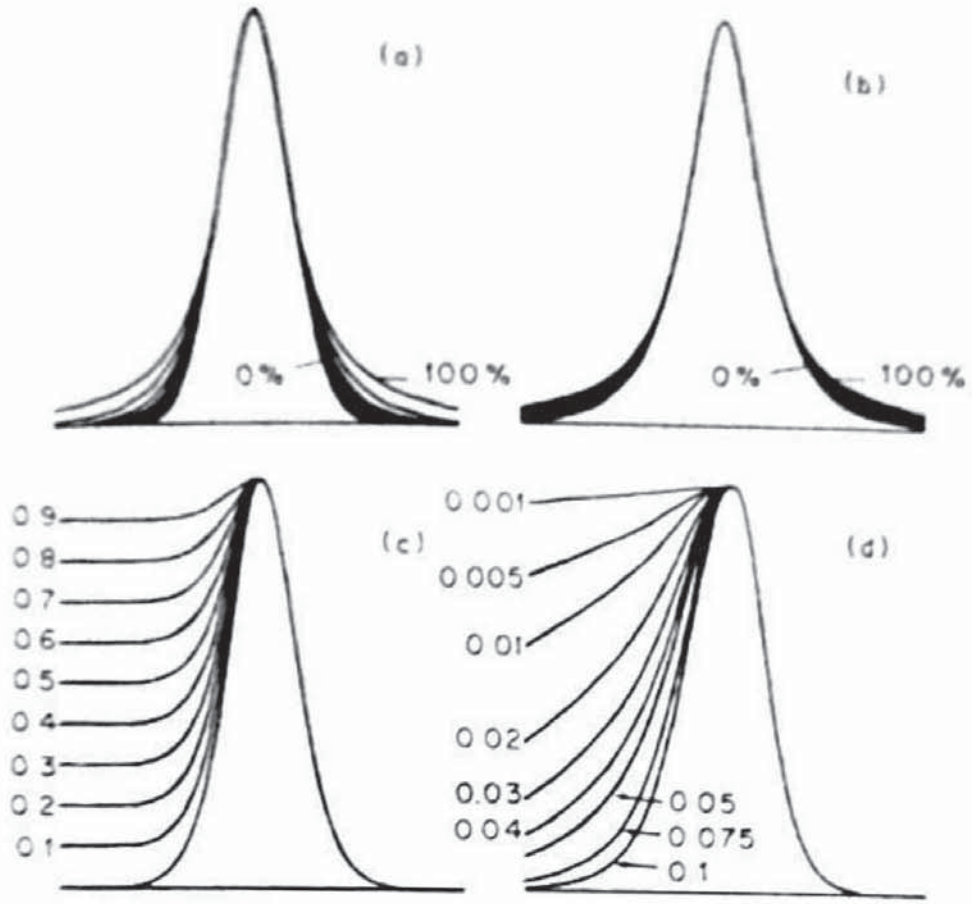

Figure A3.6 Possible peak shapes obtained with a Gaussian/Lorentzian product function by varying the mixing ratio and tail parameters. (a) Variation of the mixing ratio in steps of 10 per cent from 10 to 100 per cent Lorentzian character. (b) As (a) but the range is in steps of 1 per cent from 88 to 100 per cent. (c) Variation of constant tail parameters. (d) Variation of exponential tail parameters.

The peak function with the tail may be represented as

$$Y = H[GL + (1 - GL)\ T] \qquad \text{(A3.7)}$$

Figure A3.6 shows the way in which peak shapes can be synthesized by the variation of the peak parameters in the Gaussian/Lorentzian product function combined with the tail parameters.

A3.5.4 Non-linear least squares curve fitting

This attempts to optimize the curve synthesis process by using the method of non-linear least squares, which recognizes that the process concerned may be complex, in that the appropriate parameters enter into the algebraic expression that describes the process in a non-linear manner. Such is the case for photo-electron spectral data which can be represented as a function $F(x/g)$ (see equation A3.5 above) which depends in a non-linear manner upon the parameters (q) described above. The process to minimize χ^2 is carried out computationally, rather than manually, by the operator of the curve synthesis

process by a procedure of guessing. A number of possible non-linear least squares methods are available. The author uses the Gauss–Newton method. In this method the requirement for the minimization of χ^2 allows one to construct the equations:

$$0 = \frac{\partial \chi^2}{\partial q_i} = -2 \sum_r w_r [y_r - F(x_r/q)] \left(\frac{\partial F}{\partial q_i}\right)_{x=x_r} \qquad \text{(A3.8)}$$

which gives k equations where k is the number of parameters q. The problem is a non-linear one, since q values enter non-linearly. If one puts

$$q_i = q_i^0 + \delta_i \qquad \text{(A3.9)}$$

where q_i is the value of q which minimizes χ^2, q_i^0 is some initial guess and δ_i is the correction requires to q_i^0 to give q_i. If

$$F_r = F(x_r/q^0) \qquad \text{and} \qquad F_r^j = \left(\frac{\partial F}{\partial q_i}\right)_{x=x_r, q=q^0} \qquad \text{(A3.10)}$$

then one can expand $F(x_r/q)$ as a Taylor series where the series is truncated after the linear terms, i.e.:

$$F(x_r/q) = F_r + \sum \delta_j F_r^j \qquad \text{(A3.11)}$$

where $j = 1,2, \ldots, k$. Then equations (A3.8) can be rewritten to give k linear equations:

$$0 \approx \sum_r w_r [y_r - F_r - \sum_j \partial_j F_r^j] F_r^j \qquad \text{(A3.12)}$$

These equations can be solved by an iterative process, the process being stopped when the δ_i values (equation A3.9) vary by an insignificant amount for all δ_i values from one iteration to the next. The process does not always move steadily to convergence and problems may arise such as the matrices calculated being singular or having a negative determinant. The process has the advantage that it allows a certain amount of valuable statistical information, such as the standard deviations of all the calculated parameters, to be calculated. Such information allows some quantitative significane to be attached to the calculated parameters. In addition to the final χ^2 value, the probability that χ^2 is less than χ^2 (calculated) can be evaluated.[24] Normally a value less than 95 per cent. is considered statistically significant, though it must be remembered that the stringency of this test is greated when the number of electron counts is large. In general the most useful approach is to compare how χ^2 or f changes for different fits to the same spectrum rather than to use the information in any absolute sense. All this information may well assist in the overall decision of the 'best fit'. Such a decision must rest upon the statistical information consistent with chemical and spectroscopic sense. Often no unique solution is provided, but the spectrum can be reduced

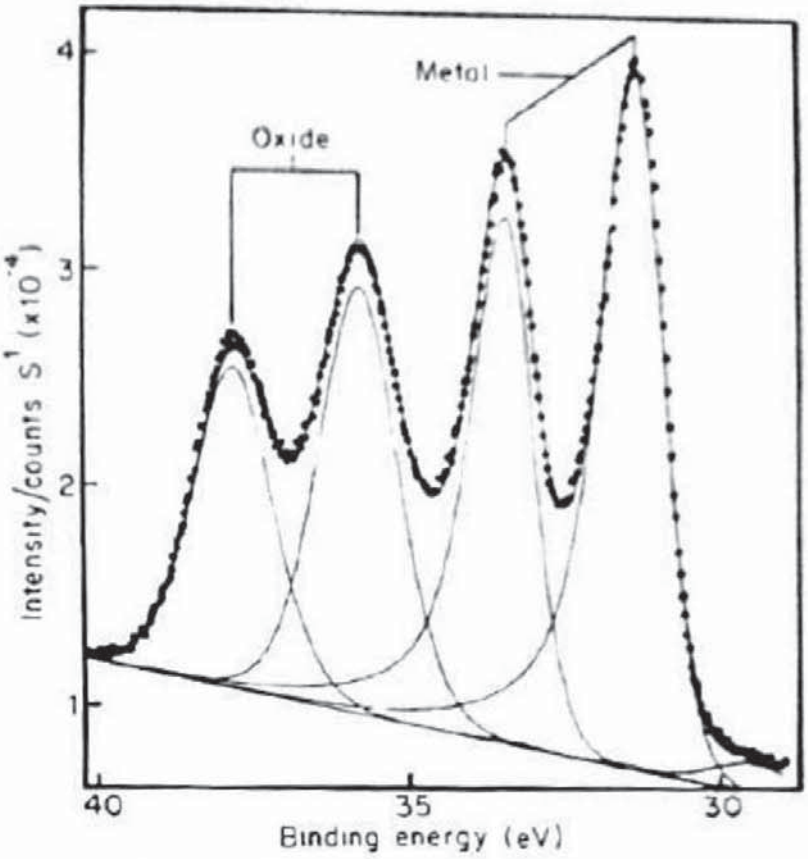

Figure A3.7 Curve-fitted W 4*f* spectrum

to a number of slightly different possibilities allowing the amount of significant information provided by a particular spectrum to be assessed. An example of such a case has been provided.[29]

The process as carried out in practice can be illustrated with the aid of the W 4*f* spectrum illustrated in Figure A3.7. This spectrum contains four clearly resolvable peaks, which for the purposes of the fit are split into two separate groups of two peaks: one group for the oxide (WO_3) and the other for the metal. Such separation into different groups is necessary when peaks are known to have different widths and tail parameters.

Each peak has even parameters associated with it:

(a) Peak centre
(b) Peak height.
(c) Peak width.
(d) Gaussian/Lorentzian peak shape mixing ratio.
(e) Constant tail height.
(f) Exponential tail slope.
(g) Constant/exponential tail mixing ratio.

Thus for n peaks are $7n$ peak parameters. In addition there are also the linear background slope and intercept. Thus a maximum of $7n + 2$ parameters can be allowed to vary or 'float' as desired. However it is impossible to

let this happen in practice and so some parameters (generally parameters d to g) are fixed.

The spectrum is fitted to the Gaussian/Lorentzian product function described above with a mixing ratio M of 0.5 for all peaks and a spin-orbit splitting intensity ratio of each doublet fixed at the expected value for $4f_{5/2}$: $4f_{7/2}$ of 1/1.333 (see Chapter 3). The tail parameters are different for the oxide and metal peaks. The asymmetry in the metal peak shape is due to conduction band interaction effects,[30-32] and in this case is accounted for by adding some exponential tail characteristic to the high binding energy side of the metal peaks (the amount being determined from a previous fit to a pure metal spectrum). We have found that using such a method is satisfactory for most purposes, though it is different from the method used by Hufner and Wertheium,[31] who first deconvoluted the instrumental broadening function from the observed data and then fit the deconvoluted data with the Doniach and Sunjic[30] lineshape. The results, shown in Table A3.2, show that the asymmetric tail in the calculation of peak intensity (area) for the metal peaks is clearly very significant.

The fit calculates a linear background slope and intercept which is often satisfactory though removal of a non-linear background can be useful (*vide infra*). X-ray satellite contributions were also taken into account, the full statellite peaks being added to each peak in the fit. The satellite contribution is very noticeable at the lower binding energy.

It should be clear that non-linear least squares curve fitting is preferable to analogue curve synthesis as it provides a quantitative handle with which to gauge the quality of the fit and, unlike analogue methods, peak parameters are perfectly reproducible. Most important is that operator subjectivity is largely eliminated.

Table A3.2 Results of curve fit to W 4*f* spectrum ($\chi^2 = 2855, f = 298$) (Figure A3.7)

	Oxide		Metal	
	5/2	7/2	5/2	7/2
Binding energy*, eV	37.66(0.01)	35.75(0.01)	33.5(0.01)	31.50(0.01)
Separation, eV	1.91(0.01)		2.00(0.01)	
PWHM†, eV	1.43(0.01)		1.01(0.01)	
Intensity $\times 10^{-7}$ (peak area)	1.127(1%)	1.503	31.720(1%)	2.293
Relative intensity	1	1.333	21.323(1%)	1.764
Exponential tail slope	20.0	20.0	1	1.333
			0.032	0.032

*Reference C 1*s* = 284.6 eV.
†Excluding exponential tail contribution.
‡Including exponential tail contribution.

A3.6 Background Removal

The accurate removal of the background contribution to a spectrum is a process that must be carried out with care since, except in the case of the trival removal of a horizontal background discussed above, it may involve distortion of the data when incorrectly carried out. Any background removal will alter absolute peak intensities and will cause problems with any quantification model which must be defined with respect to clear background conditions. There is no definite way to remove a background and the whole process is still controversial (see Chapter 5).

A rather crude removal of the background may be achieved by removal of a linear background drawn as a straight line between the first and last set of points in a spectrum. The correct choice of a first and last set of points, or a suitable average over them, has a critical effect upon the resulting background. Such a process is best not carried out directly but may be included in the curve-fitting process as described above and illustrated in Figure A3.7. This means that the original data are not altered and if a non-linear background has been removed, as described below, then such a linear background would be expected to be horizontal, as shown in Figure A3.9 below.

The removal of a non-linear background requires a complete understanding of the processes that give rise to background electrons. Such a process will involve inelastic electron ejection processes, but the background must be distinguished from any peaks, which may be broad and difficult to distinguish, that may arise from specific elastic processes such as satellite peaks of various sorts and Auger electron peaks. In addition any angular dependence of the background (which may be machine dependent since β factors will differ for different machines; see Chapter 5) and inhomogeneities in the material may cause problems. The problems that may arise from plasmon losses and asymmetric broadening being confused with the inelastic background has been pointed out.[33] The most common method of non-linear background subtraction, often called the Shirley method, considers the background at any point due to inelastically scattered electrons, is assumed to arise solely from the scattering of electrons of higher kinetic energy and is thus proportional to the integrated photo-electron intensity to higher kinetic energy. The method has been used by a number of workers[34-38] and various refinements have been introduced. Bishop[39] has modified this model to include a linearly falling contribution to the background of inelastically ejected electrons as the energy falls from high to low kinetic energy. In general the non-linear background removal becomes more and more prone to error as the energy range over which the background is subtracted is increased, so while modified models such as that due to Bishop may help, problems due to features such as negative peaks may appear when the energy range is large. It is important to ensure that the beginning and end of the spectral region that is to be back-

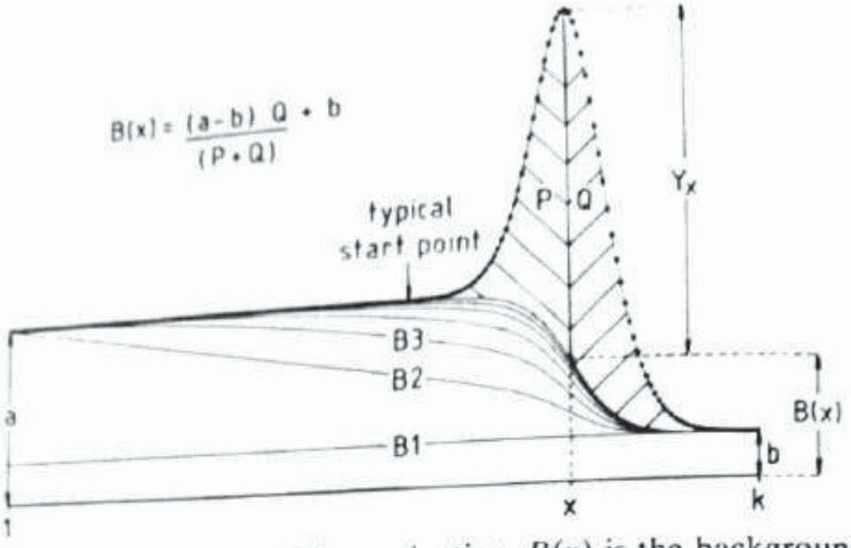

Figure A3.8 Inelastic background determination. $B(x)$ is the background at point x in the spectrum which contains k equally spaced points

ground subtracted represents points on the background profile (rather than a part of some specific peak) or else the background removal process will remove significant peak intensity.

Non-linear background subtraction may be performed in the way used by the author,[15] which is illustrated in Figure A3.8. In such a spectrum the value of the background at a point x in a spectral array of k equally spaced points of separation h is

$$B(x) = \frac{(a-b)Q}{P+Q} + b \tag{A3.13}$$

where a is the average start point, b the average end point, $(P + Q)$ the total background subtracted (BS) peak area and Q the (BS) peak area from point x to point k. Using the trapezoidal rule:

$$Q = h\left[\left(\sum_{i=x}^{k} y_i\right) - 0.5(y_x + y_k)\right] \tag{A3.14}$$

the (BS) areas are calculated initially by choosing a linear constant background of magnitude b, line B1 in Figure A3.8. Substitution in equation (A3.13) leads to the background B2 which is then used to calculate new (BS) areas resulting in the background B3. The process is repeated until $(P = Q)$ remains essentially unchanged on successive iterations. Typically the start point is chosen close to the peak to minimize the number of required iterations. In Figure A3.8 the start point is somewhat removed from the peak to illustrate the iterative process; however the final result will be the same.

The term $0.5\ (y_x + y_k)$ is the correction introduced by the trapezoidal rule to the simple sum of points over the range x to k. In determining $(P = Q)$,

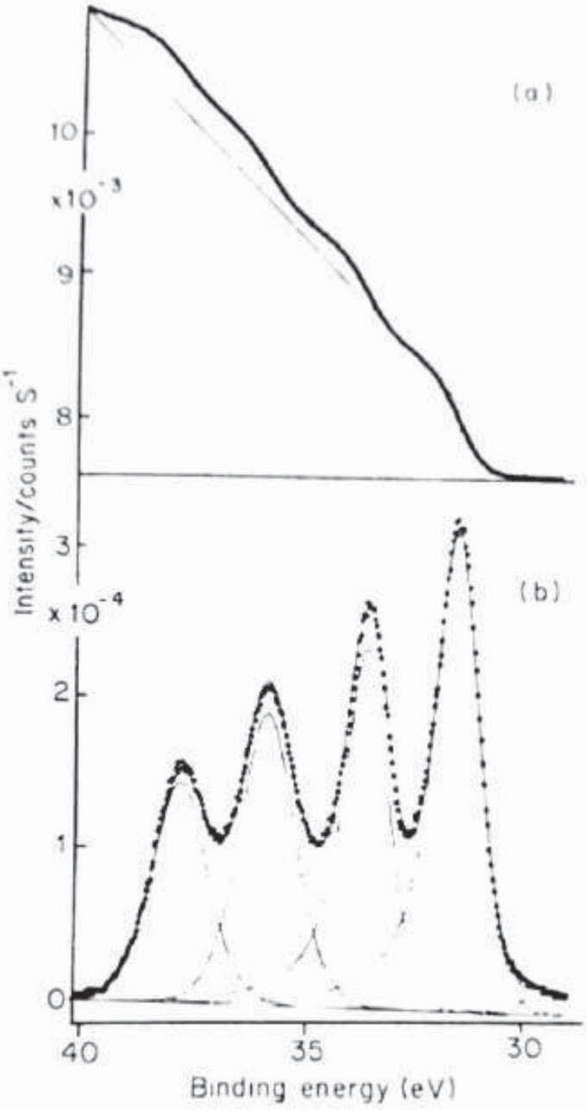

Figure A3.9 W 4*f* spectral region. (a) Inelastic integral background spectrum in comparison with linear background. (b) Spectrum with integral background subtracted and curve fitted

where $x = 1$, y_1 and y_k both zero, the latter correction is insignificant. As x increases the correction does become more significant since y_k increases.

Figure A3.9(a) shows the calculated background for the W 4*f* region of Figure A3.7 compared with the computer-calculated linear background from the fit. It is generally true that a linear background underestimates the 'true background' to the high binding energy side of a peak, the converse being true at the lose binding energy side. This could be of major significance in determination of peak areas and subsequent peak area ratios. In this case, as shown by the fit in Figure A3.9(b), the effect is minimal. A point to note, however, is that at the low binding energy side of the peak there is still intensity due to an X-ray satellite. The satellite is accounted for by allowing the fitted background slope to vary such that a sloping linear background is

calculated, but it is much less than before. A horizontal background could have been obtained by estimating the position of the true background intensity at the low binding energy side of the peak prior to subtraction.

A3.7 Difference Spectra

Difference spectra can be a very useful method for data analysis of a range of similar samples subjected to different amounts of chemical treatment. The simple subtraction of one spectrum from another is a trivial operation, but the proper use of difference spectra requires this subtraction process to be carried out with care and according to clearly defined criteria. The application of this technique to XPS has recently been discussed[15] and it has been shown that there are a number of points, specific to XPS, that need to be considered.

A3.7.1 Alignment

The first step in any difference spectra process is to ensure that the two spectra have been correctly aligned, i.e. that their data points correspond directly in kinetic energy value. This generally requires that the two spectra contain the same number of data points. Careful checks of calibration must then be carried out to ensure this correct alignment. It has been shown[15] that small differences in spectral alignment can cause large differences in the resulting difference spectra, stressing the importance of carrying out this operation with care and accuracy. Methods for using difference spectra to obtain good spectral alignment have been discussed.[15]

A3.7.2 Normalization

When the spectra have been correctly aligned it is then necessary to carry out a normalization process before the difference spectra is calculated. This requires that all the points in one spectrum be multiplied by this factor before the spectra are subtracted. The process of normalization requires that one knows the exact proportion of one spectrum in the spectrum from which it is to be subtracted. When one is attempting to subtract two spectra, each of which contains clearly separated chemically shifted peaks, the process is trivial, but such cases would hardly benefit from difference spectra. The typical difference spectrum is obtained from spectra that contain a number of overlapping peaks which makes normalization non-trivial and central to the difference spectral process. Thus one needs to know the correct answer before carrying out the process! Normally the two spectra are treated by appropriate preliminary methods such as smoothing (using the same smoothing parameters) and background subtraction (bearing in mind the problems discussed above). Then the maximum points in the two spectra are identified and the

spectra adjusted so that these maximum points are the same (ten thousand in the spectra illustrated here). After this preliminary process normalization can be carried out and it is possible to identify three types of normalization process that can be carried out in a clearly defined manner:

(a) Height normalization.
(b) Optimal normalization.
(c) Area normalization.

Height normalization and area normalization are processes that can be carried out easily. Optimal normalization represents an attempt to obtain the 'correct' normalization factor by an iterative procedure. The normalization process can be illustrated (Figure A3.10) using model C 1*s* spectra A and B, where spectrum B consists of a number of overlapping chemically shifted peaks B, B1, B2 and B3 and spectrum A is a single peak. Spectrum B is then subtracted from spectrum A to hopefully reveal the weaker peaks B1, B2 and B3.

A3.7.2.1 Height normalization

Having carried out the preliminary procedures on the aligned spectra, described above, then a normalization factor x can be defined. If the height of

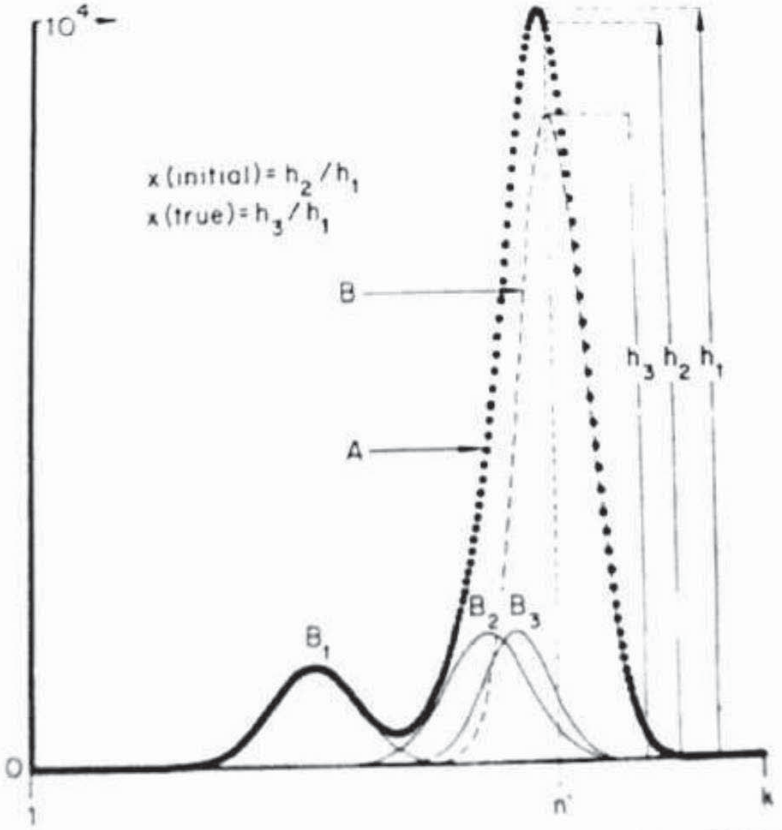

Figure A3.10 Model C 1*s* 'oxidized' spectrum, A, comprising 'unoxidized' component B, and chemically shifted components B1, B2 and B3

the peak maximum of the most intense peak in a spectrum to be subtracted (which will be called spectrum B) from another spectrum composed of a number of peaks (which will be called spectrum A) is h_3, and the height in spectrum A at this peak maximum is h_1, then

$$x = h_3/h_1$$

as illustrate in Figure A3.10. Unfortunately x is not generally known though it must be less than unity. Simple height normalization is then carried out with x = unity. This type of height normalization can be applied to assist in alignment of the two spectra.[15]

A3.7.2.2 Optimal normalization

Optimal normalization is based upon the idea that it might be possible to obtain a better value for x than unity by using iterative methods. The method used by the author[15] decreases x below unity and then follows certain properties of the resulting difference spectrum until x is considered to be at its optimum value. The most successful test criterion in model spectra was found to be that the difference spectrum should maintain a negative slope in the region bounded by the peak maximum of spectrum B and the right-hand side of spectrum A (points n' and k in Figure A3.10), i.e.:

$$(\mathrm{A} - \mathrm{B})\,(n) > (\mathrm{A} - \mathrm{B})\,(n - 1) \qquad \text{(A3.16)}$$

where n varies from n' to $(k - 1)$.

Starting with a value of $x = x(\text{initial}) = h_2/h_1$ (thus ensuring that the calculated value of x will always be less than or equal to 1.0) the procedure then tests expression (A3.16).[16] If the criterion is not satisfied for a particular pair of points the value of x is reduced by an amount $0.01x(\text{initial})$, and the test begins again. When (A3.16) is satisfied over the whole region, n' to k, the value of x is $x(\text{optimal})$ and the spectra are optimally normalized (ON). Using this process with model spectra it was possible to obtain a value of x of 0.854, very close to the correct value of 0.855 for the example chosen. In real spectra it has been found that the range of the test must be reduced from the right-hand side of spectrum A by C channels (Figure A3.10) or else the optimal value of x may fall to zero!

A3.7.2.3 Area normalization

The value of x is chosen to be the ratio of the total area of the spectrum of interest(spectrum A) and the total area of the reference spectrum(spectrum B). In contrast to the height and area normalized spectra this normalization factor will be greater than unity. The resulting difference spectrum will contain negative peaks corresponding to the fact that spectrum A contains other

features than just spectrum B; the less of spectrum B in spectrum A then the larger will be the negative peak. If x(optimal) is obtained as above and x(area normalization) is also evaluated, these two normalization factors can give useful quanitities. Thus the fraction of the reference spectrum(B) in the spectrum of interest(A) will be x(area normalization)/x(optimal) and thus the difference between this fraction and unity is the fraction of the total area due to spectral features other than the reference spectrum. Thus if the reference spectrum were that of a pure metal and the spectrum of interest contained metal and oxide, such a calculation would allow the amount of oxide in the spectrum to be evaluated. This might usefully be compared with curve-fitting results.

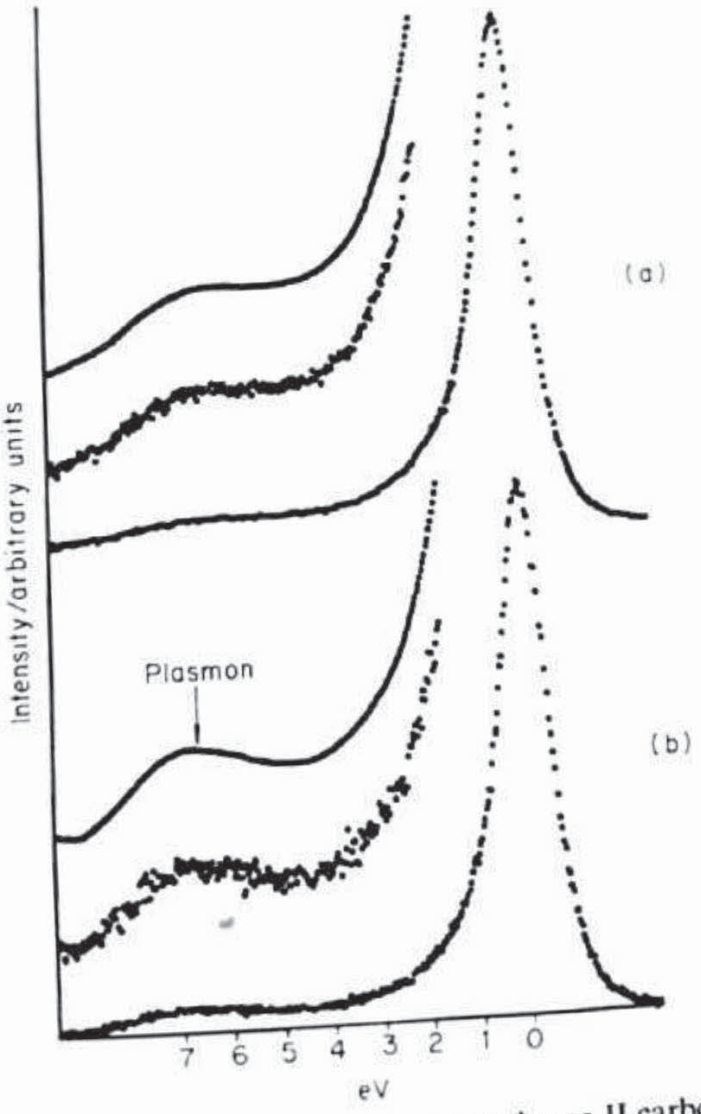

Figure A3.11 C 1*s* spectra obtained from untreated type II carbon fibres: (a) B1, at ambient temperature, (b) B2, after heat treatment to 1400 °C. In addition to the original spectrum, the plasmon region is shown magnified and smoothed (P = 21, 15 times)

A3.7.3 Examples of difference spectra

Figure A3.12 illustrates the difference spectrum obtained when the two spectra illustrated in Figure A3.11 are subtracted. The two spectra show only small visual differences, but the difference spectra highlight these differences. Thus the area normalized spectrum shows that there are more chemically shifted C 1s groups in B1 than in B2, since there is a large negative peak in the spectrum corresponding to the 'graphitic' carbon (chemical shift shown as zero). The height normalized spectrum is shown, together with other spectra corresponding to smaller values of x. The optimal normalization factor is satisfied with $C = 30$ for $x = 0.95$. As expected, the value of x(optimal) varies as C is varied, as shown in Figure A3.13, but 0.95 corresponds to a

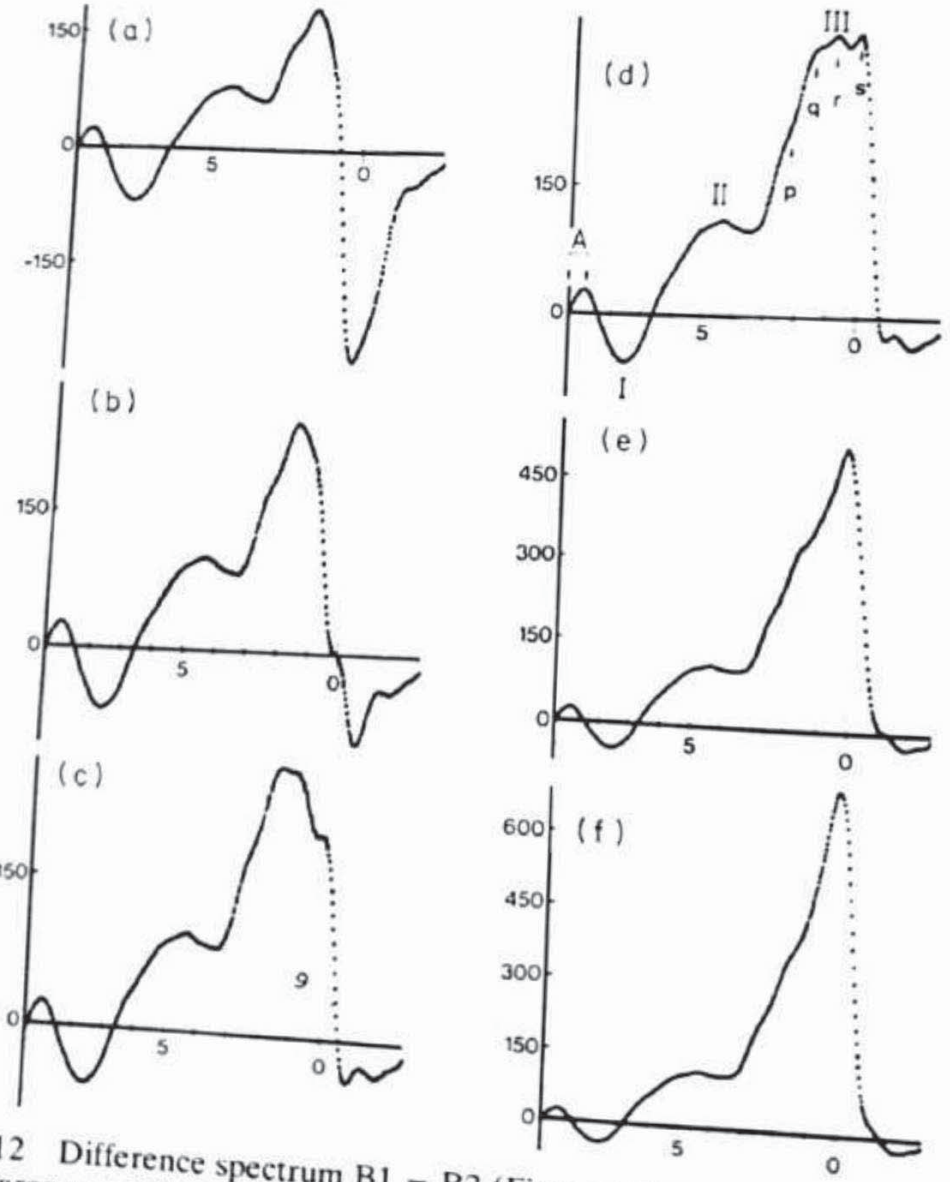

Figure A3.12 Difference spectrum B1 − B2 (Figure A3.11). Various normalization factors: (a) area normalized $z = 1.03$, (b) height normalized $x = 1.0$, (c) $x = 0.98$, (d) $x = 0.97$, (e) optimally normalized $x = 0.95$, (f) $x = 0.93$

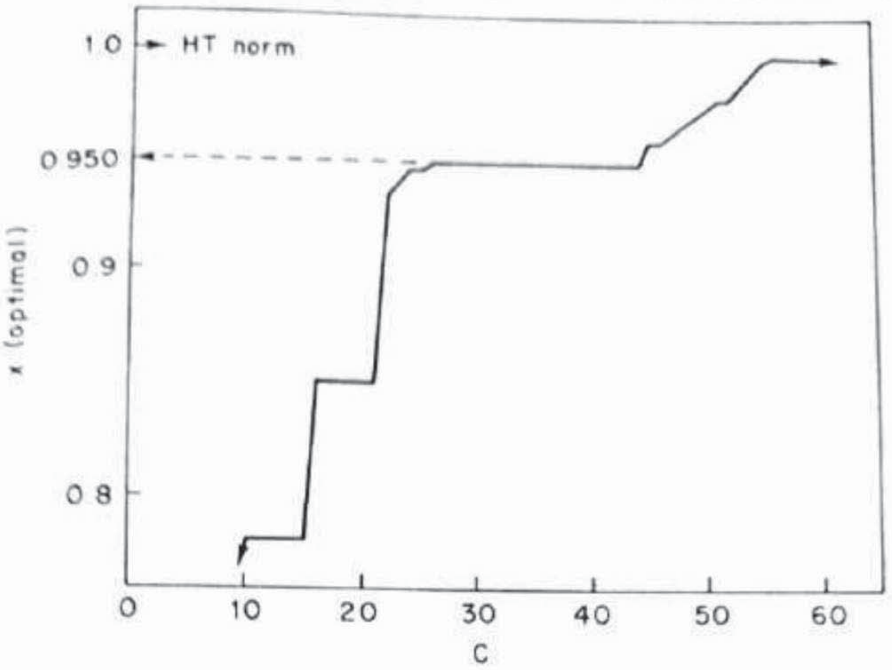

Figure A3.13 Variation of x (optimal) with C for the difference B1(3)−B2(1)

plateau in the graph which makes it seen a suitable value. In fact, the spectrum with $x = 0.97$ seems to contain more information, which may mean that it represents a more suitable choice of x than the optimal value which may mean that the test is too severe. Region I is thought to correspond to a difference in the plasmon intensity in the two spectra, and regions II and III to differences in surface C/O groups. Clearly the choice of x(optimal) in real spectra requires subjective decisions and is not uniquely defined as are area and height normalized spectra. However, real information is present and, when combined with other data analysis methods, can lead to useful chemical information.

A3.8 Conclusions

Data analysis clearly has a vital role to play in the interpretation of X-ray photo-electron spectroscopy. This appendix has attempted to present the main techniques that are currently available and provide suitable illustrations of their application. Much time and effort can be spent upon data analysis, and one needs to be careful not to over-interpret the data. However, there are many systems where spectral changes are very small but highly significant, and in such cases careful data analysis may provide the only means of extracting useful results. The ready availability of cheap data-collection systems should encourage more workers to collect digital data, and hopefully use such techniques to improve spectral accuracy. Great care must be taken in data analysis that changes the original data or attempts to provide automated

information on peak positions, peak intensities or even elemental composi-
tions. Such an analysis may be based upon approximations and assumptions
about the sample that makes these methods incorrect and highly misleading
when used in certain situations. Notwithstanding the need for care and discre-
tion in their application, the wider application of data analysis methods will
clearly make an important contribution to the future useful development of
photo-electron spectroscopy.

Acknowledgement

I would like to thank the American Chemical Society for permission to repro-
duce many of the figures in this appendix. I would also like to thank Dr
Andrew Proctor for his contribution, while a research student and postdoc-
toral fellow, to a number of the data analysis methods described here.

References

1. A. Savitsky and M. J. E. Golay, *Anal. Chem.*, **36**, 1627 (1964).
2. F. B. Hildebrand, *Introduction to Numerical Analysis*, Chap. 7, McGraw-Hill, New York (1956).
3. A. Proctor and P. M. A. Sherwood, *Anal. Chem.*, **52**, 2315 (1980).
4. W. F. Maddams, *Appl. Spec.*, **34**, 245 (1980).
5. J. O. Lephardt, *Transform Techniques in Chemistry* (Ed. P. R. Griffiths), Chap. 11, p. 285, Plenum Press, New York (1978).
6. G. Horlick, *Anal. Chem.*, **44**, 943 (1972).
7. K. R. Betty and G. Horlick, *Appl. Spec.*, **30**, 23 (1976).
8. T. A. Maldacker, J. E. Davis and L. B. Rogers, *Anal. Chem.*, **46**, 637 (1974).
9. D. W. Kirmse and A. W. Westerberg, *Anal. Chem.*, **43**, 1035 (1971).
10. C. A. Bush, *Anal. Chem.*, **46**, 890 (1974).
11. G. L. Turin, *IRE Trans. Inform. Theory*, **IT-6**, 311 (1960).
12. R. R. Ernst, *Advances in Magnetic Resonance* (Ed. J. S. Waugh), Vol. 2, p. 1, Academic Press, New York (1966).
13. W. F. Maddams, *Appl. Spec.*, **34**, 245 (1980).
14. A. F. Carley and R. W. Joyner, *J. Electron Spectrosc.*, **16**, 1 (1979).
15. A. Proctor and P. M. A. Sherwood, *Anal. Chem.*, **54**, 13 (1982).
16. H. P. Yule, *Anal. Chem.*, **38**, 103 (1966).
17. T. Inouye, T. Harper and N. C. Rasmussen, *Nucl. Instr. Methods*, **67**, 125 (1969).
18. A. W. Westerberg, *Anal. Chem.*, **41**, 1770 (1969).
19. J. R. Morrey, *Anal. Chem.*, **40**, 905 (1968).
20. A. E. Panlath and M. M. Millard, *Appl. Spec.*, **33**, 502 (1979).
21. J. J. Pireaux, *Appl. Spec.*, **30**, 219 (1976).
22. D. C. Champery, *Fourier Transforms and Their Physical Applications*, p. 17, Academic Press, New York (1973).
23. R. O. Ansell, T. Dickinson, A. F. Povey and P. M. A. Sherwood, *J. Electroanal Chem.*, **98**, 79 (1979).
24. J. W. Perram, *J. Chem. Phys.*, **49**, 4245 (1968).
25. A. Baruya and W. F. Maddams, *Appl. Spec.*, **32**, 563 (1978).
26. E. Caulcott, *Significance Tests*, Routledge and Kegan Paul, London (1973).

27. J. S. Bendat and A. G. Piersol, *Random Data: Analysis and Measurement Procedures*, Wiley-Interscience, New York (1971).
28. F. E. Fisher, *Fundamental Statistical Concepts*, Canfield Press, San Francisco (Harper and Row) (1973).
29. A. Proctor and P. M. A. Sherwood, *Surf. Interface Anal.*, **2**, 191 (1980).
30. S. Doniach and M. Sunjic, *J. Phys.*, **C3**, 285 (1970).
31. S. K. Hufner and G. K. Wertheim, *Phys. Rev.*, **B11**, 678 (1975).
32. G. K. Wertheim and D. N. E. Buchanan, *Phys. Rev.*, **B16**, 2613 (1975).
33. G. K. Wertheim and S. Hufner, *Phys. Rev. Lett.*, **35**, 53 (1975).
34. D. A. Shirley, *Phys. Rev.*, **B5**, 4709 (1972).
35. M. O. Krause, T. A. Carlson and R. D. Dismukes, *Phys. Rev.*, **170**, 37 (1968).
36. D. W. Fischer, *Advan. X-ray Anal.*, **13**, 159 (1969).
37. A. Barrie and F. J. Street, *J. Electron Spectrosc.*, **7**, 1 (1975).
38. N. S. McIntyre and D. G. Zetaruk, *Anal. Chem.*, **49**, 1521 (1975).
39. H. E. Bishop, *Surf. Interface Anal.*, **3**, 272 (1981).

Practical Surface Analysis
by Auger and X-ray Photoelectron Spectroscopy
Edited by D. Briggs and M. P. Seah

Appendix 4

Auger and Photoelectron Energies and the Auger Parameter: A Data Set

C. D. Wagner
29 Starview Drive, Oakland CA 94618, USA

This is a comprehensive survey of $N(E)$-type Auger line energies from the literature to 1982. It includes data on the sharpest Auger line and, where available, the most intense photo-electron line. From these are calculated the modified Auger parameter, which is the difference in the line energies plus the energy of the exciting radiation or, more simply,

$$\alpha' = \text{KE(Auger)} - \text{KE(photo-electron)} + h\upsilon = \text{KE(Auger)} + \text{BE(photo-electron)}$$

where the zero reference for both the Auger and photo-electrons is the Fermi edge. This quantity is useful because it is not subject to problems with determination of steady state charge, and because its chemical shifts reflect changes in screening energy (75–7). Compilations similar to this have appeared in earlier versions, including plots of Auger energy versus photo-electron energy, termed chemical state plots (77–21, 78–8, 79–11, 79–12).

There are some problems, of course, in selecting the lines to be included. We are guided by emphasizing those lines that can be observed in conventional ESCA or XPS spectra. It was decided not to attempt to include valence-type or cvv Auger lines because they are usually composed of broad bands, and vary greatly in line distribution with the chemical state. Thus, we do not include the elements through $Z = 7$ (nitrogen) and compilations already exist for available data for oxygen (80–21) and fluorine (77–21) so these data need not be repeated here. The rule against including cvv lines is bent with inclusion of some fragmentary data on the wide LVV lines of sulphur and chlorine, the $LM_{23}V$ lines of Ti, V, Cr, and Mn and the LVV lines of Fe, Co and Ni. Similarly, there are included data on the $M_{45}VV$ lines of Mo, Ru, Rh, and Pd. Finally, in the *NOO* series, there are data on the *NVV* of Pt and Au. Data on Auger lines for transitions higher in energy than that accessible by Al K X-rays are supplied for Al, Si, P, S, Cl, Ar, Br, Kr, fragmentary

data for the $L_3M_{45}M_{45}$ lines of Sr, Y, Zr, Nb and Mo, and the higher energy $M_5N_{67}N_{67}$ series for the heavy metals, Ta, W, Os, Pt, Au, Hg, Tl, Pb and Bi. There are no data for Rb or for any of the rare earths. With the latter the Auger lines are too broad to be analytically useful in this way. There are also no data available on the actinides. In summary, there are entries for all of the stable elements except $Z = 10$, Rb, the rare earths, Hf, Re, Ir, and the actinides. Values for both a high and low energy Auger series are shown for S, Cl, Ar, Pt, Au and Pb. In the $M_{45}N_{45}N_{45}$ and $N_{67}O_{45}O_{45}$ series, the $M_5N_{45}N_{45}$ and $N_6O_{45}O_{45}$ components are the ones cited, because in insulating compounds they appear sharper and more easily measured accurately than the M_4 and N_7 counterparts.

The selection of the companion photo-electron line is simpler. It is the 1s line through Na, the $2p_{3/2}$ line through Zn, the $3d_{5/2}$ line through Ba, and the $4f_{7/2}$ line through Hf–Bi. In the overlapping regions this is somewhat arbitrary. Thus, the 1s energy is also supplied where it was available in the data for Mg and the following elements through Ar, even though they may require higher energy sources than Mg or Al X-rays to be produced. Data on $2p_{3/2}$ line energies are supplied for Ga, Ge, As, Se, and Br. Some data on 4*d* energies are included for antimony and tellurium. Data on the $3d_{5/2}$ line are supplied for tungsten compounds.

In this tabulation a serious attempt has been made to assemble the line energy data in as self-consistent a manner as possible. To this end we emphasize the following:

(a) Data on gas phase materials are assumed to have good accuracy, usually inherent to using mixtures with rare gas standards. These data are presented without change. A comprehensive review of gas phase photoelectron line energies has appeared, and information there on gas phase referencing may be useful (80–22). All data from gas phase are referenced to the vacuum level and are indicated here by the symbol 'v'.

(b) References 80–4*, 82–1*, and 82–2* are all recent efforts to obtain accurate line energies of easily prepared solids relative to the Fermi level. The values shown in this tabulation are corrected to Au $4f_{7/2}$ = 84.00; their absolute values are actually, respectively, 83.98, 84.1 and 84.00.

(c) For all of the other data on solids, we have made the assumption of a common energy scale with a spectrometer work function such that Au $4f_{7/2}$ = 84.0, Ag $3d_{5/2}$ = 368.2 and Cu $2p_{3/2}$ = 932.6. Data on any of these elements afford the opportunity to adjust the position of the voltage scale of the reference on this common basis. Similarly, data on insulators accompanied by a valid method of charge reference, such as gold decoration, use of adventitious hydrocarbon or use of a hydrocarbon moiety of the sample, assuming hydrocarbon C1s = 284.8 eV, permits adjustment also. When adjustment to the data is done for these reasons,

the reference is followed by 'r'. References supplying no single natural line energy, or no referral to the Fermi level, are designated 'n'. Often, though the articles may not state it, it is assumed that papers from a given laboratory closely spaced in time have the same reference for one end of the voltage scale (usually Au $4f_{7/2}$). The data for insulators not charge referenced, or of doubtful charge reference validity, are not included, but in many cases the Auger parameters are included because they are independent of charge correction.

References including 1*s* and 2*p* lines for Na, Mg, Al and Si, and those with $2p_{3/2}$ and 3*d* lines for Zn, Ga, Ge, As and Se afford the possibility to check on the magnitude of the voltage scale, because these line differences for the elements should be equal to the X-ray energy. This was possible for a few references, and minor corrections in high binding energy lines were made and noted by 'c', using X-ray energy data from (67–1). It is not possible to make corrections for non-linearity in the voltage scales.

Older data from a given laboratory supplanted by later data have been omitted in favour of the later data. Some data appearing to be clearly inconsistent with those of most other workers have been omitted. These are usually older studies, of the order of ten years, before instruments were developed to their present state. Some data hitherto unpublished by the author are included as reference 82–5. Most are data obtained in conjunction with reference (79–12), and some for reference (79–11), and were obtained in the same way as data in those references.

Some studies emphasize the changes in line energy, where lines from both chemical or physical states are present in the same spectrum. There are included in the data as, e.g. Mg → Mg ox, with values of line energy changes indicated by Δ. Where there is a change of phase, e.g. Zn → Zn (g), the reference level is of course the same.

The order of presentation of compounds for each element is roughly in decreasing Auger parameter, but with regard to clustering of similar compounds.

References

66–1 H. Körber and W. Mehlhorn, *Z. Physik*, **191**, 217 (1966).

66–2 A. Fahlman, R. Nordberg, C. Nordling and K. Siegbahn, *Z. Physik*, **192**, 476 (1966).

67–1 J. A. Bearden, *Rev. Mod. Phys.*, **39**, 78 (1967).

69–1 K. Siegbahn, C. Nordling, G. Johansson, J. Hedman, P. F. Heden, K. Hamrin, U. Gelius, T. Bergmark, L. O. Werme, R. Manne and Y. Baer, *ESCA Applied to Free Molecules*, North Holland Publishing Company, Amsterdam (1969).

69–2 L. Ramqvist, K. Hamrin, G. Johansson, A. Fahlman and C. Nordling, *J. Phys. Chem. Solids*, **30**, 1835 (1969).

70–1 D. W. Langer and C. J. Vesely, *Phys. Rev.*, **B2**, 4885 (1970).

70-2 R. Spohr, T. Bergmark, N. Magnusson, L. O. Werme, C. Nordling and K. Siegbahn, *Phys. Scr.*, **2**, 31 (1970).
70-3 S. Aksela, M. Pessa and M. Karras, *Z. Physik*, **237**, 381 (1970).
71-1 S. Aksela, *Z. Physik*, **244**, 268 (1971).
72-1 L. O. Werme, T. Bergmark and K. Siegbahn, *Phys. Scr.*, **6**, 141 (1972).
73-1 G. Schon, *Acta Chem. Scand.*, **27**, 2623 (1973).
73-2 G. Johansson, J. Hedman, A. Berndtsson, M. Klasson and R. Nilsson, *J. Electron Spectrosc. Relat. Phenom.*, **2**, 295 (1973).
73-3 S. P. Kowalczyk, L. Ley, F. R. McFeely, R. A. Pollak and D. A. Shirley, *Phys. Rev.*, **B8**, 3583 (1973).
73-4 W. B. Perry and W. L. Jolly, *Chem. Phys. Lett.*, **23**, 529 (1973).
73-5 S. P. Kowalczyk, R. A. Pollak, F. R. McFeely, L. Ley and D. A. Shirley, *Phys. Rev.* **B8**, 2387 (1973).
73-6 G. Schon, *J. Electron Spectrosc.*, **2**, 75 (1973).
73-7 G. Schon, *Surf. Sci.*, **35**, 96 (1973).
73-8 C. D. Wagner and P. Biloen, *Surf. Sci.*, **35**, 82 (1973).
73-9 L. O. Werme, T. Bergmark and K. Siegbahn, *Phys. Scr.*, **8**, 149 (1973).
74-1 H. Aksela and S. Aksela, *J. Phys. B. Atom. Mol. Phys.*, **7**, 1262 (1974).
74-2 S. Aksela and H. Aksela, *Phys. Lett.*, **48A**, 19 (1974).
74-3 B. Breukmann and V. Schmidt, *Z. Physik*, **268**, 235 (1974).
74-4 J. E. Castle and D. Epler, *Proc. Roy. Soc. London*, **A339**, 49 (1974).
74-5 N. E. Erickson, *J. Vac. Sci. Technol.*, **11**, 226 (1974).
74-6 H. Hillig, B. Cleff, W. Mehlhorn and W. Schmitz, *Z. Physik*, **268**, 225 (1974).
74-7 M. Klasson, A. Berndtsson, J. Hedman, R. Nilsson, R. Nyholm and C. Nordling, *J. Electron Spectrosc.*, **3**, 427 (1974).
74-8 S. P. Kowalczyk, L. Ley, F. R. McFeely, R. A. Pollak and D. A. Shirley, *Phys. Rev.*, **B9**, 381 (1974).
74-9 T. D. Thomas and R. W. Shaw, *J. Electron Spectrosc.*, **5**, 1081 (1974).
74-10 P. Larson, *J. Electron Spectrosc.*, **4**, 213 (1974).
74-11 W. B. Perry and W. L. Jolly, *Inorg. Chem.*, **13**, 1211 (1974).
75-1 L. Fiermans, R. Hoogewijs and J. Vennik, *Surf. Sci.*, **63**, 390 (1977).
75-2 J. C. Fuggle, L. M. Watson, D. J. Fabian and S. Affrossman, *J. Phys. F. Metal. Phys.*, **5**, 375 (1975).
75-3 H. C. Halder, J. Alonso and W. E. Swartz, *Z. Naturforsch.*, **30a**, 1485 (1975).
75-4 C. K. Jørgenson and H. Berthou, *Chem. Phys. Lett.*, **36**, 432 (1975).
75-5 L. Ley, F. R. McFeely, S. P. Kowalczyk, J. G. Jenkin and D. A. Shirley, *Phys. Rev.*, **B11**, 600 (1975).
75-6 E. D. Roberts, P. Weightman and C. E. Johnson, *J. Phys. C. Sol. State Phys.*, **8**, 1301 (1975).
75-7 C. D. Wagner, *Faraday. Disc. Chem. Soc.*, **60**, 291 (1975).
76-1 L. Asplund, P. Kelfve, H. Siegbahn, O. Goscinzki, H. Fellner-Feldegg, K. Hamrin, B. Blomster and K. Siegbahn, *Chem. Phys. Lett.*, **40**, 353 (1976).
76-2 M. K. Bahl, R. O. Woodall, R. L. Watson and K. J. Irgolic, *J. Chem. Phys.*, **64**, 1210 (1976).
76-3 G. Dufour, J.-M. Mariot, P.-E. Nilsson-Jatko and R. C. Karnatak, *Phys. Scr.*, **13**, 370 (1976).
76-4 H. C. Halder, J. Alonso and W. E. Swartz, *Phys. Rev.*, **B13**, 2418 (1976).
76-5 K. S. Kim, S. W. Gaarenstroom and N. Winograd, *Chem. Phys. Lett.*, **41**, 503 (1976).
76-6 O. Keski-Rahkonen and M. O. Krause, *J. Electron Spectrosc.*, **9**, 371 (1976).
76-7 N. S. McIntyre, T. E. Rummery, M. G. Cook and D. Owen, *J. Electrochem. Soc.*, **123**, 1165 (1976).

76–8 R. Reisfeld, C. D. Jørgenson, A. Bornstein and H. Berthou, *Chimia*, **30**, 451 (1976).
76–9 P. Weightman, *J. Phys. C. Sol. State Phys.*, **9**, 1117 (1976).
76–10 J. D. Nuttall and T. E. Gallon, *J. Phys. C. Sol. State Phys.*, **9**, 4063 (1976).
76–11 J. E. Castle, L. B. Hazell and R. D. Whitehead, *J. Electron Spectrosc.*, **9**, 247 (1976).
77–1 H. Aksela, S. Aksela, J. S. Jen and T. D. Thomas, *Phys. Rev.*, **A15**, 985 (1977).
77–2 L. Asplund, P. Kelfve, B. Blomster, H. Siegbahn, K. Siegbahn, R. L. Lozes and U. I. Wahlgren, *Phys. Scr.*, **16**, 273 (1977).
77–3 L. Asplund, P. Kelfve, B. Blomster, H. Siegbahn and K. Siegbahn, *Phys. Scr.*, **16**, 268 (1977).
77–4 M. K. Bahl and R. L. Watson, *J. Electron Spectrosc.*, **10**, 111 (1977).
77–5 M. K. Bahl, R. L. Watson and K. J. Irgolic, *J. Chem. Phys.*, **66**, 5526 (1977).
77–6 N. R. Armstrong and R. H. Quinn, *Surf. Sci.*, **67**, 451 (1977).
77–7 T. A. Carlson, W. B. Dress and G. L. Nyberg, *Phys. Scr.*, **16**, 211 (1979).
77–8 J. C. Fuggle, *Surf. Sci.*, **69**, 581 (1977).
77–9 J. C. Fuggle, E. Källne, L. M. Watson, and D. J. Fabian, *Phys. Rev.*, **B16**, 750 (1977).
77–10 S. W. Gaarenstroom and N. Winograd, *J. Chem. Phys.*, **67**, 3500 (1977).
77–11 R. Hoogewijs, L. Fiermans and J. Vennik, *J. Electron Spectrosc.*, **11**, 171 (1977).
77–12 R. Hoogewijs, L. Fiermans and J. Vennik, *J. Microsc. Spec. Electron*, **1**, 109 (1977).
77–13 J. Haber and L. Ungier, *J. Electron Spectrosc.*, **12**, 305 (1977).
77–14 A. W. C. Lin, N. R. Armstrong and T. Kuwana, *Anal. Chem.*, **49**, 1228 (1977).
77–15 J. M. Mariot and G. Dufour, *Chem. Phys. Lett.*, **50**, 219 (1977).
77–16 J. F. McGilp and P. Weightman, *J. Phys. C. Sol. State Phys.*, **9**, 3541 (1977).
77–17 J. H. Fox, J. D. Nuttall and T. E. Gallon, *Surf. Sci.*, **63**, 390 (1977).
77–18 V. I. Nefedov, A. K. Zhumadilov and T. Y. Konitova, *J. Struct. Chem.*, **18**, 692 (1977).
77–19 R. B. Shalvoy, G. B. Fisher and P. J. Stiles, *Phys. Rev.*, **B15**, 1680 (1977).
77–20 J. Väyrynen, S. Aksela and H. Aksela, *Phys. Scr.*, **16**, 452 (1977).
77–21 C. D. Wagner, in *Handbook of X-ray and Ultra-violet Photoelectron Spectroscopy*, (Ed. D. Briggs). Heyden and Sons, 1977, Chap. 7 and Appendix 3, pages 387–392.
77–22 E. Antonides, E. C. Janse and G. A. Sawatzky, *Phys. Rev.*, **B15**, 1669 (1977).
77–23 A. Barrie and F. J. Street, *J. Electron Spectrosc.*, **7**, 1 (1977).
77–24 S. Aksela, H. Aksela, M. Vuontisjarvi, J. Väyrynen and E. Lähteenkorva, *J. Electron Spectrosc.*, **11**, 137 (1977).
78–1 M. K. Bahl, R. L. Watson and K. J. Irgolic, *J. Chem. Phys.*, **68**, 3272 (1978).
78–2 J. Haber, T. Machej, L. Ungier and J. Ziolkowski, *J. Sol. State Chem.*, **25**, 207 (1978).
78–3 J. M. Mariot and G. Dufour, *J. Electron Spectrosc.*, **13**, 403 (1978).
78–4 Y. Mizokawa, H. Iwasaki, R. Nishitani and S. Nakamura, *J. Electron Spectrosc.*, **14**, 129 (1978).
78–5 R. Romand, M. Roubin and J. P. Deloume, *J. Electron Spectrosc.*, **13**, 229 (1978).
78–6 P. Steiner, F. J. Reiter, H. Höchst, S. Hüfner and J. C. Fuggle, *Phys. Lett.*, **66A**, 229 (1978); *Phys. Stat. Solidi*, **90**, 45 (1978).
78–7 P. M. Th. M. Van Attekum and J. M. Trooster, *J. Phys. F. Metal Phys.*, **8**, L169 (1978).
78–8 C. D. Wagner, *J. Vac. Sci. Technol.*, **15**, 518 (1978).

79–1 A. J. Ashe, M. K. Bahl, K. D. Bomben, W. T. Chan, J. Gimzewski, P. A. Sitton and T. D. Thomas, *J. Am. Chem. Soc.*, **101**, 1764 (1979).

79–2 H. Aksela, J. Vayrynen and S. Aksela, *J. Electron Spectrosc.*, **16**, 339 (1979).

79–3 C. R. Brundle and D. Seybold, *J. Vac. Sci. Technol.*, **16**, 1186 (1979).

79–4 R. G. Cavell and R. Sodhi, *J. Electron Spectrosc.*, **15**, 145 (1979).

79–5 S. M. Barlow, P. Bayat-Mokhtari and J. E. Gallon, *J. Phys. C. Sol. State Phys.*, **12**, 5577 (1979).

79–6 H. Kuroda, T. Ohta and Y. Sato, *J. Electron Spectrosc.*, **15**, 21 (1979).

79–7 R. Kumpula, J. Vayrynen, T. Rantala and S. Aksela, *J. Phys. C. Sol. State Phys.*, **12**, L809 (1979).

79–8 M. Pessa, A. Vuoristo, M. Villi, S. Aksela, J. Väyrynen, T. Rantala and H. Aksela, *Phys. Rev.*, **B20**, 3115 (1979).

79–9 A. C. Parry-Jones, P. Weightman and P. T. Andrews, *J. Phys. C. Sol. State Phys.*, **12**, 1587 (1979).

79–10 T. Rantala, J. Vayrynen, R. Kumpula and S. Aksela, *Chem. Phys. Lett.*, **66**, 384 (1979).

79–11 C. D. Wagner, L. H. Gale and R. H. Raymond, *Anal. Chem.*, **51**, 466 (1979).

79–12 C. D. Wagner, W. M. Riggs, L. E. Davis, J. F. Moulder and G. E. Muilenberg, *Handbook of X-Ray Photoelectron Spectroscopy*, Perkin-Elmer Corporation, Physical Electronics Division, Eden Prairie, Minnesota (1979).

79–13 D. M. Zehner and H. H. Madden, *J. Vac. Sci. Technol.*, **16**, 562 (1979).

79–14 L. Hilaire, P. Légaré, Y. Holl and G. Maire, *Solid State Comm.*, **32**, 157 (1979).

79–15 J. E. Castle and R. H. West, *J. Electron Spectrosc.*, **16**, 195 (1979).

79–16 G. D. Nichols and D. A. Zatko, *Inorg. Nucl. Chem. Lett.*, **15**, 401 (1979).

79–17 J. E. Castle, L. B. Hazell and R. H. West, *J. Electron Spectrosc.*, **16**, 97 (1979).

79–18 V. Y. Young, R. A. Gibbs and N. Winograd, *J. Chem. Phys.*, **70**, 5714 (1979).

80–1 E. J. Aitken, M. K. Bahl, K. D. Bomben, J. K. Gimzewski, G. S. Nolan and T. D. Thomas, *J. Am. Chem. Soc.*, **102**, 4874 (1980).

80–2 S. Aksela, J. Väyrynen, H. Aksela and S. Pennanen, *J. Phys. B. Atom Molec Phys.*, **13**, 3745 (1980).

80–3 C. W. Bates and L. E. Galan, *Proc. Ninth IMEKO Symp. on Photon Detectors*, Budapest, Hungary, 9–12 September, 1980 pp. 100–129.

80–4 R. J. Bird and P. Swift, *J. Electron Spectrosc.*, **21**, 227 (1980).

80–5 M. K. Bahl, R. L. Watson and K. J. Irgolic, *J. Chem. Phys.*, **72**, 4069 (1980).

80–6 J. E. Castle and R. H. West, *J. Electron Spectrosc.*, **18**, 355 (1980).

80–7 S. Evans, *Proc. Roy. Soc. London*, **A370**, 107 (1980).

80–8 R. A. Gibbs, N. Winograd and V. Young, *J. Chem. Phys.*, **72**, 4799 (1980).

80–9 J. Hedman and N. Martensson, *Phys. Scr.*, **22**, 176 (1980).

80–10 P. Kelfve, B. Blomster, H. Siegbahn, K. Siegbahm, E. Sanhueza and O. Goscinski, *Phys. Scr.*, **21**, 75 (1980).

80–11 L. L. Kazmerski, P. J. Ireland, P. Sheldon, T. L. Chu, S. S. Chu and C. L. Lin, *J. Vac. Sci. Technol.*, **17**, 1061 (1980).

80–12 H. Van Doveren and J. A. Th. Verhoeven, *J. Electron Spectrosc.*, **21**, 265 (1980).

80–13 J. A. Th. Verhoeven and H. Van Doveren, *Appl. Surf. Sci.*, **5**, 361 (1980).

80–14 J. Väyrynen, S. Aksela, M. Kellokumpu, and H. Aksela, *Phys. Rev.*, **A22**, 1610 (1980).

80–15 C. D. Wagner, *J. Electron Spectrosc.*, **18**, 345 (1980).

80–16 C. D. Wagner and J. A. Taylor, *J. Electron Spectrosc.*, **20**, 83 (1980).

80–17 P. Weightman and P. T. Andrews, *J. Phys. C. Sol. State Phys.*, **13**, L815, L821 (1980).

80-18 P. Weightman and P. T. Andrews, *J. Phys. C. Sol. State Phys.*, **13**, 3529 (1980).
80-19 S. J. Yang and C. W. Bates, *Appl. Phys. Lett.*, **36**, 675 (1980).
80-20 N. H. Turner, J. S. Murday and D. E. Ramaker, *Anal. Chem.*, **52**, 84 (1980).
80-21 C. D. Wagner, D. A. Zatko and R. H. Raymond, *Anal. Chem.*, **52**, 1445 (1980).
80-22 A. A. Bakke, H.-W. Chen and W. L. Jolly, *J. Electron Spectrosc.*, **20**, 333 (1980).
81-1 G. Van der Laan, C. Westra, C. Haas and G. A. Sawatzky, *Phys. Rev.*, **B23**, 4369, (1981).
81-2 N. S. McIntyre, S. Sunder, D. W. Shoesmith and F. W. Stanchell, *J. Vac. Sci. Technol.*, **18**, 714 (1981).
81-3 M. Schärli and J. Brunner, *Z. Physik*, **B42**, 285 (1981).
81-4 J. A. Taylor, *Appl. Surf. Sci.*, **7**, 168 (1981).
81-5 J. A. Taylor and J. W. Rabalais, *J. Chem. Phys.*, **75**, 1735 (1981).
81-6 J. Väyrynen, *J. Electron Spectrosc.*, **22**, 27 (1981).
81-7 S. Aksela, M. Kellokumpu, H. Aksela and J. Väyrynen, *Phys. Rev.*, **A23**, 2374 (1981).
81-8 C. D. Wagner, H. A. Six, W. T. Jansen and J. A. Taylor, *Appl. Surf. Sci.*, **9**, 203 (1981).
82-1. C. J. Powell, N. E. Erickson and T. Jach, *J. Vac. Sci. Technol.*, **20**. 625 (1982)
82-2. M. P. Seah and M. T. Anthony, Appendix 1 of this book.
82-3 P. Swift, *Surf. Inter. Anal.*, **4**, 47 (1982).
82-4 J. A. Taylor, *J. Vac. Sci. Technol.*, **20**, 751 (1982).
82-5 C. D. Wagner, unpublished data.
82-6 R. H. West and J. E. Castle, *Surf. Inter. Anal.*, **4**, 68 (1982).
82-7 C. D. Wagner, D. E. Passoja, H. F. Hillery, T. G. Kinisky, H. A. Six, W. T. Jansen and J. A. Taylor, *J. Vac. Sci. Technol.*, **21**, 933 (1982).
82-8 C. D. Wagner and J. A. Taylor, *J. Electron Spectrosc.*, **28**, 211 (1982).
82-9 R. M. Henry, T. A. B. Fryberger and P. C. Stair, *J. Vac. Sci. Technol.*, **20**, 818 (1982).
82-10 M. Polak, *J. Electron Spectrosc.* (in press).
82-11 S. Aksela and J. Sivonen, *Phys. Rev.*, **A23**, 1243 (1982).
82-12 L. Pederson, *J. Electron Spectrosc.*, **28**, 203 (1982).

NEON	1s	$KL_{23}L_{23}$	α′	Ref.
Ne (implanted in Fe)	863.4	818.0	1681.4	75-7 r
Ne (implanted in diamond)	863.1	818.7	1681.8	80-7
Ne (g)	870.31 v	804.56 v	1674.87	74-9
Ne (g)	870.37 v	804.52 v	1674.89	73-2
Ne (g)	870.2 v	804.8 v	1675.0	69-1
Ne (g)	870.0 v	804.15 v	1674.15	66-1
SODIUM				
Na	1071.8 c	944.3	2066.1 c	77-23 r
Na	1071.5 c	994.2	2065.7 c	73-3
Na		994.5		78-6 n
NaI	1071.6	991.2	2062.8	75-7 r
NaI			2062.2	74-8
NaI			2063.7	79-6
NaBr	1071.7	990.6	2062.3	75-7 r
NaBr			2063.1	79-6
Na → Na ox	Δ +0.7	−4.5	−3.8	77-23
Na ox	1072.7	989.8	2062.5	77-23 r
Na ox			2062.0	74-8
Na ox		998.8		66-2 n
Na_3Sb			2064.8	80-3
Na_2KSb			2065.1	80-3
$NaBiO_3$	1071.3	990.9	2062.2	79-11 r
Na_2MoO_4	1070.9	991.0	2061.9	79-11 r
Na_2CrO_4	1071.2	990.9	2062.1	79-11 r
$Na_2Cr_2O_7$	1071.6	990.4	2062.0	79-11 r
Na_2PdCl_4	1071.8	990.2	2062.0	75-7 r
NaCl	1071.6	990.3	2061.9	75-7 r
NaCl			2062.8	79-6
NaSCN	1071.3	990.5	2061.8	75-7 r
Na_2SeO_3	1070.8	991.0	2061.8	75-7 r
$Na_2S_2O_4$	1071.2	990.6	2061.8	75-7 r
$Na_2S_2O_3$	1071.6	990.1	2061.7	75-7 r
Na_2WO_4	1071.3	990.4	2061.7	79-11 r
Na_2SO_3	1071.4	990.2	2061.6	79-11 r
Na_2SO_3			2062.6 c	80-20 r
Na thioglycollate	1071.2	990.4	2061.6	79-11 r
Na_2TeO_4	1071.1	990.5	2061.6	75-7 r
$NaAsO_2$	1070.9	990.7	2061.6	75-7 r
Na_2HPO_4	1071.6	989.9	2061.5	79-12 r
Na_2HPO_4	1071.5	989.7	2061.2	82-3
$Na_2SnO_3 \cdot 3H_2O$	1071.1	990.3	2061.4	79-11 r
$NaNO_2$	1071.6	989.8	2061.4	75-7 r
Na_2CO_3	1071.5	989.8	2061.3	79-11 r
$Na_2C_2O_4$	1070.8	990.5	2061.3	79-11 r

SODIUM—*cont.*	1s	$KL_{23}L_{23}$	α'	Ref.
Na_3PO_4	1071.1	990.2	2061.3	82-3
Na salt of EDTA*	1070.8	990.4	2061.2	79-11 r
$NaHCO_3$	1071.3	989.8	2061.1	79-11 r
$Na_2IrCl_6 \cdot 6H_2O$	1071.9	989.2	2061.1	75-7 r
albite ($NaAlSi_3O_8$)	1072.2	988.9	2061.1	82-7 r
NaH_2PO_4	1072.0	989.1	2061.1	82-3
$NaPO_3$	1071.7	989.3	2061.0	75-7 r
$NaPO_3$	1071.6	989.4	2061.0	82-3
Na_2SO_4	1071.2	989.8	2061.0	75-7 r
Na_2SO_4			2062.1c	80-20 r
Na_2SO_4			2061.9	79-6
NaOAc	1071.1	989.9	2061.0	75-7 r
Na benzenesulphonate	1071.3	989.7	2061.0	79-11 r
NaH_2PO_2	1071.1	989.8	2060.9	82-3
NaOOCH	1071.1	989.8	2060.9	79-11 r
natrolite ($Na_2Al_2Si_3O_{10} \cdot 2H_2O$)	1072.4	988.5	2060.9	82-7 r
$NaNO_3$	1071.4	989.4	2060.8	79-11 r
$NaNO_3$			2062.2	79-6
Na zeolite A ($NaAlSiO_4$)	1071.7	988.9	2060.6	82-7 r
hydroxysodalite	1070.5	989.8	2060.3	82-7 r
Na_2ZrF_6	1071.5	988.7	2060.2	75-7 r
Na_2TiF_6	1071.6	988.5	2060.1	75-7 r
Na_3AlF_6	1071.9	988.2	2060.1	79-11 r
NaF	1071.2	988.6	2059.8	75-7 r
NaF			2061.0	79-6
$NaBF_4$	1072.7	987.1	2059.8	75-7 r
Na_2GeF_6	1071.7	988.1	2059.8	75-7 r
Na_2SiF_6	1071.7	987.7	2059.4	75-7 r
Na (g)	1078.6 v	976.7 v	2055.3	74-6

*Ethylenediaminetetracetic acid

MAGNESIUM	2p	$KL_{23}L_{23}$	α'	1s	Ref.
Mg	49.95	1185.5	1235.45		79-12 r
Mg		1185.9			78-7 n
Mg	49.5*	1185.5	1235.0	1303.2 c	78-6 n
Mg	49.6	1185.7	1235.3		77-11 r
Mg	49.6	1185.6	1235.2	1303.2 c	77-8
Mg		1184.9			77-7 r
Mg	49.4	1186.5 c	1235.9 c	1303.0 c	75-3, 76-4
Mg	49.4	1185.3	1234.7	1303.0	75-5
Mg	50.0	1185.6	1235.6		75-7 r
Mg		1183.0 v			77-20

*From 2s = 88.6, assuming 2s − 2p = 39.1.

MAGNESIUM—*cont.*	2*p*	$KL_{23}L_{23}$	α'	1*s*	Ref.
Mg_2Cu	49.5	1186.0	1235.5	1302.6	75-2*
Mg_3Au	49.4	1185.7	1235.1	1302.7	75-2*
Mg_3Bi	50.3	1184.9	1235.2	1303.6	75-2*
Mg → Mg ox	Δ +1.3	−6.1	−4.8		79-11
Mg → Mg ox	Δ +1.4	−5.9	−4.5		77-11
Mg → Mg ox	Δ +0.8	−5.1	−4.3	+1.3	77-8
Mg → Mg ox	Δ +1.2	−5.2	−4.0	+1.5	77-7 r
Mg → Mg ox	Δ +1.5	−6.2	−4.7	+0.6	75-3, 76-4
Mg → Mg ox	Δ	−6.2			73-8
MgO	50.4	1180.4	1230.8	1304.0	79-11 r
MgO (single crystal)			1231.6		77-11
Mg acetylacetonate	50.1	1180.5	1230.6	1304.0	79-11 r
Mg cyclohexanebutyrate	50.7	1180.0	1230.7	1304.2	79-11 r
Mg erucate	50.7	1180.2	1230.9	1304.4	79-11 r
$MgSeO_4$	51.1	1180.7	1231.8	1304.7	79-11 r
$MgSO_4 \cdot 7H_2O$	51.6	1178.8	1230.4	1305.2	79-11 r
talc, $Mg_3Si_4O_{11} \cdot H_2O$	50.46	1180.3	1230.76		82-7 r
MgF_2	50.95	1178.15	1229.1	1305.0	80-15 r
MgF_2	50.9	1178.0	1228.9	1304.8	79-11 r
Mg (g)		1167.0 v			77-20
Mg (g)		1167.1 v			74-3
Mg (s) → Mg (g)		Δ −16.0			77-20

*Line energies from 75-2 corrected by +0.3 eV kinetic energy, based upon later work from same laboratory, 77-8.

ALUMINIUM	2*p*	$KL_{23}L_{23}$	α'	1*s*	α'	Ref.
Al	72.92	1393.21	1466.13			81-8 r,
Al	72.85	1393.29	1466.14			82-7 r
Al		1393.2				82-4
						78-7 n
Al		1393.2				77-7
Al		1393.0				76-3 r
Al			1466.2			79-15
Al				1558.2	2953.2	79-17
AlAs	73.6	1391.2	1464.8			82-4
AlN	74.0	1388.9	1462.9			81-5

ALUMINIUM—*cont.*	2*p*	$KL_{23}L_{23}$	α'	1*s*	α'	Ref.
Al ox	74.15*	1387.48	1461.63			81-8 r
Al → Al ox	Δ +2.7	−7.4	−4.7			82-4
Al → Al ox	Δ +2.8	−7.4	−4.6			77-7
Al → Al ox		−6.5		+3.0		76-11
				+3.0	−3.5	
Al_2O_3 sapphire	74.10	1387.87	1461.97			81-8 r
Al_2O_3 sapphire, heated 450°	74.32	1387.68	1462.00			81-8 r
α-Al_2O_3	73.85	1388.24	1462.09			81-8 r
Al_2O_3 corundum					2948.5	82-6
Al_2O_3			1461.9			79-15
γ-Al_2O_3	73.72	1387.83	1461.55			81-8 r
AlO(OH) boehmite	74.22	1387.60	1461.82			81-8 r
$Al(OH)_3$ bayerite	73.90	1387.62	1461.52			82-7 r
$Al(OH)_3$ bayerite	74.3	1387.7	1462.0			82-4
$Al(OH)_3$ gibbsite	74.00	1387.43	1461.43			81-8 r
AlF_3			1460.7			79-15
kaolinite	74.68	1386.73	1461.41			82-7 r
kaolinite					2948.6	79-17
pyrophyllite	74.71	1386.75	1461.46			82-7 r
pyrophyllite					2948.9	82-6
muscovite mica	74.25	1387.06	1461.31			82-7 r
muscovite mica					2948.8	82-6
albite	74.34	1386.47	1460.81			82-7 r
albite					2947.7	82-6
natrolite	74.25	1386.53	1460.78			82-7 r
					2947.8	82-6
spodumene	74.32	1387.13	1461.45			82-7 r
sillimanite	74.58	1386.86	1461.44			82-7 r
andalusite					2948.5	82-6
almandine					2948.9	82-6
anorthite					2948.5	82-6
beryl					2949.2	82-6
cordierite					2948.7	82-6
epidote					2948.6	82-6
kyanite					2948.85	82-6
microcline					2946.9	82-6
plagioclase					2948.0	82-6
staurolite					2949.1	82-6
stilbite					2946.9	82-6
sodalite					2947.9	82-6

*From C 1*s* charge reference

ALUMINIUM—*cont.*	2*p*	$KL_{23}L_{23}$	α'	1*s*	α'	Ref.
molecular sieve type A	73.66	1386.90	1460.56			81-8 r
molecular sieve type X	74.13	1386.25	1460.38			81-8 r
molecular sieve type Y	74.45	1385.85	1460.30			81-8 r
H Zeolon	74.82	1385.52	1460.34			82-7 r
hydroxysodalite	73.95	1486.35	1460.3			82-7 r
SILICON						
Si	99.44	1616.68	1716.12			81-8 r
Si	99.6	1616.3	1715.9			81-4
Si	99.6	1616.4	1716.0			80-6 n
Si vapour deposited	99.7	1616.2	1715.9	1839.3 c	3455.5 c	74-7 r
Si		1616.4				77-7
Si					3456.3	79-17
$PdSi_{0.6}$	99.8	1617.4	1717.2			80-16 r
$MoSi_2$	99.56	1617.20	1716.76			81-8 r
$MoSi_x$	99.4	1617.4	1716.8			81-8 r
SiC			1714.1			80-6
SiC					3453.7	82-6
Si_3N_4	101.9*	1612.2	1714.1			81-4
Si_3N_4			1713.7		3454.15	80-6, 82-6
phenylsilicone resin	102.74	1609.96	1712.70			82-7 r
methylsilicone resin	102.92	1608.80	1711.72			82-7 r
poly-dimethyl-silicone	102.40	1609.38	1711.78			82-7 r
Si ox	103.43	1608.27	1711.70			81-8 r
Si ox (on Si100)	103.4	1608.6	1712.0			81-4
SiO_2 (on Si100)			1711.9			81-4
SiO_2 vapour deposited	103.4	1608.8	1712.2	1842.7 c	3451.5 c	74-7 r
SiO_2 α-cristobalite	103.25	1608.64	1711.89			81-8 r
SiO_2 α'-quartz	103.65	1608.6	1712.25			82-7 r
SiO_2 quartz			1712.2		3452.4	80-6, 82-6
SiO_2 Vycor	103.5	1608.5	1712.0			78-8 r

*Formed by N_2^+ bombardment of Si(100) wafer.

SILICON—*cont.*	2*p*	$KL_{23}L_{23}$	α'	1*s*	α'	Ref.
SiO_2 gel	103.59	1607.87	1711.46			82-7 r
SiO_2 gel	104.1	1607.4	1711.5			78-8 r
SiO_2 gel			1711.3			80-6
$ZnSiO_3$			1711.8			80-6
hemimorphite	101.96	1610.52	1712.48			82-7 r
					3452.7	82-6
wollastonite	102.36	1609.99	1712.35			82-7 r
pseudo-wollastonite	102.16	1610.27	1712.43			82-7 r
talc	103.13	1608.93	1712.06			82-7 r
talc			1712.3		3453.6	80-6, 82-6
kaolinite	102.98	1609.03	1712.01			82-7 r
kaolinite			1711.9		3451.5	80-6, 79-17
pyrophyllite	102.88	1609.20	1712.08			82-7 r
pyrophyllite			1712.1		3453.1	80-6, 82-6
muscovite mica	102.36	1609.64	1712.00			82-7 r
muscovite			1712.0		3452.5	80-6, 79-17
sillimanite	102.64	1609.48	1712.12			82-7 r
spodumene	102.46	1609.59	1712.05			82-7 r
almandine			1712.4		3453.0	80-6, 82-6
anorthite			1712.3		3452.4	80-6, 82-6
biotite			1712.15			80-6
bentonite			1712.1			80-6
lepidolite			1712.0			80-6
microcline			1711.95		3452.0	80-6, 82-6
beryl			1711.7		3452.1	80-6, 82-6
stilbite			1711.7		3451.9	80-6, 82-6
andalustite					3452.6	82-6
staurolite					3453.6	82-6
epidote					3452.7	82-6
uvarovite					3452.2	82-6
kyanite					3452.6	82-6
cordierite					3452.7	82-6

SILICON—*cont.*	2*p*	$KL_{23}L_{23}$	α'	1*s*	α'	Ref.
olivine					3452.2	82-6
enstatite					3452.6	82-6
asbestos					3452.5	82-6
zircon					3452.65	82-6
serpentine					3453.1	82-6
soda glass	102.95	1608.72	1711.67			82-7 r
albite	102.63	1609.26	1711.89			82-7 r
albite					3452.3	82-6
natrolite	102.22	1609.62	1711.84			82-7 r
natrolite					3452.4	82-6
hydroxysodalite	101.65	1610.7	1712.35			82-7 r
sodalite					3452.35	82-6
plagioclase					3452.4	82-6
molecular sieve type A	101.43	1610.09	1711.52			81-8 r
molecular sieve type X	102.16	1609.40	1711.56			81-8 r
molecular sieve type Y	102.84	1608.63	1711.47			81-8 r
H Zeolon	103.28	1608.40	1711.68			82-7 r
$SiCl_4$ (g)	110.17 v	1600.16 v	1710.33			80-10
$Si(OMe)_4$ (g)	107.70 v	1601.81 v	1709.51			80-10
$Si(OEt)_4$ (g)	107.56 v	1602.27 v	1709.83			80-10
$SiMe_4$ (g)	105.94 v	1603.74 v	1709.68			80-10
$SiEt_4$ (g)	106.03 v	1604.3 v	1710.33			80-10
$SiCl_3Ph$ (g)	108.81 v	1601.95 v	1710.76			80-10
$SiCl_3C_3H_5$ (g)	108.92 v	1601.51 v	1710.43			80-10
$SiCl_3Et$ (g)	108.97 v	1601.34 v	1710.31			80-10
$SiCl_3C_2H_3$ (g)	109.05 v	1601.29 v	1710.34			80-10
$SiCl_3Me$ (g)	109.15 v	1600.96 v	1710.11			80-10
$SiCl_3H$ (g)	109.44 v	1600.3 v	1709.74			80-10
$SiCl_2MeC_2H_3$ (g)	108.07 v	1602.08 v	1710.15			80-10
$SiCl_2Et_2$ (g)	107.85 v	1602.52 v	1710.37			80-10
$SiCl_2Me_2$ (g)	108.10 v	1601.82 v	1709.92			80-10
$SiCl_2MeH$ (g)	108.53 v	1601.17 v	1709.70			80-10
$SiClMe_2C_3H_5$ (g)	106.98 v	1603.18 v	1710.16			80-10
$SiClEt_3$ (g)	106.6 v	1603.8 v	1710.4			80-10
$SiClMe_3$ (g)	107.06 v	1602.80 v	1709.86			80-10
$SiMe_3CH_2Cl$ (g)	106.23 v	1603.62 v	1709.85			80-10
$SiMe(OEt)_3$ (g)	107.09 v	1602.70 v	1709.79			80-10
$SiMe_2(OEt)_2$ (g)	106.69 v	1603.00 v	1709.69			80-10
$SiMe_3OEt$ (g)	106.29 v	1603.29 v	1709.58			80-10
SiF_4 (g)	111.70 v	1595.34 v	1707.04			80-10
SiH_4 (g)	107.1 v	1601.2 v	1708.3	1847.0	3448.2	74-11, 79-4

PHOSPHORUS	2*p*	$KL_{23}L_{23}$	α'	1*s*	Ref.
Gap	128.7	1858.9	1987.6		80-16 r
P (red)	130.2	1857.0	1987.2		81-3 r
$NaPO_3$	134.7	1848.3	1983.0		78-8 r
Na_2HPO_4	133.1	1850.8	1983.9		80-16 r
$SPCl_3$ (g)	141.15 v	1842.6 v	1983.75		79-4
$OPCl_3$ (g)	141.35 v	1841.3 v	1982.65		79-4
PCl_3 (g)	140.15 v	1842.4 v	1982.55		79-4
SPF_3 (g)	142.85 v	1839.1 v	1981.95		79-4
C_6H_5P, phosphazene (g)	136.1 v	1845.3 v	1981.4		79-1
PF_5 (g)	144.65 v	1836.2 v	1980.85		79-4
OPF_3 (g)	143.25 v	1836.9 v	1980.15		79-4
PF_3 (g)	142.05 v	1837.4 v	1979.45		79-4
PH_3 (g)	137.35 v	1842.0 v	1979.35	2150.5 v	79-4
PH_3 (g)	137.3 v	1841.4 v	1978.7		79-1
SULPHUR					
WS_2	162.8	2115.6	2278.4		78-8 r
$NiWS_2$	162.6	2115.9	2278.5		78-8 r
NiS	162.8	2116.1	2778.9		80-16 r
$Na_2S_2O_3$ (central S)	168.6	2107.8	2276.4		78-8 r
(peripheral S)	162.5	2112.5	2275.0		78-8 r
Na_2SO_3	166.6	2108.5	2275.1		82-8 r
$CuSO_4$	169.1	2108.0	2277.1		80-16 r
SF_6	174.4	2100.45	2274.85		82-8 r
SF_6 (g)	180.4 v	2092.6 v	2273.0	2490.1 v	76-6
SF_6 (g)	180.28 v	2092.52 v	2272.80		77-2
CS_2	163.6	2111.65	2275.25		82-8 r
CS_2 (g)	170.03 v	2101.40 v	2271.43		76-1
SO_2	167.4	2106.2	2273.6		82-8 r
SO_2 (g)	174.8 v	2095.5 v	2270.3	2483.7 v	76-6
SO_2 (g)	174.84 v	2095.40 v	2270.24		77-2
COS (g)	170.8 v	2099.2 v	2270.0		76-1
H_2S (g)	170.2 v	2098.7 v	2268.9	2478.5 v	76-6
H_2S (g)	170.44 v	2098.42 v	2268.86		77-2
H_2S (g)		2099.1 v		2477.7 v	79-4
		LLV			
S (s)	164.25	152	316		82-5

CHLORINE	$2p_{3/2}$	*LVV*	α'	1*s*	Ref
poly(vinyl chloride)	200.1	182.3	382.4		79-12 r
KCl	199.3	181.0	380.3		77-18 r
$KClO_3$	206.5	181.0	387.5		77-18 r
$KClO_4$	208.7	180.7	389.4		77-18 r

CHLORINE—cont.	$2p_{3/2}$	$KL_{23}L_{23}$	α'	1s	Ref.
CCl_4 (g)	207.04 v	2375.72 v	2582.76		80-1
$CHCl_3$ (g)	206.86 v	2375.52 v	2582.38		80-1
CCl_3F (g)	207.20 v	2374.93 v	2582.13		80-1
t-C_4H_8Cl (g)	205.38 v	2376.64 v	2582.02		80-1
s-C_4H_9Cl (g)	205.62 v	2376.17 v	2581.79		
80-1					
n-C_3H_7Cl (g)	205.81 v	2375.77 v	2581.58		80-1
CH_2Cl_2 (g)	206.62 v	2375.15 v	2581.77		80-1
CCl_2F_2 (g)	207.47 v	2374.18 v	2581.66		80-1
C_2H_3Cl (g)	205.92 v	2375.46 v	2581.38		80-1
Cl_2 (g)	207.82 v	2373.72 v	2581.54		80-1
$CClF_3$ (g)	207.83 v	2373.30 v	2581.13		80-1
CH_3Cl (g)	206.26 v	2374.51 v	2580.77		80-1
ClF (g)	209.18 v	2370.73 v	2579.91		80-1
HCl (g)	207.38 v	2371.98 v	2579.36		80-1
HCl (g)		2372.2 v		2829.2 v	79-4

ARGON	$2p_{3/2}$	$L_3M_2M_3^*$	$L_2M_2M_3^*$	α'	1s	$KL_{23}L_{23}$	Ref.
Ar (implanted in Fe)	241.7		216.9*	458.6			75-7 r
Ar (implanted in Be)		211.0 v	212.8 v				79-13 n
Ar (adsorbed on Ag)		210.6 v	212.7 v				76-10
Ar (multilayer on Ag)		207.6 v					76-10
Ar (g)	248.62 v	203.49 v	205.61 v	453.17†			73-2
Ar (g)					3205.9 v	2660.51 v	69-1, 77-3

*Centre of unresolved peaks.
†Calculated for mean of Auger peaks listed.

POTASSIUM

K				547.9†			80-3
K_3Sb				546.8†			80-3
Na_2KSb				547.0†			80-3
KI	292.8		250.8*	543.6			75-7 r
KBr	293.1	248.3	250.7	542.6			79-12 r
KCl	292.5		250.4*	542.9			82-5
KNO_3	292.9		249.3*	542.2			75-7 r
K_2SO_4				542.5			80-20
K_2SO_3				542.3			80-20
KF	292.5		249.6*	542.1			75-7 r
$KSbF_6$	293.7		248.6*	542.3			75-7 r
K (g)	300.7 v	236.67 v	239.51 v	540.2†			81-7

*Peaks composed mainly of $L_3M_{23}M_{23}{}^1D_2$ and $L_2M_{23}M_{23}{}^1D_2$ respectively. Values centred between these columns are for the unresolved doublet.
†Auger parameter based upon $L_2M_{23}M_{23}$. The others are based upon Auger energies of the unresolved doublet.

CALCIUM	$2p_{3/2}$	$L_3M_2M_3^*$	$L_2M_2M_3^*$	α'	Ref.
Ca	345.9		298.2	644.1	
$CaCl_2$	348.3		291.9	640.2	80-12 r
CaO	346.5		291.9	638.4	75-7 r
CaO	347.3		292.5	639.8	82-5
$Ca \rightarrow CaO$	Δ +1.4		−5.7	−4.3	80-12 r
$CaSO_4$	347.6		291.2	638.8	80-12
$CaCO_3$	347.0		291.8	638.8	82-5 r
wollastonite (Ca silicate)	347.0		291.5	638.5	79-12 r
CaF_2	347.9		288.9	636.8	82-7 r
					82-5
SCANDIUM					
Sc_2O_3	401.9	334.9		736.8	79-12 r
Sc oxalate	403.3	333.5		736.8	82-5
Sc acetylacetonate	402.2	333.4		735.6	82-5
ScF_3	405.0	329.8		734.8	82-5

*Peaks composed mainly of $L_3M_{23}M_{23}{}^1D_2$ and $L_2M_{23}M_{23}{}^1D_2$, respectively. Values centred between these columns are for the unresolved doublet.

TITANIUM	$2p_{3/2}$	$L_3M_{23}M_{23}$	α'	$KL_{23}L_{23}$	α'	Ref.
Ti			836.6			77-6
TiO_2			840.3			77-6
		$L_3M_{23}V$				
Ti	454.0	419.1	873.1			79-12 r
TiN	455.7	420.0	875.7			79-11 r
TiC	454.6	418.2	872.8			79-11 r
TiO_2	458.7	414.9	873.6			82-5
TiO_2	458.5	414.7	873.2			79-11 r
TiO acetylacetonate	458.4	414.8	873.2			79-11 r
titanocene dichloride	457.2	414.9	872.1			79-11 r
Na_2TiF_6	462.6	409.8	872.4			79-11 r
K_2TiF_6	462.1	409.4	871.5			79-11 r
$Ti \rightarrow TiC$	Δ +1.3			−1.5	−0.2	69-2
$Ti \rightarrow TiN$	Δ +1.5			−1.9	−0.4	69-2
$Ti \rightarrow TiO$	Δ +1.0			−1.6	−0.6	69-2
$Ti \rightarrow TiO_2$	Δ +4.9			−5.8	−0.9	69-2
VANADIUM						
V	512.15	472.0	984.15			79-12 r
$V \rightarrow VC$	Δ + 1.8			−2.4	−0.6	69-2
CHROMIUM						
Cr	574.3	527.2	1101.5			79-12 r

MANGANESE	$2p_{3/2}$	$L_3M_{23}V$	α'	Ref.
Mn	639.0	586.4	1225.4	79-12 r
		582.8 v		81-6
Mn	642.4	584.9	1227.3	82-5
MnO_2	642.3	583.9	1226.2	79-11 r
MnO_2				
	642.8	580.9	1223.7	79-11 r
$MnCl_2$	642.3	582.4	1224.7	79-11 r
$MnSiO_3$	641.7	582.0	1223.7	79-11 r
$K_3Mn(CN)_6$	640.8	582.2	1223.0	79-11 r
$Mn(C_{24}H_{27}N_7)(PF_6)_2$*				
		561.6 v		81-6
Mn (g)		Δ −21.2		81-6
Mn (s) → Mn (g)				

*The nitrogen ligand contains three pyridine rings.

IRON	$2p_{3/2}$	L_3VV*	α'	Ref.
Fe	706.95	702.4	1409.35*	79-12 r
Fe_2O_3	711.0	703.1	1414.1	79-11 r
Fe_2O_3	710.9	702.0	1412.9	82-5
$FeWO_4$	711.5	703.1	1414.6	79-11 r
$Fe_2(WO_4)_3$	711.1	702.5	1413.6	79-11 r
FeS	710.4	703.2	1413.6	79-11 r
FeS_2	707.4	702.7	1410.1	79-11 r
Fe^{II} acetylacetonate	711.5	700.8	1412.3	79-11 r
Fe^{III} acetylacetonate	711.8	700.3	1412.1	79-11 r
Fe cyclohexanebutyrate	712.0	700.8	1412.8	79-11 r
Fe dithiodibutylcarbamate	711.3	701.2	1412.5	79-11 r
$FeSO_4 \cdot 7H_2O$	711.0	700.4	1411.4	79-11 r
$Fe(C_{10}H_8N_2)_3(PF_6)_2$†	708.2	699.6	1407.8	79-11 r
$K_3Fe(CN)_6$	709.9	698.4	1408.3	79-11 r
$K_4Fe(CN)_6$	708.5	698.9	1407.4	79-11 r
K_3FeF_6	713.8	698.6	1412.4	79-11 r

*The Auger line for all but Fe and FeS_2 is very broad, ca. 8 eV wide, and accuracy of the line energy is therefore limited.
†Ligand is $C_5H_5NCH{=}NCH_3$.

COBALT	$2p_{3/2}$	L_3VV	α'	Ref.
Co	778.1	773.2	1551.3	79-12 r
Co	778.2	773.0	1551.2	77-13
Co_3O_4	780.0	773.6	1553.6	82-5
Co_3O_4	780.3	773.9	1554.2	79-11 r
Co_3O_4	779.3	773.6	1552.9	77-13
CoO	780.2	773.6	1553.8	82-5

COBALT—*cont.*	$2p_{3/2}$	L_3VV	α'	Ref.
$CoSiO_3$	781.5	770.4	1551.9	79-11 r
Co_2SiO_4	781.3	770.6	1551.9	79-11 r
Co cyclohexanebutyrate	781.6	770.0	1551.6	79-11 r
Co dibutyldithiocarbamate	779.5	770.2	1549.7	79-11 r
$Co(NH_3)_6Cl_3$	781.7	768.6	1550.3	79-11 r
$Co(N_4$-tetramethylethylenediamine$)(NO_3)_2$	780.0	770.1	1550.1	79-11 r
$K_3Co(CN)_6$	781.9	766.8	1548.7	79-11 r
$Co(C_{24}H_{27}N_7)(PF_6)_2$*	780.5	773.4	1553.9	79-11 r
$CoSiF_6$	783.6	768.2	1551.8	79-11 r

*The nitrogen ligand contains three pyridine rings.

NICKEL	$2p_{3/2}$	L_3VV	α'	Ref.
Ni	852.7•	846.2•	1698.9•	82-1• r
Ni	852.5	846.2	1698.7	79-12 r
Ni	852.6	845.9	1698.5	76-5
Ni	852.7	845.8	1698.5	74-4 r
Ni	852.9	846.1	1699.0	80-8
Ni (s) → Ni (implanted in C)	Δ +0.9	−0.7	+0.2	80-8
NiO	853.5	846.0*	1699.5	82-5
NiO	853.5	846.4*	1699.9	79-11 r
NiO	854.1	845.8	1699.9	74-4
Ni cyclohexanebutyrate	856.3	842.5	1698.8	79-11 r
Ni acetylacetonate	855.7	842.9	1698.6	79-11 r
KNi biuret	856.8	841.9	1698.7	79-11 r
Ni trifluoroacetate	856.9	841.8	1698.7	79-11 r
$NiSiO_3$	856.9	841.4	1698.3	79-11 r
Ni dimethylglyoxime	854.8	842.4	1697.2	79-11 r
$Ni(C_{24}H_{27}N_7)(PF_6)_2$†	855.4	842.1	1697.5	79-11 r
$K_2Ni(CN)_4$	855.4	840.3	1695.7	79-11 r
NiF_2	857.4	842.4	1699.8	79-11 r
$NiSiF_6$	858.7	840.4	1699.1	79-11 r

*Taken as the centre of a broad square line.
†The nitrogen ligand contains three pyridine rings.

COPPER	$2p_{3/2}$	$L_3M_{45}M_{45}$	α'	Ref.
Cu	932.67•	918.65•	1851.32•	82-2•
Cu	932.68•	918.62•	1851.30•	80-4•
Cu	932.6•	918.8•	1851.4•	82-1•
Cu	932.6	918.4	1851.0	79-12 r

COPPER—*cont.*	$2p_{3/2}$	$L_3M_{45}M_{45}$	α'	Ref.
Cu	932.8	918.5	1851.3	77-9 r
Cu	932.8	918.3	1851.1	73-2
Cu	932.6	918.6	1851.2	75-7 r
Cu	932.6	918.8	1851.4	77-10
Cu	932.7 c	918.6	1851.3	76-5
Cu				
Cu	932.2	919.0	1851.2	73-7
Cu	932.4	919.0	1851.4	76.7
Cu	933.0	918.4	1851.4	78-5
Cu	933.1	918.2	1851.3	78-2
Cu				
Cu	932.8	918.0	1850.8	73-5
Cu	933.0	918.1	1851.1	73-2
Cu	932.6	918.9	1851.5	81-2 r
Cu		918.9		70-3
Cu				
Al_2Cu	933.9	918.0	1851.9	77-9 r
CuAgSe	932.3	917.6	1849.9	78-5
Cu_2Se	932.3	917.5	1849.8	78-5
CuSe	932.4	918.3	1850.7	78-5
Cu_2S	932.5	917.4	1849.9	75-7 r
$Cu \rightarrow Cu_2S$	Δ + 0.07	−1.37	−1.30	82-5
$Cu \rightarrow Cu_2S$	Δ + 0.1	−1.8	−1.7	74-10
CuS	932.6	917.8	1850.4	78-5
Cu_2O	932.6	916.6	1849.2	82-5
Cu_2O	932.4	917.2	1849.6	77-10
Cu_2O	932.2	917.6	1849.8	76-7 r
Cu_2O	933.1	916.2	1849.3	78-2 r
$Cu \rightarrow Cu_2O$	Δ −0.11	−2.00	−2.11	82-5
$Cu \rightarrow Cu_2O$	Δ + 0.1	−2.3	−2.2	74-10
$Cu \rightarrow Cu_2O$	Δ	−2.3		81-2
$Cu \rightarrow Cu_2O$	Δ 0.0	−2.2	−2.2	73-5
CuO	933.8	917.9	1851.7	82-5
CuO	933.6	918.1	1851.7	77-10
CuO	933.8	917.8	1851.6	78-2 r
CuO	933.5	917.9	1851.4	76-7 r
CuO	933.0	917.9	1850.9	73-7
$Cu \rightarrow CuO$	Δ +0.96	−0.88	+0.08	82-5
$Cu \rightarrow CuO$	Δ +1.2	−1.0	+0.2	74-10
$Cu \rightarrow CuO$	Δ +1.3	−0.8	+0.5	81-2
$Cu \rightarrow Cu(OH)_2$	Δ +2.5	−2.7	−0.2	81-2
CuCl	932.4	915.6	1848.0	77-10
CuCl	932.6	915.0	1847.6	75-7 r
$CuCl_2$	934.4	915.5	1849.9	77-10

COPPER—*cont.*	$2p_{3/2}$	$L_3M_{45}M_{45}$	α'	Ref.
$CuCl_2$	935.2	915.1	1850.3	79-11 r
$CuCl_2$	934.8	915.3	1850.1	81-1 r
$CuBr_2$	933.3	916.9	1850.2	81-1 r
CuCN	933.1	914.5	1847.6	75-7 r
$Cu_2Mo_3O_{10}$	932.0	916.5	1848.5	78-2 r
$CuSO_4$	935.5	915.9	1851.4	82-5
$CuSO_4$	935.5	915.6	1851.1	77-18 r
$Cu(NO_3)_2$	935.5	915.3	1850.8	77-18 r
$CuCO_3$	935.0	916.3	1851.3	79-11 r
$CuMoO_4$	934.5	916.6	1851.1	78-2 r
$CuSiO_3$	934.9	915.2	1850.1	79-11 r
$CuC(CN)_3$	933.2	914.5	1847.7	77-18 r
$Cu(C_{24}H_{27}N_7)(PF_6)_2$*	934.0	915.9	1849.9	79-11 r
CuF_2	937.0	914.8	1851.8	79-11 r
CuF_2	936.1	916.0	1852.1	77-10
CuF_2	936.8	914.4	1851.2	81-1 r
Cu → Cu atoms in SiO_2	Δ 0.7	−4.1	−3.4	79-18
Cu → Cu (g)	Δ 2.5	−13.2	−10.7	82-11

*The nitrogen ligand contains three pyridine rings.

ZINC	$2p_{3/2}$	$L_3M_{45}M_{45}$	α'	Ref.
Zn	1021.65	992.2	2013.85	79-12 r
Zn	1021.6	992.3	2013.9	77-15 r
Zn	1021.7	992.5	2014.2	73-6
Zn	1021.4 c	992.0	2013.4 c	76-5
Zn	1022.0	991.8	2013.8	74-8
Zn	1021.7 c	992.0	2013.7 c	77-10
Zn	1021.9	992.4	2014.3	74-4 r
Zn	1021.4 c	992.3	2013.7 c	77-12 n
Zn		988.4 c		77-17
Zn		988.2 v		77-20
Zn		991.7		70-3
ZnTe	1021.6 c	991.3	2012.9 c	77-12 n
ZnTe			2012.2	70-1
ZnSe	1022.0 c	989.5	2011.5 c	77-12 n
ZnSe			2010.2	70-1
ZnS	1021.6 c	989.7	2011.3 c	77-10
ZnS	1021.9 c	988.2	2010.1 c	77-12 n
ZnS			2011.9	70-1

ZINC—cont.	$2p_{3/2}$	$L_3M_{45}M_{45}$	α'	Ref.
	1022.5 c	988.7	2011.2 c	77-10
ZnI_2			2011.1 c	77-12
ZnI_2			2010.3 c	77-12
$ZnBr_2$	1023.4	987.3	2010.7	75-7 r
$ZnBr_2$				
	1021.7	988.2	2009.9	73-6
ZnO	1022.1 c	987.6	2009.7 c	77-12 n
ZnO	1022.1 c	987.7	2009.8 c	77-10
ZnO			2010.3	70-1
ZnO	1021.9	988.6	2010.5	82-5
ZnO	1022.2	987.4	2009.6	74-8
ZnO				
Zn → Zn ox	Δ + 0.3	−4.2	−3.9	79-11
Zn → Zn ox	Δ	−4.2		77-17
Zn → Zn ox	Δ + 0.2	−3.5	−3.3	74-4
$ZnCl_2$			2009.2 c	77-12
Zn acetylacetonate	1021.4	987.7	2009.1	75-7 r
$Zn(C_{24}H_{20}N_4)(BF_4)_2$*	1021.3	988.3	2009.6	79-11 r
hemimorphite (Zn silicate)	1021.96	987.30	2009.26	82-7 r
ZnF_2	1021.8 c	986.2	2008.0 c	77-10
ZnF_2			2008.2 c	77-12 n
ZnF_2	1022.8	986.7	2009.5	75-7 r
ZnF_2			2007.4	74-8
Zn (g)		973.3 v		74-2
Zn (g)		974.5 v		77-20
Zn → Zn (g)	Δ 3.15	−13.1	−9.9	79-7

*The nitrogen ligand contains three pyridine rings.

GALLIUM	3*d*	$L_3M_{45}M_{45}$	α'	$2p_{3/2}$	Ref.
Ga	18.7	1068.1	1086.8		79-12 r
Ga	18.7	1068.1	1086.8	1116.6 c	82-5, 75-7 r
Ga	18.6	1068.3	1086.9	1116.5 c	73.6
Ga	18.4	1068.2	1086.6		77-22
Ga	18.5	1069.0	1087.5	1116.4 c	74-4 r
Ga	18.5	1068.1	1086.6		78-4 r
GaAs (cleaved)	19.2	1066.4	1085.6		79-3 n
GaAs (cleaved)	19.4	1066.2	1085.6		78-4 r
GaAs (sputtered)	19.0	1067.1	1086.1		78-4 r
GaAs (chem etch)	19.3	1066.2	1085.5		78-4 r
GaP	19.3	1066.2	1085.5		82-5
GaN	19.54	1064.5	1084.04		80-9 r
Ga → Ga ox	Δ +2.0	−6.3	−4.3		82-5
Ga → Ga ox	Δ +2.6	−6.4	−3.8		74-4

GALLIUM—*cont.*	3*d*	$L_3M_{45}M_{45}$	α'	$2p_{3/2}$	Ref.
Ga_2O_3	21.0	1061.9	1082.9		78-4 r
Ga_2O_3	20.3	1062.8	1083.1	1117.9	73-6 r
GaAs → Ga ox	Δ +1.0	−3.5	−2.5		79-3

GERMANIUM	3*d*	$L_3M_{45}M_{45}$	α'	$2p_{3/2}$	$\alpha'^{\dagger}$	Ref.
Ge	29.0	1145.4	1174.4			77-19 r
Ge	29.15	1145.2	1174.35	1217.2 c	2362.4 c	79-12 r
Ge	29.5*	1145.0*	1174.5	1217.4*	2362.4	77-16
Ge	29.0	1145.0	1174.0	1217.0 c	2362.0 c	74-4 r
Ge	29.2	1144.9	1174.1			77-22
$GeTe_2$	30.0	1144.8	1174.8			77-19 r
$GeSe_2$	30.9	1143.8	1174.7			77-19 r
GeS_2	30.5	1143.7	1174.2			77-19 r
Ge → Ge ox	Δ +4.1	−8.0	−3.9	+3.8	−4.2	74-4
Ge → Ge ox	Δ +3.8	−7.9	−4.1	+3.7	−4.2	82-5, 75-7
						75-7 r
GeO_2	32.7	1137.7	1170.4	1220.6	2358.3	82-5, 75-7 r
GeO_2					2358.9	76-8
Na_2GeF_6	33.3	1135.7	1169.0	1221.3	2357.0	82-5, 75-7 r
K_2GeF_6					2357.15	76-8
$GeBr_4$ (g)	38.95 v	1130.32 v	1169.27			73-4
$GeCl_4$ (g)	39.6 v	1129.01 v	1168.61			73-4
$GeMe_4$ (g)	35.63 v	1132.64 v	1168.27			73-4
GeH_3Br (g)	37.65 v	1129.81 v	1167.46			73-4
GeH_3Cl (g)	37.77 v	1129.4 v	1167.17			73-4
GeH_3Me (g)	36.44 v	1130.55 v	1166.99			73-4
GeH_4 (g)	36.9 v	1129.5 v	1166.4			73-4
GeF_4 (g)	41.55 v	1124.28 v	1165.83			73-4

*Vacuum-level referenced values corrected by a 4.3 eV work function.
†Based upon $2p_{3/2}$ and $L_3M_{45}M_{45}$.

ARSENIC	3*d*	$L_3M_{45}M_{45}$	α'	$2p_{3/2}$	Ref.
As	41.8	1225.0	1266.8	1323.4 c	76-2
As	41.5	1226.1	1267.6		75-6 r
As	41.5	1225.2	1266.7	1323.1	82-5, 79-11 r
As	42.1	1225.0	1267.1	1323.7 c	74-4 r
As	41.6	1225.4	1267.0	1323.3	82-4
GaAs (cleaved)	41.3	1224.5	1265.8		79-3 n
GaAs (chem etch)	41.2	1225.0	1266.2	1323.0	82.4

ARSENIC—*cont.*	3*d*	$L_3M_{45}M_{45}$	α'	$2p_{3/2}$	Ref.
GaAs (sputtered)	41.0	1225.5	1266.5	1322.7	82-4
GaAs (sputtered)	40.9	1225.4	1266.3	1322.8	79-12 r
NbAs	40.8	1226.0	1266.8		76-2
As_2Te_3		1225.0			76-2
As_2Se_3	43.0	1223.3	1266.3	1324.7	76-2
As_2S_3	43.5	1222.0	1265.5	1325.6	76-2 r
As_4S_4	43.1	1222.7	1265.8	1325.1	76-2 r
Ph_3AsS	44.1	1220.0	1264.1	1325.9	76-2 r
Me_3AsS	44.0	1219.3	1263.3	1325.8	76-2 r
AsI_3	43.5	1222.9	1266.4	1325.6	76-2 r
$MeAsI_2$	43.5	1222.3	1265.8	1325.1	76-2 r
$AsBr_3$	45.3	1218.1	1263.4	1327.4	76-2 r
Ph_3As	42.4	1221.1	1263.5	1324.3	76-2 r
As_2O_3	44.4	1218.9	1263.3	1326.7	76-2
As_2O_3	45.0	1218.8	1263.8	1326.4	79-11 r
As_2O_3	44.9	1218.7	1263.6	1326.6	82-4 r
As_2O_5	46.2	1217.4	1263.6	1328.1	76-2 r
As_2O_5	44.9	1218.6	1263.5	1328.8	74-4 r
$NaAsO_2$	44.2	1219.4	1263.6	1325.6	79-11 r
$NaAsO_2$	44.3	1219.6	1263.9		82-4 r
Na_2HAsO_4	45.5	1217.1	1262.6	1326.8	79-11 r
Ph_3AsO	44.3	1219.5	1263.8	1325.5	76-2
$PhAsO(OH)_2$	45.2	1218.4	1263.6	1326.8	76-2
Ph_2AsOOH	44.4	1219.0	1263.4	1326.8	76-2
Me_2AsOOH	44.6	1218.4	1263.0	1326.3	76-2
$(C_{10}H_{21})_2AsOOH$	44.0	1219.0	1263.0	1325.5	76-2
$BuAsO(OH)_2$	45.1	1218.3	1263.4	1327.0	76-2
$KAsF_6$	47.8	1213.8	1261.6	1330.0	79-11 r
$GaAs \rightarrow As_2O_3$	Δ 3.1	−5.9	−2.8		79-3
	3*s*	$L_2M_{45}M_{45}$			
C_5H_5As (arsabenzene) (g)	211.2	1248.2			79-1
$AsMe_3$ (g)	211.1	1247.9			79-1
AsH_3 (g)	212.4	1245.1			79-1

SELENIUM	$3d_{5/2}$	$L_3M_{45}M_{45}$	α'	$2p_{3/2}$	α'†	Ref.
Se	55.5	1307.0	1362.5			80-5 r
Se	55.7	1306.7	1362.4			79-11 r
Se	55.5	1306.6*	1362.1*	1434.2 c	2740.8 c	79-12 r
Se	56.3	1305.8	1362.1	1435.0 c	2740.8 c	74-4 r

SELENIUM—*cont.*	$3d_{5/2}$	$L_3M_{45}M_{45}$	α'	$3p_{3/2}$	$L_3M_{23}M_{45}$	Ref.
Se				161.9	1178.2	77-18 r
$USe_{1.88}$				161.1	1180.0	77-18 r
Ph_2Se	56.0	1303.8	1359.8			80-5 r
Ph_2Se_2	56.0	1304.1	1360.1			80-5 r
$Se{=}C(NH_2)_2$	55.0	1305.2	1360.2			80-5 r
Ph_2SeI_2	58.3	1301.9	1360.2			80-5 r
Ph_2SeCl_2	57.9	1302.7	1360.6			80-5 r
$C_7H_8SeCl_3$	58.1	1302.6	1360.7			80-5 r
SeO_2	59.0	1301.4	1360.4			80-5 r
H_2SeO_3	59.2	1300.8	1360.0			80-5 r
H_2SeO_4	61.2	1297.9	1358.1			80-5 r
Ph_2SeO	57.8	1301.7	1359.5			80-5 r
Na_2SeO_3	58.5	1301.2	1359.7			79-11 r
Na_2SeO_3				164.9	1173.1	77-18 r
Na_2SeO_4	60.6	1298.9	1359.5			79-11 r
$MgSeO_4$	59.5	1299.2	1358.7			79-11 r
$(NH_4)_2SeO_4$	59.2	1300.1	1359.3			79-11 r
K_2SeO_4				165.9	1173.1	77-18 r

*±0.5 eV. †Based upon $2p_{3/2}$ and $L_3M_{45}M_{45}$.

BROMINE	$3d_{5/2}$	$L_3M_{45}M_{45}$	α'	$2p_{3/2}$	Ref.
KBr	68.7	1388.0	1456.7		80-16 r
LiBr	68.9	1389.2	1458.1	1548.8	78-8 r
NaBr	68.9	1388.3	1457.2	1549.0	78-8 r
$C_{16}H_{33}NMe_3Br$	67.5	1390.1	1457.6	1547.5	78-8 r
$KBrO_3$	74.8	1384.4	1459.2	1553.9	78-8 r
tetrabromophenol-sulphonphthalein*	70.5	1387.9	1458.4	1550.5	78-8 r
CBr_4 (g)	76.7 v	1378.9 v	1455.6		70-2
$CHBr_3$ (g)	76.8 v	1378.6 v	1455.4		70-2
CH_2Br_2 (g)	76.6 v	1378.1 v	1454.7		70-2
CH_3Br (g)	76.3 v	1377.6 v	1453.9		70-2
KRYPTON					
Kr (g)	93.8 v	1460.4 v	1554.2		73-2, 72-1
STRONTIUM					
SrF_2		1640.6			78-8 r
YTTRIUM					
Y_2O_3		1736.5			78-8 r
ZIRCONIUM					
Zr ox		1831.0			78-8 r
NIOBIUM					
Nb ox		1919.7			78-8 r

MOLYBDENUM	$3d_{5/2}$	$L_3M_{45}M_{45}$	α'			
				$M_{45}VV$	α'	
Mo	227.9			222.8	450.7	79-12 r
Mo	228.0	2038.8	2266.8			80-16 r
Mo ox	232.7	2032.2	2264.9			80-16 r
Mo → Mo ox	Δ +4.7	−6.6	−1.9			80-16
$MoSi_2$	227.7	2039.0	2266.7			82-7 r

*The indicator, bromophenol blue.

RUTHENIUM	$3d_{5/2}$	$M_{45}VV$	α'	Ref.
Ru	280.2	274.2	554.4	79-12 r
$Ru_3(CO)_{12}$	280.9	271.8	552.7	82-5
RHODIUM				
Rh	307.2	301.3	608.5	79-12 r
Rh acetylacetonate	310.0	298.8	608.8	79-11 r
$Rh(NO_3)_3 \cdot 2H_2O$	310.7	297.7	608.4	79-11 r
$RhCl_3 \cdot 3H_2O$	310.0	298.2	608.2	79-11 r
Na_3RhCl_6	310.0	297.7	607.7	79-11 r
$Rh_6(CO)_{16}$	308.6	298.7	607.3	79-11 r
$Rh(NH_3)_5Cl_3$	310.0	297.1	607.1	79-11 r
$(PH_3P)_3RhBr$	309.5	297.5	607.0	79-11 r
$(PH_3P)_3RhHCO$	309.5	297.4	606.9	79-11 r
$(PH_3P)_3RhCl$	307.5	297.3	604.8	79-11 r

PALLADIUM	$3d_{5/2}$	$M_4N_{45}N_{45}$	α'	Ref.
Pd	335.1	327.8	662.9	79-12 r
Pd	334.6	328.5	663.1	79-14 n
Pd	335.1	327.8	662.9	80-17
$Mg_{75}Pd_{25}$	336.2	326.4	662.6	80-17
$Al_{80}Pd_{20}$	337.4	325.5	662.9	80-17
$Ag_{30}Pd_{50}$	334.6	328.8	663.4	80-17
$Ag_{80}Pd_{20}$	334.9	329.8*	664.7	80-17
$Ag_{90}Pd_{10}$	334.9	329.7*	664.6	80-17
$Pt_{50}Pd_{50}$	334.6	327.5	662.1	79-14 n
$Au_{40}Pd_{60}$	334.5	327.5	662.0	79-14 n
Pd ox	336.4	326.3	662.7	79-14 n
$PdSO_4$	338.7	324.8	663.5	79-11 r
Pd acetylacetonate	338.1	324.9	663.0	79-11 r
$Pd(NO_3)_2$	338.2	324.7	662.9	79-11 r
$PdBr_2$	337.7	324.9	662.6	79-11 r
$Pd(CN)_2$	338.7	323.7	662.4	79-11 r
$PdCl_2$	338.0	325.2	662.2	79-11 r
$(cyC_8H_{12})_2PdCl_2$	338.5	323.8	662.3	79-11 r
$Pd(NH_3)_4Cl_2$	338.4	323.8	662.2	79-11 r
$(Ph_3P)_2PdCl_2$	338.0	323.6	661.6	79-11 r
Na_2PdCl_4	338.0	323.4	661.4	79-11 r
K_2PdCl_4	337.9	323.1	661.0	79-11 r
$(Ph_3P)_4Pd$	335.1	324.4	659.5	79-11 r

*Line distribution is unusual.

SILVER	$3d_{5/2}$	$M_4N_{45}N_{45}$	α'	Ref.
Ag	368.28•	357.84•	726.12•	82-2•
Ag	368.1	357.9	726.0	79-12 r
Ag	368.2	358.1	726.3	77-9 r
Ag	368.3	358.0	726.3	77-10
Ag	368.3	358.0	726.3	73-1
Ag	368.4	357.5*	725.9	78-5
Ag	368.2	357.6*	725.8	77-10
Ag	368.2	357.9	726.1	79-9
Ag		357.8		78-3 r
Ag		359.3		71-1
Ag		353.7 v		76-10
$Mg_{21}Ag_{79}$	368.3	358.1*	726.4	80-18
$Mg_{30}Ag_{50}$	368.7	357.9*	726.6	80-18
$Mg_{97}Ag_3$	368.8	358.2*	727.0	80-18
$AlAg_2$	368.7	357.7	726.4	77-9 r
$Al_{40}Ag_{60}$	368.8	357.7*	726.5	80-18
$Al_{95}Ag_5$	369.0	357.5*	726.5	80-18
Ag_2S	368.2	356.8*	725.0	78-5
Ag_2S			724.7	80-20
Ag_2Se	367.9	357.0*	724.9	78-5
AgCuSe	367.9	356.9*	724.8	78-5
Ag_2O	368.5	356.0*	724.5	78-5
Ag_2O	367.9	356.6	724.5	73-1
Ag_2O	367.8	356.7*	724.5	77-10
AgO	367.6	357.2	724.8	73-1
AgO	367.4	356.6*	724.0	77-10
AgI	368.0	356.1*	724.1	77-10
$AgOOCCF_3$	368.8	355.1	723.9	75-7 r
Ag_2SO_4	368.3	354.2	722.5	75-7 r
Ag_2SO_4	367.9	355.1*	723.0	77-10
Ag_2SO_4			722.5	80-20
AgF	367.7	355.3*	723.0	77-10
AgF_2	367.3	355.6*	722.9	77-10
Ag (g)		341.8*		80-14

*6.0 eV added to value for $M_5N_{45}N_{45}$ to give value for $M_4N_{45}N_{45}$.

CADMIUM	$3d_{5/2}$	$M_4N_{45}N_{45}$	α'	Ref.
Cd	405.0	383.6	788.6	79-12 r
Cd	404.9	383.7	788.6	75-7 r
Cd	405.0	384.0*	789.0	77-10
Cd	405.3	383.5*	788.8	79-9

CADMIUM—*cont.*	$3d_{5/2}$	$M_4N_{45}N_{45}$	α'	Ref.
		385.6		
Cd		380.5 v*		71-1
Cd		380.4 v		77-20
Cd		380.1 v		77-24
Cd				76-9
$CdSe_{0.85}Te_{0.15}$	404.9	382.2	787.1	
CdTe	405.2	382.4	787.6	82-10 r
CdTe	405.0	382.6*	787.6	82-10 r
CdSe	405.3	381.5*	786.8	77-10
CdSe	405.0	381.7	786.7	77-10
				82-10 r
CdS	405.3	381.3*	786.6	77-10
CdI_2	405.4	381.2*	786.6	77-10
CdO	404.2	382.4*	786.6	77-10
$Cd(OH)_2$	405.1	380.0	785.1	79-11 r
CdF_2	405.8	378.8	784.6	75-7 r
CdF_2	405.9	379.0	784.9	77-10
Cd → Cd (g)	Δ +2.95	−11.8	−8.85	79-7
Cd (g)		368.2 v		77-24
Cd (g)		368.3 v*		77-20
Cd (g)		367.9 v		74-1

*6.8 eV added to value for $M_5N_{45}N_{45}$ to give value for $M_4N_{45}N_{45}$.

INDIUM

In	443.84	410.41	854.25	79-8
In	443.8	410.4	854.2	79-12 r
In	444.0	410.5	854.5	77-14 r
In	444.3	410.1	854.4	75-7 r
In	444.0	410.2	854.2	79-9
In	443.6	410.5	854.1	80-11 n
In	443.4	411.5	854.9	79-16 n
In		411.1		71-1
InTe	444.3	409.2	853.5	79-11 r
In_2Te_3	444.5	408.9	853.4	79-11 r
InSe	445.0	408.0	853.0	79-11 r
In_2Se_3	444.8	408.3	853.1	79-11 r
InS	444.5	408.3	852.8	79-11 r
In_2S_3	444.7	407.3	852.0	79-11 r
In_2S_3	444.3	408.0	852.3	79-16 n
In_2S_3	444.4	408.9	853.3	80-11 n
InP	444.0	410.0	854.0	80-11 n
In → In ox	Δ +1.2	−3.6	−2.4	75-7
In_2O	444.3	406.8	851.1	77-21 r
In_2O	444.0	406.6	850.6	80-11 n

INDIUM—*cont.*	$3d_{5/2}$	$M_4N_{45}N_{45}$	α'	Ref.
In_2O_3	444.3	406.4	850.7	77-21 r
In_2O_3	444.9	406.3	851.2	77-14 r
In_2O_3	444.9	407.2	852.1	80-11 n
In_2O_3	443.7	407.2	850.9	79-16 n
$In(OH)_3$	445.0	405.0	850.0	79-11 r
$In(OH)_3$	445.8	404.8	850.6	80-11 n
$In(OH)_3$	444.6	405.4	850.0	79-16 n
InI_3	445.8	405.8	851.6	77-21 r
InI_3 (red)	445.3	406.5	851.8	79-16 n
InI_3 (yellow)	445.7	405.8	851.5	79-16 n
$InBr_3$	446.0	404.8	850.8	77-21 r
$InBr_3$	445.7	405.2	850.9	79-16 n
InCl	444.8	405.7	850.5	77-21 r
$InCl_3$	446.0	404.6	850.6	77-21 r
$InCl_3$	445.8	403.8	849.6	80-11 n
$InCl_3$	445.7	404.8	850.5	79-16 n
InF_3	446.2	403.7	849.9	75-7 r
InF_3	445.9	403.7	849.6	79-16 n
$(NH_4)_3InF_6$	445.6	404.1	849.7	77-21 r
$(NH_4)_3InF_6$	445.3	404.0	849.3	79-16 n
$InCl_3$ (g)		394.1 v*		80-2
InCl (g)		393.95 v*		80-2
In (g)		393.25 v*		80-2

*7.6 eV added to value for $M_5N_{45}N_{45}$ to give value for $M_4N_{45}N_{45}$

TIN	$3d_{5/2}$	$M_4N_{45}N_{45}$	α'	Ref.
Sn	484.87	437.27	922.14	79-8
Sn	484.85	437.6	922.45	79-12 r
Sn	485.0	437.4	922.4	75-7 r
Sn	484.9	437.5	922.4	77-14 r
Sn	484.8	437.4*	922.2	79-9
Sn		434.0 v		79-5
SnS	485.6	435.7	921.3	75-7 r
Sn → Sn ox	Δ +1.5	−4.7	−3.2	75-7
Sn → Sn ox	Δ	−4.1		79-5
SnO	486.8	432.15	918.95	82-5
SnO	486.7	432.0	918.7	79-11 r
SnO_2	487.3	431.8	919.1	79-11 r
SnO_2	486.6	432.4	919.0	82-5
SnO_2	486.6	432.6	919.2	77-14 r

Tin—*cont.*	$3d_{5/2}$	$M_4N_{45}N_{45}$	α'	Ref.
	486.7	431.7	918.4	75-7 r
Na_2SnO_3	485.9	432.4	918.3	79-11 r
$(R_3Sn)_2O$	487.4	430.8	918.2	75-7 r
$NaSnF_3$		420.24 v		79-8
$SnCl_2$ (g)				

[a] 8.5 eV added to value for $M_5N_{45}N_{45}$ to give value for $M_4N_{45}N_{45}$.

ANTIMONY	$3d_{5/2}$	$M_4N_{45}N_{45}$	α'	$4d$	Ref.
	528.02	464.29	992.31	31.94	79-8
Sb	528.25	463.9	992.15		79-12 r
Sb	528.2	464.2	992.4		75-7 r
Sb		465.7			71-1
Sb					
			991.5		80-3
Cs_3Sb			990.7		80-3
K_3Sb			990.6		80-3
Na_2KSb			990.6		80-3
Na_3Sb					
Sb_2S_3	529.5	462.1	991.6		75-7 r
Sb_2S_5	529.3	462.2	991.5		75-7 r
Sb_2O_5	530.0	459.7	989.7		75-7 r
$KSbF_6$	532.9	454.4	987.3		75-7 r
Sb_4 (g)		452.95 v			78-9, 79-2

TELLURIUM					
Te	572.85	492.13	1064.98	40.26	79-8
Te	572.9	492.2	1065.1		79-12 r
Te	573.1	491.8	1064.9	40.5	77-4
Te		492.2			71-1
Te → Te ox	Δ +3.7	−5.2	−1.5		75-7
CdTe	572.7	490.8	1063.5		82-10 r
$CdSe_{0.65}Te_{0.35}$	572.6	491.1	1063.7		82-10 r
TeO_2	576.1	487.1	1063.2	43.4	77-5
TeO_3	577.3	485.5	1062.8	44.6	77-5
$Te(OH)_6$	577.1	485.1	1062.2	45.0	77-5 r
Ph_2Te_2	573.9	488.5	1062.4	42.8	77-5[a] r
$PhTeI_3$	575.8	488.2	1064.0	44.8	77-5 r
Ph_2TeI_2	575.4	487.8	1063.2	44.4	77-5 r
Et_2TeI_2	575.3	487.6	1062.9	44.2	77-5 r
Me_2TeI_2	575.6	487.6	1063.2	42.8	77-5 r
$TeBr_4$	576.7	487.3	1064.0	44.0	77-5
$PhTeBr_3$	576.6	486.8	1063.4	43.9	77-5 r
Ph_2TeBr_2	576.2	486.7	1062.9	43.5	77-5 r
$FC_6H_4TeBr_3$	576.3	487.0	1063.3	43.7	77-5 r

TELLURIUM—*cont.*	$3d_{5/2}$	$M_4N_{45}N_{45}$	α'	$4d$	Ref.
$BuTeBr_3$	576.6	486.5	1063.1	43.9	77-5 r
$MePhTeBr_2$	576.0	486.6	1062.6	43.2	77-5 r
$TeCl_4$	576.9	486.1	1063.0	44.3	77-5
p-$MeOC_6H_4TeCl_3$	576.7	485.9	1062.6	44.4	77-5 r
Ph_2TeCl_2	576.2	486.3	1062.5	43.8	77-5 r
$(NH_4)_2TeCl_6$	576.9	486.4	1063.3	45.3	77-5 r
$Te(thiourea)_2Cl_2$	574.7	488.3	1063.0	42.0	77-5 r
p-MeC_6H_4TeOOH	576.1	486.6	1062.7	43.7	77-5 r
Na_2TeO_4	576.8	485.5	1062.3		75-7 r
Te_2 (g)		479.20 v			79-2, 79-8

*All 77-5 references with 'r' are assumed to be referenced to adventitious carbon C 1s, necessitating a correction.

IODINE	$3d_{5/2}$	$M_4N_{45}N_{45}$	α'	Ref.
LiI	619.7	517.0	1136.7	79-12 r
NaI	618.9	517.2	1136.1	79-11 r
KI	618.7	517.0	1135.7	79-11 r
NiI_2	619.0	518.8*	1137.8	77-10
CuI	619.0	518.6*	1137.6	77-10
ZnI_2	619.8	517.5*	1137.3	77-10
AgI	619.4	518.3*	1137.7	77-10
CdI_2	619.2	518.5*	1137.7	77-10
InI_3	619.9	517.2	1137.1	79-11 r
KIO_4	624.1	513.3	1137.4	79-11 r
I_2 (g) → I (g)		Δ −3.25		79-10

*11.5 eV added to the value for $M_5N_{45}N_{45}$ to provide value for $M_4N_{45}N_{45}$.

XENON				
Xe (implanted in graphite)	669.65	545.2	1214.85	79-12 r
Xe (implanted in diamond)	668.9	545.4*	1214.3	80-7 n
Xe (implanted in Fe)	670.2	544.8	1215.0	75-7 r
Xe (adsorbed on Pt)	669.5	544.2	1213.7	74-5 n
Xe (g) → Xe (adsorbed on Mo)	Δ −1.2	+6.3	+5.1	82-9
Xe (g) → Xe (adsorbed on MoO_2)	Δ −3.5	+7.1	+3.6	82-9
Na_4XeO_6	674.1	541.4	1215.5	77-21
Na_4XeO_6			1216.3*	75-4
Xe (g)	676.4 v	532.7 v	1209.1	69-1, 72-1
Xe (g)		532.8 v		73-9

*12.7 eV added to $M_5N_{45}N_{45}$ value to give value for $M_4N_{45}N_{45}$.

CESIUM	$3d_{5/2}$	$M_4N_{45}N_{45}$	α'	Ref.
Cs			1296.6	80-3
Cs			1297.1	80-19
Cs_3Sb			1296.1	80-3

CESIUM—*cont.*	$3d_{5/2}$	$M_4N_{45}N_{45}$	α'	Ref.
CsI			1294.0	80-3
Cs_2O_4			1293.1	80-19
CsCl	724.9	568.7	1293.6	82-5
CsOH	724.15	568.7	1292.85	79-12 r
Cs_2SO_4	723.9	568.4	1292.3	77-21 r
BARIUM				
Ba	779.3*	602.0*	1381.3	80-12 r
Ba ox	779.1	598.4	1377.5	80-12 r
Ba → Ba ox	Δ −0.2	−3.6	−3.8	80-12
BaO	779.85	597.5	1377.35	79-12 r
$BaSO_4$	780.8	596.1	1376.9	77-12 r
Ba erucate	780.2	596.2	1376.4	82-5
Ba cyclohexanebutyrate	780.1	596.1	1376.2	82-5
Ba chloranilate	779.6	596.7	1376.3	82-5
BaF_2	779.7	597.2	1376.9	82-5

*These data are assumed to supersede those in 80-13.

TANTALUM	$4f_{7/2}$	$M_5N_{67}N_{67}$	α'	$M_4N_{67}N_{67}$	$3d_{5/2}$	Ref.
Ta	21.9	1674.65	1696.55			80-16 r
TUNGSTEN						
WC	32.5	1729.1	1761.6	1791.5	1807.7	78-8 r
WS_2	33.0	1728.5	1761.5	1790.8	1807.7	78-8 r
$NiWS_2$	32.8	1728.7	1761.5	1791.1	1807.7	78-8 r
$K_4W(CN)_8$	32.8	1725.6	1758.4	1787.9	1807.5	78-8 r
$(C_5H_5)_2WCl_2$		1725.9		1787.9	1808.5	78-8 r
WO_3	36.1	1723.8	1759.9	1786.3	1810.6	78-8 r
H_2WO_4	36.1	1723.9	1760.0	1786.3	1810.5	78-8 r
$W(OPh)_6$	37.3	1723.8	1761.1	1786.2	1811.3	78-8 r
$CoWO_4$	36.0	1725.0	1761.0	1787.2	1810.7	78-8 r
$CuWO_4$	36.1	1725.3	1761.4	1786.9	1810.7	78-8 r
$NiWO_4$	36.0	1724.3	1760.3	1786.6	1811.2	78-8 r
$Fe_2(WO_4)_3$	36.3	1723.8	1760.1	1786.3	1810.8	78-8 r
$Na_2WO_4 \cdot 2H_2O$	36.4	1722.8	1759.2	1785.3	1810.4	78-8 r
Li_2WO_4	35.7	1722.8	1758.5	1785.1	1810.6	78-8 r
OSMIUM						
K_2OsCl_6	56.2			1907.7		78-8 r
$K_4Os(CN)_6$	57.2			1909.8		77-12 r
PLATINUM					$N_{67}W$	
Pt	71.1				63.4	82-5
Pt	71.3	1960.7	2032.0	2041.1		78-8 r
K_2PtCl_4	73.4			2035.2		75-7 r

GOLD						
Au	84.0*	2015.9*	2099.9*			
Au	84.0	2015.7	2099.7			82-1 * r
Au	84.0					80-16 r
Au	84.0	2015.8	2099.8	2101.2	69.4*	82-5
Au		2015.9		2101.3		78-8 r
						81-3 r

*Probably mainly component N_7VV.

MERCURY	$4f_{7/2}$	$M_4N_{67}N_{67}$	α'	$N_6O_{45}O_{45}^*$	α'	$N_7O_{45}O_{45}$	Ref.
Hg	99.9						
Hg (g)				80.55	180.45	77.75	82-5
						63.5 v	77-1
THALLIUM							
Tl	117.8						
						85.1	82-5
LEAD							
Pb	137.0	2180.5	2317.5				
Pb	136.8						80-16 r
Pb	136.8			96.25	233.05	92.95	82-5
PbTe	137.25			96.25	233.05		82-12
PbSe	137.6			95.45	232.7		82-12
PbS	137.5			94.75	232.35		82-12
PbO	137.25			94.55	232.05		82-12
PbO_2	137.4			92.85	230.1		82-12
PbI_2	138.35			93.05	230.45		82-12
$PbBr_2$	138.8			93.35	231.7		82-12
$PbCl_2$	138.9			92.6	231.4		82-12
PbF_2	138.5			92.1	231.0		82-12
$Pb(OH)_2$	137.95			90.6	299.1		82-12
$Pb(NO_3)_2$	138.5			91.95	229.9		82-12
$PbSiO_3$	138.65			91.7	230.2		82-12
$PbSO_4$	140.0			91.1	229.75		82-12
$PbTiO_3$	138.0			90.1	230.1		82-12
$PbCrO_4$	138.3			92.6	230.6		82-12
$PbZrO_3$	138.5			92.75	231.05		82-12
$Pb(IO_4)_2$	138.2			91.7	230.2		82-12
$PbWO_4$	138.7			92.7	230.9		82-12
PbNCN	137.5			91.8	230.5		82-12
$Pb(OAc)_2$	138.5			94.0	231.5		82-12
				91.45	229.95		82-12

*This component, made up chiefly of $N_6O_{45}O_{45}$ lines, is believed to be most easily measurable in most compounds (cf. Ref. 77-1).

BISMUTH	$4f_{7/2}$	$N_6O_{45}O_{45}$*	α'	$N_7O_{45}O_{45}$	Ref.
Bi	157.0	103.7	260.7	100.1	82-5

*This component, made up chiefly of $N_6O_{45}O_{45}$ lines, is believed to be most easily measurable in most compounds (cf. Ref. 77–1).

Practical Surface Analysis
by Auger and X-ray Photoelectron Spectroscopy
Edited by D. Briggs and M. P. Seah

Appendix 5

Empirically Derived Atomic Sensitivity Factors for XPS

The following empirically derived set of atomic sensitivity factors, relative to F 1*s* = 1.00, is obtained from a combination of data from the Varian IEE and Physical Electronics (Perkin-Elmer) 550 spectrometers. These spectrometers utilize scanning by varying the retarding voltage applied to the emitted electrons, with the analyser operated at constant-pass energy. This gives a transmission function for the spectrometer varying with the inverse of the electron kinetic energy. The factors therefore should be applicable to other spectrometers with the same transmission characteristics (cf. M. P. Seah, *Surf. Interface Anal.*, **2**, 222, 1980), but will not be applicable to those operating in a different mode. These data are reproduced from C. D. Wagner, L. E. Davis, M. V. Zeller, J. A. Taylor, R. M. Raymond and L. H. Gale, *Surf. Interface Anal.*, **3**, 211 (1981).

	Strong line		Secondary line‡	
	Area 1*s*	Height† 1*s*	Area 2*s*	Height 2*s*
Li	0.020	0.020		
Be	0.059	0.059		
B	0.13	0.13		
C	0.25	0.25		
N	0.42	0.42		
O	0.66	0.66	0.025	0.025
F	1.00	1.00	0.04	0.04
Ne	1.5	1.5	0.07	0.07
Na	2.3	2.3	0.13	0.12
Mg	3.5•§	3.3	0.20	0.15

	Strong line			Secondary line‡	
	Area		Height†	Area	Height†
	$2p_{3/2}$	$2p$	$2p_{3/2}$	$2s$	$2s$
Mg		0.12	0.12	0.20	0.15
Al		0.185	0.18	0.23	0.17
Si		0.27	0.25	0.26	0.19
P		0.39	0.36	0.29	0.21
S		0.54	0.49	0.33	0.24
Cl		0.73	0.61	0.37	0.25
Ar		0.96	0.75	0.40	0.26
K	0.83	1.24	0.83	0.43	0.26
Ca	1.05	1.58	1.05	0.47	0.26
Sc	(1.1)	(1.65)	(1.1)	0.50	0.26
Ti	(1.2)	(1.8)	(1.2)	0.54	0.26
				$3p$	$3p$
Ti	(1.2)¶	(1.8)	(1.2)	0.21	0.15
V	(1.3)	(1.95)	(1.3)	0.21	0.16
Cr	(1.5)	(2.3)	(1.5)	(0.21)	(0.17)
Mn	(1.7)	(2.6)	(1.7)	(0.22)	(0.19)
Fe	(2.0)	(3.0)	(2.0)	(0.26)	(0.21)
Co	(2.5)	(3.8)	(2.5)	(0.35)	(0.25)
Ni	(3.0)	(4.5)	(3.0)	(0.5)	(0.3)
Cu	(4.2)	(6.3)	(4.2)	(0.65)	(0.4)
Zn	4.8		4.8	0.75	0.40
Ga	5.4		5.4	0.84	0.40
Ge	6.1•		6.0•	0.92	0.40
As	6.8•		6.8•	1.00	0.43

	Area		Height	Area		Height
	$3d_{5/2}$	$3d$	$3d_{5/2}$	$3p_{3/2}$	$3p$	$3p_{3/2}$
Ga		0.31	0.31		0.84	0.40
Ge		0.38	0.37		0.91	0.40
As		0.53	0.51		0.97	0.42
Se		0.67	0.64		1.05	0.48
Br		0.83	0.77		1.14	0.54
Kr		1.02	0.91	0.82	1.23††	0.60
Rb		1.23	1.07	0.87	1.30	0.67
Sr		1.48	1.24	0.92	1.38	0.69
Y		1.76	1.37	0.98	1.47	0.71
Zr		2.1	1.5	1.04	1.56	0.72

	Strong line			Secondary line‡		
	Area		Height	Area		Height
	$3d_{5/2}$	$3d$	$3d_{5/2}$	$3p_{3/2}$	$3p$	$3d_{5/2}$
Nb	1.44	2.4	1.57	1.10		0.72
Mo	1.66	2.75	1.74	1.17		0.73
Tc	1.89	3.15	1.92	1.24		0.73
Ru	2.15	3.6	2.15	1.30		0.73
Rh	2.4	4.1	2.4	1.38		0.74
Pd	2.7	4.6	2.7	1.43		0.74
Ag	3.1	5.2	3.1	1.52		0.75
Cd	3.5		3.5	1.60		0.75
In	3.9		3.9	1.68		0.75
Sn	4.3		4.3	1.77		0.75
	Area		Height†	Area		Height
					$4d$	$4d$
Sb	4.8		4.8		1.00	0.86
Te	5.4		5.4		1.23	0.97
I	6.0		6.0		1.44	1.08
Xe	6.6		6.6		1.72	1.16
Cs	7.2		7.0		2.0	1.25
Ba	7.9		7.5		2.35	1.35
La		(10)¶			(2)	
Ce		(10)			(2)	
Pr		(9)			(2)	
Nd		(7)			(2)	
Pm		(6)			(2)	
Sm		(5)			(2)	
Eu		(5)			(2)	
Gd	(3)•				(2)	
Tb	(3)•				(2)	
		$4d$		$4p_{3/2}$		
Dy		(2)¶		(0.6)¶		
Ho		(2)		(0.6)		
Er		(2)		(0.6)		
Tm		(2)		(0.6)		
Yb		(2)		(0.6)		
Lu		(2)		(0.6)		

	Strong line			Secondary line‡		
	Area		Height	Area		Height
	$4f_{7/2}$	$4f$	$4f_{7/2}$	$4d_{5/2}$	$4d$	$4d_{5/2}$
Hf		2.05	1.70	1.42	2.35	0.90
Ta		2.4	1.89	1.50	2.50	0.90
W		2.75	2.0	1.57	2.6	0.90
Re		3.1	2.1	1.66	2.75	0.90
Os		3.5	2.2	1.75	2.9	0.90
Ir	2.25	3.95	2.4	1.84		0.90
Pt	2.55	4.4	2.55	1.92		0.90
Au	2.8	4.95	2.8	2.05		0.90
Hg	3.15	5.5	3.15	2.15		0.95

	Area		Height	Area	Height	Area		Height
	$4f_{7/2}$	$4f$	$4f_{7/2}$	$4d_{5/2}$	$4d_{5/2}$	$5d_{5/2}$	$5d$	$5d_{5/2}$
Tl	3.5	6.15	3.5	2.25	0.95		0.9	0.55
Pb	3.85	6.7	3.82	2.35	1.00		1.0	0.6
Bi	4.25	7.4	4.25	2.5	1.00		1.1	0.65
Th	7.8		7.8	3.5	1.2	0.9	1.5	0.9
U	9.0		9.0	3.85	1.3	1.0	1.6	1.0

†Height sensitivity factors based on line widths for strong lines of 3.1 eV, typical of lines obtained in survey spectra on insulating samples. When spin doublets are unresolved, data are for the convoluted peak height.

‡Factors for the strong lines are insensitive to the radiation source (Mg or Al). Factors for the secondary lines (2*s*, 3*p*, 4*d* and 5*d*) are dependent to an extent upon the photon energy. Values shown are average for Al and Mg. For more accurate results, multiply the factors by 0.9 when Mg radiation is used and by 1.1 when Al radiation is used.

§Starred data are for peaks obtained only by using Al X-rays.

¶Data in parentheses indicate great variability with chemical state, because of the prevalence of multielectron processes. Data shown for the series Ti–Cu are for diamagnetic forms; data for paramagnetic forms will be lower in general. Data for the rare earths are based on few experimental points, and should be regarded only as a rough approximation.

††Many of the area data are suppled for spin doublets for 3*p* and 4*d* because of the considerable width of many of those lines. Data for combined spin doublets in the 2*p* series for transition metals and the 3*d* for the rare earths are supplied because of the prevalence of shake-up lines, which make it desirable to deal with the doublet as a whole.

Practical Surface Analysis
by Auger and X-ray Photoelectron Spectroscopy
Edited by D. Briggs and M. P. Seah

Appendix 6

*(a) Line Positions** from Mg X-rays, by Element (BE Scale)

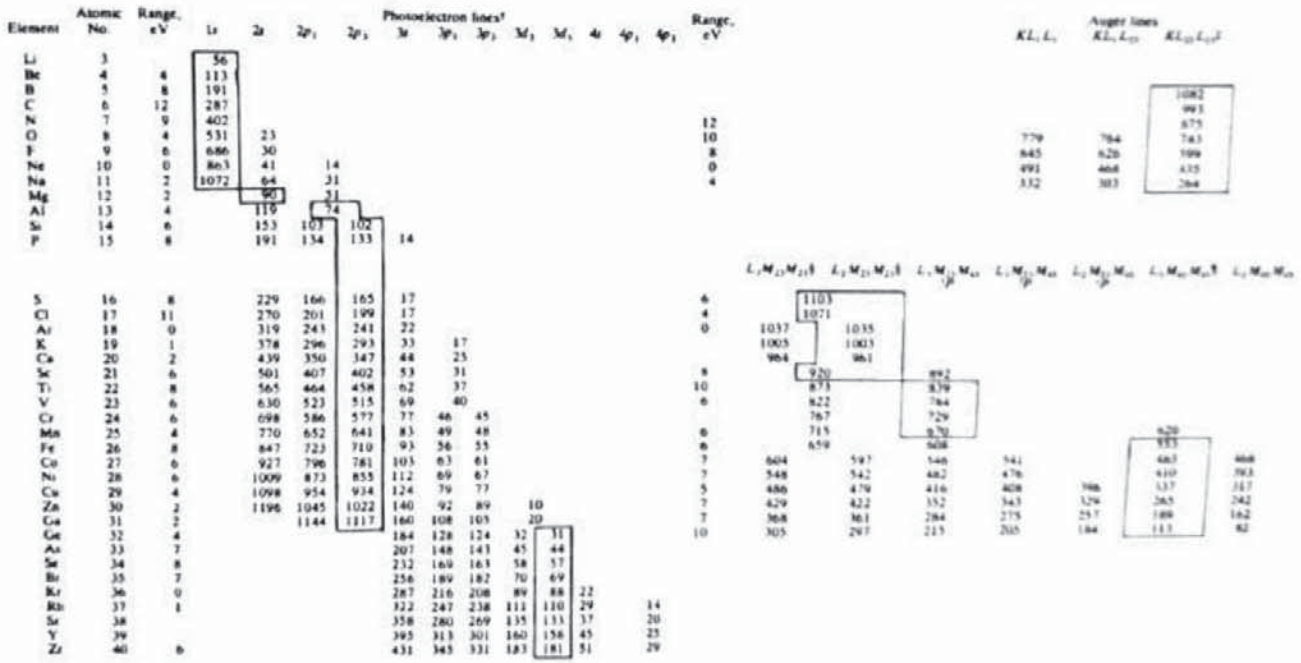

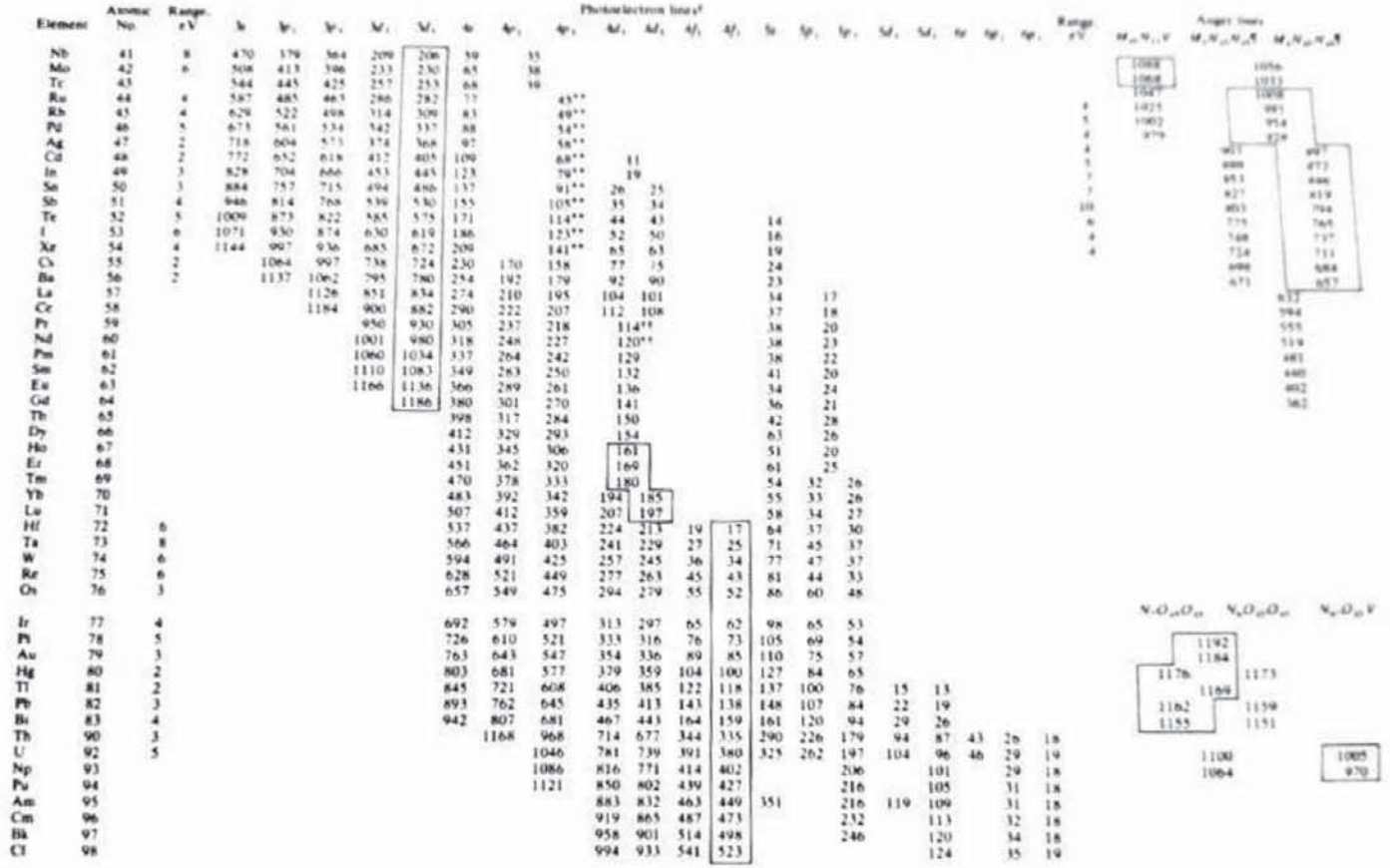

*Lines enclosed in boxes are the most intense and are the most suitable for use of line energies in identifying chemical states.
†For brevity, $2p_3$ equals $2p_{3/2}$, $3d_5$ equals $3d_{5/2}$, etc.
‡Includes *KVV* designation when L_{23} is not a core level.
§Designation is oversimplified.
¶Includes *LVV* when *M* levels are not in core, and *MVV* when *N* levels are not in core.
**No simple $4p_{1/2}$ line exists for this group of elements.
††The 4*d* doublet for these elements is complex and is variable with chemical state because of multiplet splitting and multielectron process.
Source: *Handbook of X-ray Photoelectron Spectroscopy*, C. D. Wagner, W. M. Riggs, L. E. Davis, J. F. Moulder and (ed.) G. E. Muilenberg, Perkin-Elmer Corporation, Eden Praire (1979).

(b) Line Positions* from Al X-rays, by Element (BE Scale)

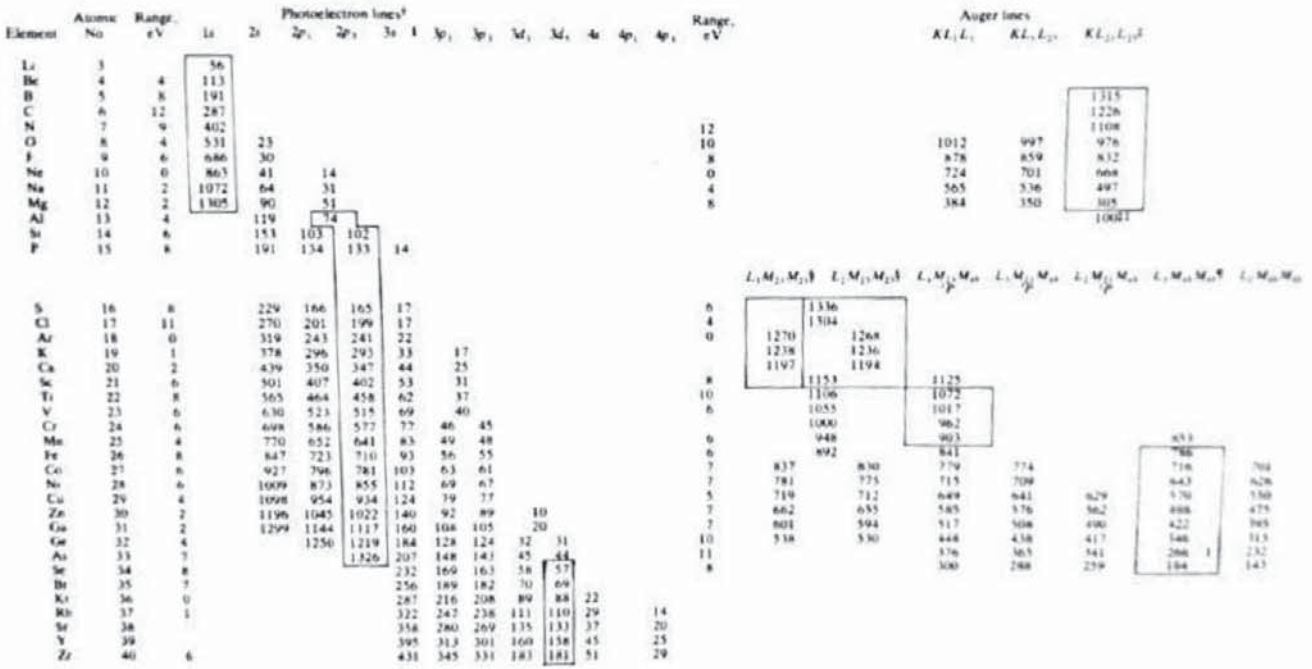

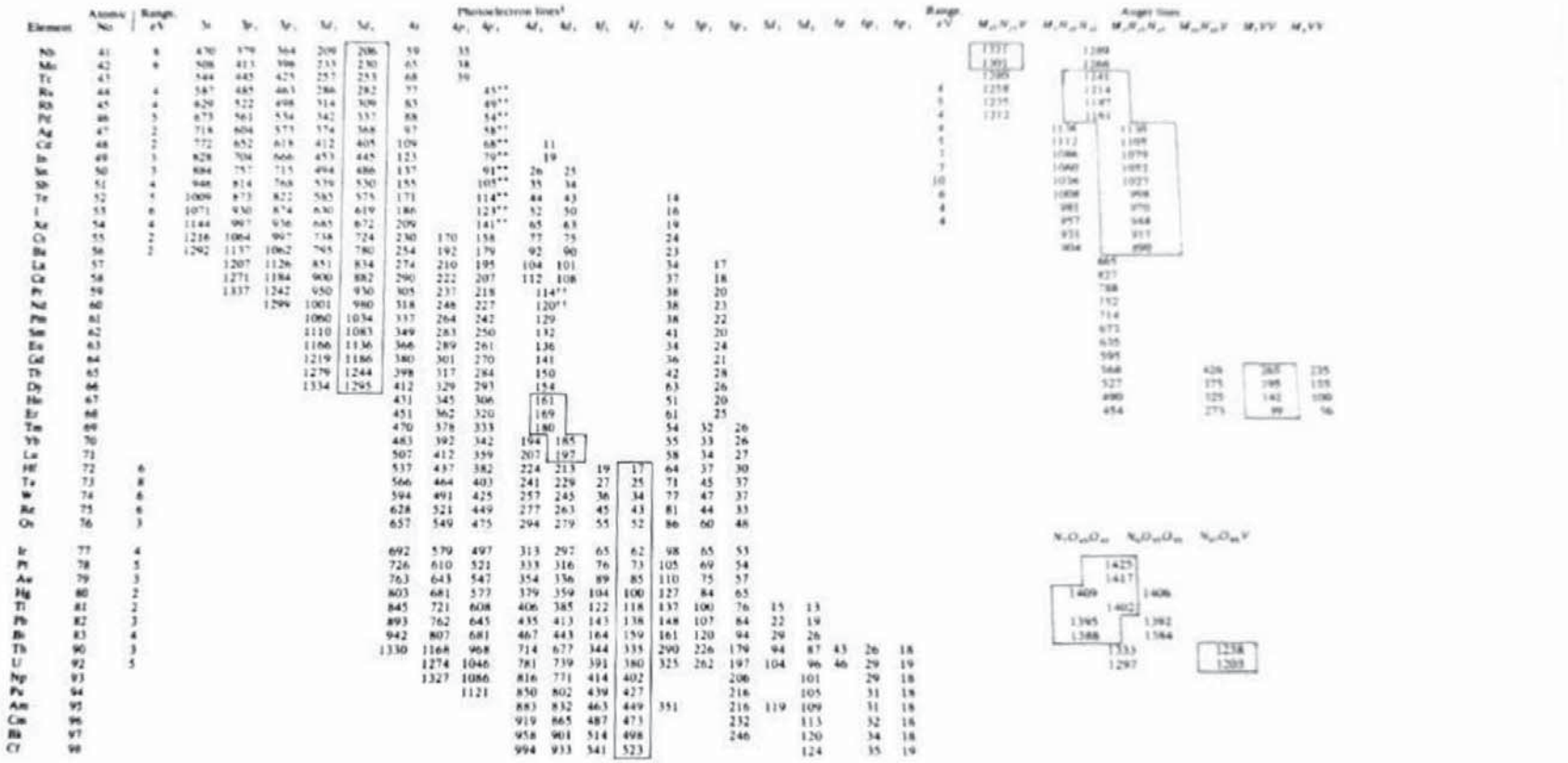

*Lines enclosed in boxes are the most intense and are the most suitable for use of line energies in identifying chemical states.
†For brevity, $2p_3$ equals $2p_{3/2}$, $3d_5$ equals $3d_{5/2}$, etc.
‡Includes KVV designation when L_{23} is not a core level.
§Designation is oversimplified.
¶Includes LVV when M levels are not in core and MVV when N levels are not in core.
**No simple $4p_{1/2}$ line exists for this group of elements.
††The $4d$ doublet for these elements is complex and is variable with chemical state because of multiplet splitting and multielectron processes.
‡‡Often observable, induced by bremsstrahlung.
Source: *Handbook of X-ray Photoelectron Spectroscopy*, C. D. Wagner, W. M. Riggs, L. E. Davis, J. F. Moulder and (ed.) G. E. Muilenberg, Perkin-Elmer Corporation, Eden Praire (1979).

Practical Surface Analysis
by Auger and X-ray Photoelectron Spectroscopy
Edited by D. Briggs and M. P. Seah

Appendix 7

(a) Line Positions from Mg X-rays, in Numerical Order

17 Hf $4f_7$	102 Si $2p_3$	206 Nb $3d_5$	359 Lu $4p_3$	575 Te $3d_5$	863 Ne $1s$	
23 O $2s$	105 Ga $3p_3$	208 Kr $3p_3$	359 Hg $4d_5$	577 Cr $2p_3$	872 Cd (A)	
25 Ta $4f_7$	108 Ce $4d_5$	213 HF $4d_5$	362 Gd (A)	594 Ce (A)	875 N (A)	
30 F $2s$	110 Rb $3d_5$	229 S $2s$	364 Nb $3p_3$	599 F (A)	882 Ce $3d_5$	
31 Ge $3d_5$	113 Be $1s$	229 Ta $4d_5$	368 Ag $3d_5$	618 Cd $3p_3$	897 Ag (A)	
34 W $4f_7$	113 Ge (A)	230 Mo $3d_5$	378 K $2s$	619 I $3d_5$	920 Sc (A)	
40 V $3p$	114 Pr $4d$	238 Rb $3p_3$	380 U $4f_7$	632 La (A)	928 Pd (A)	
41 Ne $2s$	118 Tl $4f_7$	241 Ar $2p_3$	385 Tl $4d_5$	641 Mn $2p_3$	930 Pr $3d_5$	
43 Re $4f_7$	119 Al $2s$	245 W $4d_5$	396 Mo $3p_3$	657 Ba (A)	934 Cu $2p_3$	
44 As $3d_5$	120 Nd $4d$	263 Re $4d_5$	402 N $1s$	666 In $3p_3$	954 Rh (A)	
45 Cr $3p_3$	124 Ge $3p_3$	264 Na (A)	402 Eu (A)	670 Mn (A)	961 Ca (A)	
48 Mn $3p_3$	132 Sm $4d$	265 Zn (A)	402 Sc $2p_3$	672 Xe $3d_5$	970 U (A)	
50 I $4d_5$	133 P $2p_3$	269 Sr $3p_3$	405 Cd $3d_5$	677 Th $4d_5$	980 Nd $3d_5$	
51 Mg $2p$	133 Sr $3d_5$	270 Cl $2s$	410 Ni (A)	684 Cs (A)	981 Ru (A)	
52 Os $4f_7$	136 Eu $4d$	279 Os $4d_5$	413 Pb $4d_5$	686 F $1s$	993 C (A)	
55 Fe $3p_3$	138 Pb $4f_7$	282 Ru $3d_5$	435 Ne (A)	710 Fe $2p_3$	1003 K (A)	
56 Li $1s$	143 As $3p_3$	284 Tb $4p_3$	439 Ca $2s$	711 Xe (A)	1005 Th (A)	
57 Se $3d_5$	150 Tb $4d$	287 C $1s$	440 Sm (A)	715 Sn $3p_3$	1022 Zn $2p_3$	
61 Co $3p_3$	153 Si $2s$	293 Dy $4p_3$	443 Bi $4d_5$	724 Cs $3d_5$	1035 Ar (A)	
62 Ir $4f_7$	154 Dy $4d$	293 K $2p_3$	445 In $3d_5$	729 Cr (A)	1071 Cl (A)	
63 Xe $4d_5$	158 Y $3d_5$	297 Ir $4d_5$	458 Ti $2p_3$	737 I (A)	1072 Na $1s$	
64 Na $2s$	159 Bi $4f_7$	301 Y $3p_3$	463 Ru $3p_3$	739 U $4d_5$	1082 B (A)	
67 Ni $3p_3$	161 Ho $4d$	306 Ho $4p_3$	483 Co (A)	743 O (A)	1083 Sm $3d_5$	
69 Br $3d_5$	163 Se $3p_3$	309 Rh $3d_3$	486 Sn $3d_5$	765 Te (A)	1088 Nb (A)	
73 Pt $4f_7$	165 S $2p_3$	316 Pt $4d_5$	498 Rh $3p_3$	768 Sb $3p_3$	1103 S (A)	
74 Al $2p$	169 Er $4d$	319 Ar $2s$	501 Sc $2s$	780 Ba $3d_5$	1117 Ga $2p_3$	
75 Cs $4d_5$	180 Tm $4d$	320 Er $4p_3$	515 V $2p_3$	781 Co $2p_3$	1136 Eu $3d_5$	
77 Cu $3p_3$	181 Zr $3d_5$	331 Zr $3p_3$	519 Nd (A)	784 V (A)	1155 Bi (A)	
85 Au $4f_7$	182 Br $3p_3$	333 Tm $4p_3$	530 Sb $3d_5$	794 Sb (A)	1162 Pb (A)	
87 Zn $3p_3$	185 Yb $4d_5$	335 Th $4f_7$	531 O $1s$	819 Sn (A)	1169 Tl (A)	
88 Kr $3d_5$	189 Ga (A)	336 Au $4d_5$	534 Pd $3p_3$	822 Te $3p_3$	1176 Hg (A)	
90 Ba $4d_5$	191 B $1s$	337 Pd $3d_5$	553 Fe (A)	834 La $3d_5$	1184 Au (A)	
90 Mg $2s$	191 P $2s$	337 Cu (A)	555 Pr (A)	839 Ti (A)	1186 Gd $3d_5$	
100 Hg $4f_7$	197 Lu $4d_5$	342 Yb $4p_3$	565 Ti $2s$	846 In (A)	1192 Pt (A)	
101 La $4d_5$	199 Cl $2p_3$	347 Ca $2p_3$	573 Ag $3p_3$	855 Ni $2p_3$		

An A in parentheses denotes Auger line. The sharpest Auger line and the two most intense photo-electron lines per element are included in the table. For brevity, $2p_3$ equals $2p_{3/2}$, $3d_5$ equals $3d_{5/2}$, etc. All lines are on the binding energy scale.
Source: *Handbook of X-ray Photoelectron Spectroscopy*, C. D. Wagner, W. M. Riggs, L. E. Davis, J. F. Moulder and (ed.) G. E. Muilenberg, Perkin-Elmer Corporation, Eden Praire (1979).

(b) Line Positions from Al X-rays, in Numerical Order

17 Hf $4f_7$
23 O $2s$
25 Ta $4f_7$
30 F $2s$
34 W $4f_7$
40 V $3p$
41 Ne $2s$
43 Re $4f_7$
44 As $3d_5$
45 Cr $3p_3$
48 Mn $3p_3$
50 I $4d_5$
52 Os $4f_7$
55 Fe $3p_3$
56 Li $1s$
57 Se $3d_5$
61 Co $3p_3$
62 Ir $4f_7$
63 Xe $4d_5$
64 Na $2s$
67 Ni $3p_3$
69 Br $3d_5$
73 Pt $4f_7$
74 Al $2p$
75 Cs $4d_5$
77 Cu $3p_3$
85 Au $4f_7$
87 Zn $3p_3$
88 Kr $3d_5$
90 Ba $4d_5$
90 Mg $2s$
99 Er (A)
100 Hg $4f_7$
101 La $4d_5$
102 Si $2p_3$
105 Ga $3p_3$
108 Ce $4d_5$
110 Rb $3d_5$
113 Be $1s$
114 Pr $4d$
118 Tl $4f_7$
119 Al $2s$
120 Nd $4d$
124 Ge $3p_3$
132 Sm $4d$
133 P $2p_3$
133 Sr $3d_5$
136 Eu $4d$
138 Pb $4f_7$
141 Gd $4d$
142 Ho (A)
150 Tb $4d$
153 Si $2s$
154 Dy $4d$
158 Y $3d_5$
159 Bi $4f_7$
161 Ho $4d$
163 Se $3p_3$
165 S $2p_3$
169 Er $4d$
180 Tm $4d$
181 Zr $3d_5$
182 Br $3p_3$
184 Se (A)
185 Yb $4d_5$
191 B $1s$
191 P $2s$
195 Dy (A)
197 Lu $4d_5$
199 Cl $2p_3$
206 Nb $3d_5$
208 Kr $3p_3$
213 Hf $4d_5$
229 S $2s$
229 Ta $4d_5$
230 Mo $3d_5$
238 Rb $3p_3$
241 Ar $2p_3$
245 W $4d_5$
263 Re $4d_5$
265 Tb (A)
266 As (A)
269 Sr $3p_3$
270 Cl $2s$
279 Os $4d_5$
282 Ru $3d_5$
287 C $1s$
293 K $2p_3$
297 Ir $4d_5$
301 Y $3p_3$
305 Mg (A)
306 Ho $4p_3$
309 Rh $3d_5$
316 Pt $4d_5$
319 Ar $2s$
320 Er $4p_3$
331 Zr $3p_3$
333 Tm $4p_3$
335 Th $4f_7$
336 Au $4d_5$
337 Pd $3d_5$
342 Yb $4p_3$
346 Ge (A)
347 Ca $2p_3$
359 Lu $4p_3$
359 Hg $4d_5$
364 Nb $3p_3$
368 Ag $3d_5$
378 K $2s$
380 U $4f_7$
385 Tl $4d_5$
396 Mo $3p_3$
402 N $1s$
402 Sc $2p_3$
405 Cd $3d_5$
413 Pb $4d_5$
422 Ga (A)
439 Ca $2s$
443 Bi $4d_5$
445 In $3d_5$
458 Ti $2p_3$
463 Ru $3p_3$
486 Sn $3d_5$
497 Na (A)
498 Zn (A)
498 Rh $3p_3$
501 Sc $2s$
515 V $2p_3$
530 Sb $3d_5$
531 O $1s$
534 Pd $3p_3$
565 Ti $2s$
570 Cu (A)
573 Ag $3p_3$
575 Te $3d_5$
577 Cr $2p_3$
595 Gd (A)
618 Cd $3p_3$
619 I $3d_5$
635 Eu (A)
641 Mn $2p_3$
643 Ni (A)
666 In $3p_3$
668 Ne (A)
672 Xe $3d_5$
673 Sm (A)
667 Th $4d_5$
686 F $1s$
710 Fe $2p_3$
715 Sn $3p_3$
716 Co (A)
724 Cs $3d_5$
739 U $4d_5$
752 Nd (A)
768 Sb $3p_3$
780 Ba $3d_5$
781 Co $2p_3$
786 Fe (A)
788 Pr (A)
822 Te $3p_3$
827 Ce (A)
832 F (A)
834 La $3d_5$
855 Ni $2p_3$
863 Ne $1s$
865 La (A)
882 Ce $3d_5$
890 Ba (A)
903 Mn (A)
917 Cs (A)
930 Pr $3d_5$
934 Cu $2p_3$
944 Xe (A)
962 Cr (A)
970 I (A)
976 O (A)
980 Nd $3d_5$
998 Te (A)
1017 V (A)
1022 Zn $2p_3$
1027 Sb (A)
1052 Sn (A)
1072 Na $1s$
1072 Ti (A)
1079 In (A)
1083 Sm $3d_5$
1105 Cd (A)
1108 N (A)
1117 Ga $2p_3$
1130 Ag (A)
1136 Eu $3d_5$
1153 Sc (A)
1161 Pd (A)
1186 Gd $3d_5$
1187 Rh (A)
1194 Ca (A)
1205 U (A)
1214 Ru (A)
1219 Ge $2p_3$
1226 C (A)
1230 Th (A)
1236 K (A)
1244 Tb $3d_5$
1268 Ar (A)
1295 Dy $3d_5$
1301 Mo (A)
1304 Cl (A)
1305 Mg $1s$
1315 B (A)
1321 Nb (A)
1326 As $2p_3$
1336 S (A)
1388 Bi (A)
1395 Pb (A)
1402 Tl (A)
1409 Hg (A)
1417 Au (A)
1425 Pt (A)

An A in parentheses denotes Auger line. The sharpest Auger line and the two most intense photo-electron lines per element are included in the table. For brevity, $2p_3$ equals $2p_{3/2}$, $3d_5$ equals $3d_{5/2}$, etc. All lines are on the binding energy scale.

Source: *Handbook of X-ray Photoelectron Spectroscopy*, C. D. Wagner, W. M. Riggs, L. E. Davis, J. F. Moulder and (ed.) G. E. Muilenberg, Perkin-Elmer Corporation, Eden Praire (1979).

Practical Surface Analysis
by Auger and X-ray Photoelectron Spectroscopy
Edited by D. Briggs and M. P. Seah

Appendix 8

Kinetic Energies of Auger Electrons: Experimental Data from Spectra Acquired by X-ray Excitation

C. D. Wagner
29 Starview Drive, Oakland, CA 94618, USA

The following table is believed to represent the best available data on the most prominent Auger lines in X-ray excited spectra. Lines presented are mostly of the core type, with no attempt made to include the valence-type lines such as *KVV* for Li–O, *LVV* for Mg–C1, *MVV* for Cr–Y and *NVV* for Ir–Hg. The low energy *NOO* lines for Tl–Bi and the rather prominent Coster–Kronig lines for the heavy metals are not included. Certain lines of very low intensity, such as *KLV*, *LMV* and *MNV* lines, and shoulders on the intense lines are also not included.

Data are presented mainly for elemental conductive states. Gas phase data are supplied when the data are significantly more detailed than the solid phase. Data on oxides are included as well for certain elements where the spectra are significantly different for element and oxide. Other tabulations should be consulted for data on chemical shifts.

Most of the data are derived from information used to produce reference 79–1. Other references of particular value for the distributions of line energies are noted. Data are Fermi level referenced unless otherwise noted. For many lines, the energies are close to those observed with conventional electron-excited, vacuum-referenced dN/dE data, customarily used in Auger electron spectroscopy, because the work function of 4–5 eV approximately offsets the difference between the peak position and the inflection point on the high-energy side. Some notations used are:

(g) = gas phase
v = referenced to vacuum level
i = interpolated or extrapolated value
b = broad line
l = low intensity

KLL	KL_1L_1 ^1S	KL_1L_{23} ^1P	KL_1L_{23} ^3P	$KL_{23}L_{23}$ ^1S	$KL_{23}L_{23}$ ^1D	Ref.
F alkali fluorides	611	630	638	653	656	68-1
Ne implanted in Fe	762	785	798 i	814	818	75-2
(g)	749 v	772 v	783 v	801 v	805 v	66-1
Na	926	955	967	989	994	74-2
Mg	1107	1140	1155	1181	1186	75-1, 78-1
Al	1302	1341	1357	1387	1393	76-1, 78-1
Si	1514	1559 i	1576	1610	1617	77-5
P GaP	1745	1794 i	1813	1852	1859	80-2
S WS_2	1991	2045	2065	2108	2116	77-3
Cl CCl_4 (g)	2245 v	2304 v	2326 v	2374 v	2383 v	69-1
Ar (g)	2508 v	2576 v	2600 v	2651 v	2661 v	77-2

LMM	$L_3M_1M_{23}$ ^1P	$L_3M_1M_{23}$ ^3P	$L_3M_{23}M_{23}$ ^1D	$L_3M_{23}M_{23}$ ^3P	$L_3M_{23}M_{45}$ ^1F	$L_3M_{23}M_{45}$ $^3D^3P$	$L_2M_{23}M_{45}$ ^1F	$L_3M_{45}M_{45}$ ^1G	$L_2M_{45}M_{45}$ ^1G	Ref.
Ar in Fe			217							75-2
(g)			204 v	206 v*						73-1
K KBr			248	250*						75-2
KBr (g)			237 v	239 v						81-1
Ca element				298*						80-1
$CaCO_3$			285	288*						
Sc Sc_2O_3	307	315		335*	363					
Ti element	346	355	383	389	419			452		71-2
TiO_2			382		415					

V	element	400	411	432	438	472			510	71-2
	V_2O_5			428	432	468				
Cr	element	446	460	l	489	527			570	71-2
	Cr_2O_3					528				
Mn	element	500 i	514 i	l	543	586			635	
	MnO_2				541	585			634	
Fe	element	548	563	591	598	647	651	l	702	715	71-2
	Fe_2O_3				597	647			703		
Co	element	605	618	648	655	710	715	723	773	789	71-2
	CoO	604	617	647	654	709			773	789	
Ni	element	661	674	709	715	775	781	l	846	863	71-2
	NiO			710		775			846		
Cu	element	716	729	768	775	840	847	859	919	939	77-1
	CuO			764		837	844	858	918		
Zn	element	774	787	826	834	905	913	928	992	1015	77-1, 6, 73-2
Ga	element	831	846	888	897	973	983	1000	1068	1095	77-1
Ge	element	890 i	895 i	953	962	1043	1054	1074	1145	1176	77-1
As	element	950	966	1020	1029	1116	1127	1152	1225	1261	77-7
Se	element	1013	1033	1086	1096	1189	1201	1230	1307	1348	
Br	bromo-methanes (g)			1143 v	1155 v	1253 v	1266 v	1300 v	1378 v	1424 v	70-1
Kr	(g)			1210 v	1223 v	1327 v	1342 v	1380 v	1460 v	1513 v	72-1
Rb											
Sr	SrF_2								1641		78-2
Y	Y_2O_3								1737		78-2
Zr	Zr oxide								1831		78-2
Nb	Nb oxide								1930		78-2
Mo	element								2039	2144	80-2

*Includes $L_2M_{23}M_{23}$ (^1D). Omitted because of low intensity are $L_2M_{23}M_{23}$, $L_3M_1M_{45}$ and $L_2M_{23}M_{45}$ (^3D).

MNN	$M_{45}N_1N_{23}$	$M_{45}N_{23}N_{23}$	$M_{45}N_1N_{45}$	$M_{45}N_{23}N_{45}$	$M_5N_{45}N_{45}$		$M_4N_{45}N_{45}$	
					^1G	$^3F_{2,3}$		Ref.
Zr	94	119	1	150				
Nb	114 b	136	145	168	200			
Mo	122	1	163	188	223			
Tc								
Ru	152							
Rh			201	231	274			
Pd			223	253 b	302			
			243	274 b	328		333	
Ag			262	296 b	352	353	358	71-1
Cd			280	b	377	379	384	71-1, 74-1
In			1	b	403	405	411	71-1
Sn			1	b	429	431	438	79-2
Sb					455	457	464	71-1
Te					482	484	492	77-4
I LiI					506	509	517	71-1
Xe in carbon					532	536	545	
(g)					520 v	524 v	533 v	72-1

	^1G	$M_5N_{45}N_{45}$ $^3F_{2,3}$	$M_4N_{45}N_{45}$	$M_5N_{45}N_{67}$	$M_4N_{45}N_{67}$	$M_5N_{67}N_{67}$	$M_4N_{67}N_{67}$	
Cs CsOH	555	559	569	630	643			
Ba element			602					80-1
BaO		585	598	669	683			
La La_2O_3		622	638	711 i	728 i			
Ce CeO_2		660		755	771			
Pr		695 i			795 i			
Nd		733 i			840 i			
Pm		770 i			885 i			
Sm Sm_2O_3		808 b			950 ib	1068	1094	
Eu		846 i			980 i	1120 i	1150 i	

Gd	884 i	1020 i	1170 i	1202 i	
Tb element	920 b	1068 b	1223	1256	
Dy	960 i	1115 i	1280 i	1318 i	
Ho	998 i	1165 i	1332 i	1372 i	
Er element	1035	1218 b	1387	1428	
Er_2O_3	1037	1221 b	1386	1429	
Tm	1080 i	1270 i	1440 i	1487 i	
Yb		1320 i	1500 i	1549 i	
Lu		1370 i	1560 i	1615 i	

	$M_{45}N_{45}N_{67}$	$M_5N_{67}N_{67}$	$M_4N_{67}N_{67}$†	Ref.
Hf	1420 i	1615 i	1669 i	
Ta	1462	1675	1733	80-2
W		1730	1792	78-2
Re		1790 i	1856 i	
Os K_2OsCl_6		1837	1908	78-2
Ir		1900 i	1975 i	
Pt		1961	2041	78-2
Au		2016	2102	80-2
Hg		2070 i	2160 i	
Tl		2128 i	2223 i	
Pb		2181	2282	80-2
Bi		2235 i	2343 i	
Th				
U				

†The difference in the binding energies of the $3d_{5/2}$ and $3d_{3/2}$ levels was used to calculate many of the $M_4N_{67}N_{67}$ energies from the $M_5N_{67}N_{67}$ energies.

Acknowledgement

Unpublished data from spectra obtained at Physical Electronics Division, Perkin-Elmer Corporation in connection with references 79-1 and 80-2 were used in assembling these data tables.

References

66–1 H. Körber and W. Mehlhorn, *Z. Phys.*, **191**, 217 (1966).
68–1 R. G. Albridge, K. Hamrin, G. Johansson and A. Fahlman, *Z. Phys.*, **209**, 419 (1968).
69–1 B. Cleff and W. Mehlhorn, *Z. Phys.*, **219**, 311 (1969).
70–1 R. Spohr, T. Bergmark, N. Magnusson, L. O. Werme, C. Nordling and K. Siegbahn, *Phys. Scr.*, **2**, 31 (1970).
71–1 S. Aksela, *Z. Phys.*, **244**, 268 (1971).
71–2 J. P. Coad, *Phys. Lett.*, **37A**, 437 (1971).
72–1 R. Spohr, T. Bergmark, N. Magnusson, L. O. Werme, C. Nordling and K. Siegbahn, *Phys. Scr.*, **2**, 31 (1970).
73–1 G. Johansson, J. Hedman, A. Berndtsson, M. Klasson and R. Nilsson, *J. Electron Spectrosc.*, **2**, 295 (1973).
73–2 G. Schön, *J. Electron Spectrosc.*, **2**, 75 (1973).
74–1 H. Aksela and S. Aksela, *J. Phys.*, **B7**, 1262 (1974).
74–2 A. Barrie and F. J. Street, *J. Electron Spectrosc.*, **7**, 1 (1977).
75–1 J. C. Fuggle, L. M. Watson, D. J. Fabian and S. Affrossman, *J. Phys.*, **F5**, 375 (1975).
75–2 C. D. Wagner, *Faraday Disc. Chem. Soc.*, **60**, 291 (1975).
76–1 G. Dufour, J.-M. Mariot, P.-E. Nilsson-Jatko and R. C. Karnatak, *Phys. Scr.*, **13**, 370 (1976).
77–1 E. Antonides, E. C. Janse and G. A. Sawatzky, *Phys. Rev.*, **B15**, 1669 (1977).
77–2 L. Asplund, P. Kelfve, B. Blomster, H. Siegbahn and K. Siegbahn, *Phys. Scr.*, **16**, 268 (1977).
77–3 L. Asplund, P. Kelfve, B. Blomster, H. Siegbahn, K. Siegbahn, R. L. Lozes and U. I. Wahlgren, *Phys. Scr.*, **16**, 273 (1977).
77–4 M. K. Bahl and R. L. Watson, *J. Electron Spectrosc.*, **10**, 111 (1977).
77–5 T. A. Carlson, W. B. Dress and G. L. Nyberg, *Phys. Scr.*, **16**, 211 (1977).
77–6 J.-M. Mariot and G. Dufour, *Chem. Phys. Lett.*, **50**, 219 (1977).
77–7 E. D. Roberts, P. Weightman and C. E. Johnson, *J. Phys. C. Sol. State Phys.*, **8**, 1301 (1975).
78–1 P. M. Th. M. Van Attekum and J. M. Trooster, *J. Phys.*, **F8**, L169 (1978).
78–2 C. D. Wagner, *J. Vac. Sci. Technol.*, **15**, 518 (1978).
79–1 C. D. Wagner, W. M. Riggs, L. E. Davis, J. F. Moulder and G. E. Muilenberg, *Handbook of X-ray Photoelectron Spectroscopy*, Physical Electronics Division, Perkin-Elmer Corporation, Eden Prairie, Minnesota, 1979.
79–2 S. M. Barlow, P. Bayat-Mokhtari and T. E. Gallon, *J. Phys. C. Sol. State Phys.*, **12**, 5577 (1979).
80–1 H. Van Doveren and J. A. Th. Verhoeven, *J. Electron Spectrosc.*, **21**, 265 (1980).
80–2 C. D. Wagner and J. A. Taylor, *J. Electron Spectrosc.*, **20**, 83 (1980).
81–1 S. Aksela, M. Kellokumpu, H. Aksela and J. Väyrynen, *Phys. Rev.*, **A23**, 2374 (1981).

Index